**TECHNISCHE
UNIVERSITÄT
WIEN**
Vienna University of Technology

DIPLOMARBEIT

Long Term Performance of an Fe/Cr Based Water Gas Shift Catalyst Processing Tar-Rich Wood Gas

ausgeführt zum Zwecke der Erlangung des akademischen Grades eines
Diplom-Ingenieurs unter der Leitung von

Univ. Prof. Dipl.-Ing. Dr. techn. Hermann Hofbauer
und der Mitbetreuung von
Dipl.-Ing. Michael Kraussler

Institut für Verfahrenstechnik,
Umwelttechnik und Technische Biowissenschaften

eingereicht an der Technischen Universität Wien,
Fakultät für Maschinenwesen und Betriebswissenschaften

von

Matthias Binder
Matrikelnummer 0626391
Columbusgasse 113/2/20
1100 Wien

Wien, 28. Oktober 2015   Matthias Binder

Abstract

Hydrogen is seen as an important renewable secondary energy carrier of the future.

Today, hydrogen is predominantly produced from fossil fuels. Hydrogen production from biomass via a thermochemical route can be an auspicious alternative for future decarbonized applications, which are based on renewable and carbon dioxide neutral produced hydrogen. Especially the dual fluidized bed (DFB) biomass steam gasification using wood chips as feedstock, seems to be a promising technology. It generates a wood gas with a high calorific value, of up to 12 $\frac{MJ}{m_{N,db}^3}$ and with a high hydrogen content, of about 40 $mol.\%_{db}$. Applying a water gas shift (WGS) unit could even increase the hydrogen yield.

In this thesis, the long term performance of a commercial Fe/Cr based WGS catalyst was investigated. For this purpose, a WGS pilot unit was operated for more than 2330 hours, processing a side stream of tar-rich wood gas, extracted upstream of the RME gas scrubber from the commercial DFB biomass steam gasification plant in Oberwart, Austria. Furthermore, steady partial load operations of the DFB gasification plant as well as of the WGS pilot unit were investigated.

Extensive chemical analyses were carried out. CO, CO_2, CH_4, N_2, O_2, C_2H_6, C_2H_4, C_2H_2, H_2S, COS, and C_4H_4S were measured. In addition, gas chromatography coupled with a mass spectrometer (GCMS) tar and ammonia analyses were performed. Furthermore, the catalyst's activity was observed by measuring the temperature profiles along the reactors of the WGS pilot unit.

A technically immaculate functionality and a steady long term operation of the WGS pilot unit could be achieved. Even partial load operation at the DFB plant did not affect the performance of the WGS pilot unit in a negative way. The WGS pilot unit was operated with a significant excess of steam. At this condition of operation, a carbon monoxide conversion up to 93 % and consequently less than 1.5 $mol.\%_{db}$ carbon monoxide was obtained at the WGS pilot unit's outlet. In addition, a significant reduction of detectable GCMS tar components was achieved along the WGS pilot unit. With the present experimental layout, no catalyst deactivation could be observed.

Kurzfassung

Wasserstoff gilt als wichtiger erneuerbarer sekundärer Energieträger der Zukunft.

Heutzutage wird Wasserstoff zum überwiegenden Teil aus fossilen Energieträgern hergestellt. Eine Wasserstoffproduktion aus Biomasse, mittels thermo-chemischem Verfahren kann eine vielversprechende Alternative für einen zukünftigen, kohlenstoff-freien Energieträger darstellen. Besonders die Zweibettwirbelschicht-Dampfvergasung von Holzhackgut ist hierfür eine vielversprechende Technologie. Sie erzeugt ein Holzgas mit einem hohen Heizwert von $12 \frac{MJ}{m_{N,db}^3}$ und einem hohen Wasserstoffanteil von etwa $40 \ mol.\%_{db}$. Der zusätzliche Einsatz einer Wassergas-Shift (WGS) Anlage erhöht die Wasserstoffausbeute.

Im Zuge dieser Arbeit wurde die Lebensdauer eines kommerziellen Fe/Cr basierten WGS Katalysators untersucht. Zu diesem Zweck wurde eine Wassergas-Shift Pilotanlage über einen Zeitraum vom mehr als 2330 Stunden mit einem teerreichen Holzgasteilstrom, welcher dem Zweibettwirbelschicht-Dampfvergasungs-Kraftwerk Oberwart, Österreich, vor dem Rapsmethylester (RME) Wäscher entnommen wurde, betrieben. Hierbei war es möglich stationäre Teillastbetriebszustände sowohl von der WGS Versuchsanlage, als auch vom Zweibettwirbelschicht-Dampfvergasungs-Kraftwerk zu untersuchen.

Während der Versuche wurden umfangreiche chemische Analysen durchgeführt. CO, CO_2, CH_4, N_2, O_2, C_2H_6, C_2H_4, C_2H_2, H_2S, COS und C_4H_4S wurden analysiert. Zusätzlich wurden mittels Gaschromatographen in Verbindung mit einem Massenspektrometer (GCMS) Teermessungen und Ammoniakanalysen durchgeführt. Um die Aktivität des Katalysators beurteilen zu können, wurde das Temperaturprofil über die Reaktoren der WGS Versuchsanlage aufgezeichnet.

Ein einwandfreier und stetiger Langzeitversuch der WGS Versuchsanlage konnte realisiert werden. Selbst der Teillastbetrieb des Zweibettwirbelschicht-Dampfvergasungs-Kraftwerks beeinflusste die Leistungsfähigkeit der WGS Versuchsanlage nicht nachteilig. Die WGS Versuchsanlage wurde mit einem deutlichen Dampfüberschuss betrieben. Mit diesen Versuchsbedingungen wurde ein Kohlenmonoxidumsatz von 93 % und damit verbunden, weniger als $1,5 \ mol.\%_{db}$ Kohlenmonoxid am Versuchsanlagenausgang erreicht. Zusätzlich konnte eine deutliche GCMS-Teer Reduktion erzielt werden. Mit dem aktuellen Versuchsanlagenaufbau konnte keine Katalysatordeaktivierung festgestellt werden.

Contents

Chapter 1

Introduction

The growing global energy demand is mostly covered by fossil primary energy sources. Since the beginning of the industrialization, usages and requirements for energy carriers changed according to the state of science and technology. Over time, consumption of fuels moved from solid coal, via liquid crude oil to a, nowadays, strong increase in natural gas. This leads to a shift from carbon to hydrogen with respect to the molar ratio of the fuels. This trend of decarbonization could be enhanced by strengthened substitution of the fossil fuels with hydrogen [5, 18].

Today, 95 % of the global hydrogen production is based on fossil fuels, which causes relevant carbon dioxide emissions. Hydrogen from renewable energy sources is discussed as an alternative to solve the dilemma of greenhouse gases, especially carbon dioxide, with a sustainable effect. This can be a step in the direction of a decarbonized energy system and hydrogen could play an important role in meeting the world's future demand for energy [1].

One energy carrier in the future could be pure hydrogen or hythane, a mixture of hydrogen and methane. Both can be produced by gasification of wood chips using DFB steam gasification technology [12, 32]. Hythane could allow hydrogen for an initial entry into the fuel market, by taking advantage of the already existing natural gas infrastructure. The addition of renewable produced hydrogen to natural gas reduces the carbon dioxide emissions. This allows the hydrogen infrastructure to slowly become established until the production and efficiency demands can be met for a hydrogen based economy [19, 30].

Chapter 2

Motivation and Aim of the Work

This thesis is based on previous work, which introduced the hydrogen production based on biomass using the DFB steam gasification technology. The DFB biomass steam gasification technology was developed at the Vienna University of Technology and already reached commercialization [12, 19]. This hydrogen production is seen as an integral part of a polygeneration system, a combined system producing multiple products like heat, electricity, gases, and fuels. A polygeneration system convinces, because it turns this multiple product output into an advantage.

Previous work successfully established fundamental workability as well as basic information about process conditions and some process optimization of a process chain generating hydrogen from wood gas, derived from the industrial scale DFB biomass steam gasification plant in Oberwart, Austria ([3, 8, 9] etc.).

The WGS reaction is an interesting technology for the adjustment of the H_2/CO ratio in wood gas for further chemical syntheses or the increase of the hydrogen yield to a maximum by converting almost all carbon monoxide with steam to hydrogen and carbon dioxide.

The aim of this work was to investigate the long term performance of a commercial Fe/Cr based WGS catalyst. Therefore, a WGS pilot unit was operated with real tar-rich wood gas on site of the DFB biomass steam gasification plant. In previous test runs the WGS pilot unit mainly processed wood gas, extracted downstream of the DFB biomass steam gasification plant's RME gas scrubber. In contrast to those previous WGS pilot unit test runs, for this present long term test run the WGS pilot unit processed tar-rich wood gas, extracted upstream of the RME gas scrubber. On one hand this leads to less energy demand on steam addition and heating at the WGS pilot unit's inlet, as processing wood gas downstream the RME gas scrubber. On the other hand this will result in a higher stress for the catalyst, because the catalyst of the WGS pilot unit would have to face a considerably higher load of impurities, especially high amounts of tar and ammonia. In a future use, this will result in a higher efficiency, caused of the higher water content in the tar-rich wood gas and higher temperature, if processing the tar-rich wood gas extracted upstream of the gas scrubber.

Chapter 3

State of the Art

This chapter provides an overview of the state of the art principles of industrial hydrogen production, biomass gasification, and previous work on hydrogen production from biomass. In the first section industrial hydrogen production is discussed, followed by biomass gasification with focus on the DFB steam gasification technology. The next section deals with the WGS reaction and is finally followed by a section which gives an overview of previous research activities related to hydrogen from biomass via thermochemical route, based on biomass gasification by a DFB steam gasification system.

3.1 Hydrogen Production

Nowadays, hydrogen is an important feedstock in chemical industry and refineries. Hydrogen is seen as an important renewable secondary energy carrier of the future and could be used directly as fuel and feedstock for further syntheses as well as for the generation and storage of electricity [2, 18, 29].

There is an approximate worldwide hydrogen production of 10^{11} to 10^{12} m_N^3 per year. This hydrogen is mainly used by four consumers: ammonia production 50 %, refinery applications 22 %, methanol production 14 %, various reduction processes 7 %. The rest of 7 % is spread to other consumers. The demand as feedstock in refineries will continue to grow, as well as the usage as an energy carrier [4, 29]. This leads to the question of hydrogen production, which is currently based on nonrenewable sources. 95 % of today's global hydrogen production is based on fossil fuels, mainly on steam reforming of natural gas. Another 4 % is generated by water electrolysis using electricity. As long as supplied electricity is related on carbon dioxide emissions, this does not solve the dilemma of greenhouse gases with a sustainable effect. Only 1 % of the total amount of hydrogen is produced by converting biomass [1].

Figure 3.1 shows the established processes for generating synthesis gas and hydrogen, based on fossil hydrocarbon containing feedstock and its use. It illustrates the processing steps for gaseous, liquid, and sold feedstocks.

All these methods cause certain carbon dioxide emissions. Therefore, and for taking decarbonization forward, hydrogen produced from renewable energy sources is needed.

Hydrogen can be produced from a variety of feedstocks. Production from hydrocarbons such as fossil fuels and biomass involves conversion technologies such as reforming, gasification, and pyrolysis. These processes provide a synthesis gas, mainly consisting of hydrogen and carbon monoxide. This synthesis gas can be subjected to downstream processes in order to produce pure hydrogen.
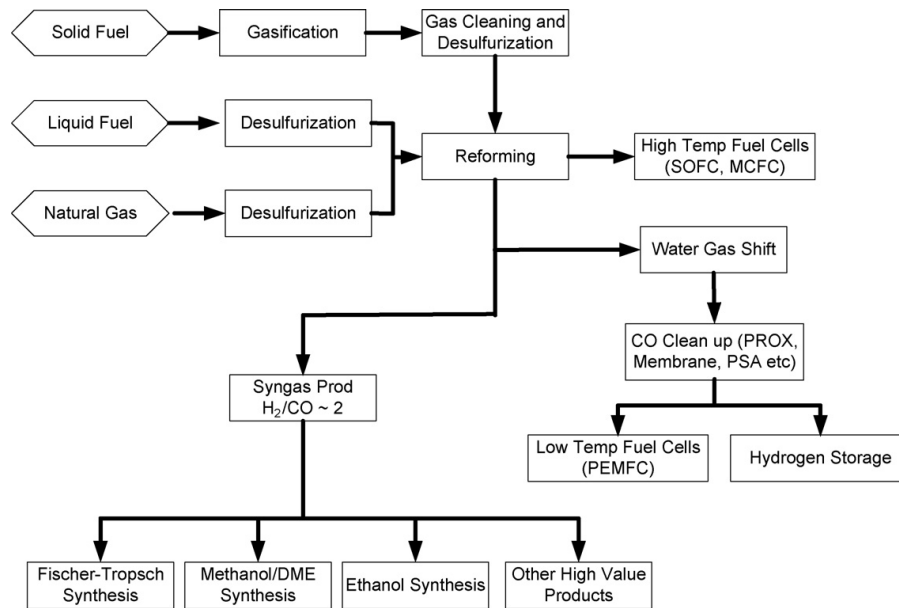

Figure 3.1: Options for synthesis gas generation or hydrogen production from hydrocarbon containing feedstock and its usage. Dimethyl ether (DME), molten carbonate fuel cell (MCFC), proton exchange membrane fuel cell (PEMFC), preferential oxidation (PROX), pressure swing adsorption (PSA), solid oxide fuel cell (SOFC), [16].

The following subsections give an overview of the main industrial production technologies for hydrogen: steam reforming of natural gas, partial oxidation, coal gasification, and electrolysis.

3.1.1 Steam Methane Reforming

Steam reforming or also called steam methane reforming (SMR) is the reaction of methane with steam in the presence of a catalyst to carbon monoxide and hydrogen (see Equation 3.1).

$$\text{Steam reforming} \qquad CH_4 + H_2O \rightleftharpoons CO + 3H_2 \qquad \Delta H_R^0 = +206 \ \frac{kJ}{mol} \quad (3.1)$$
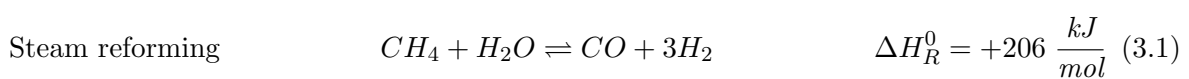
This reaction is strongly endothermic. In order to produce hydrogen, the synthesis gas exiting the reformer is usually subjected to a WGS unit. Figure 3.2 illustrates the hydrogen production based on natural gas using SMR with its main process steps.
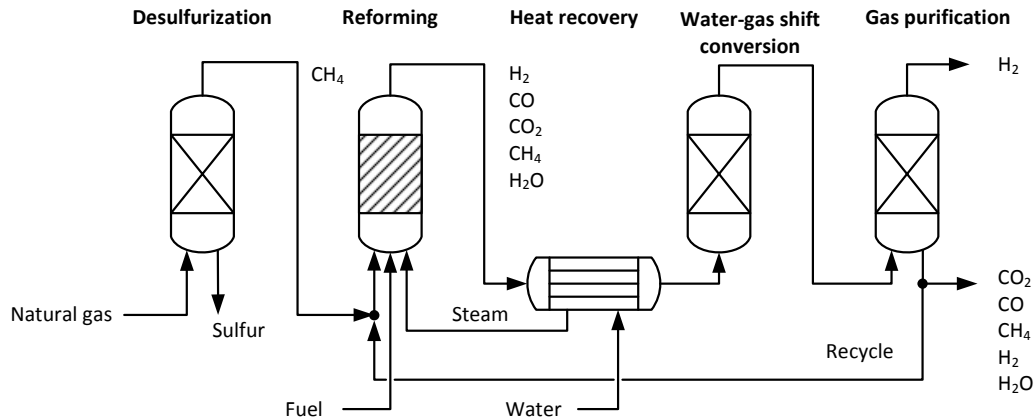

Figure 3.2: Hydrogen production using the steam methane reforming (SMR) process with its process steps [3].

After desulfurization, steam reforming is carried out. Typical reaction conditions for steam reforming are at a temperature range between 500 to 900 °C. Because of the endothermic reaction, externally heating is needed. In conventional endothermic steam reforming technologies, heat is supplied by burning fuel outside reactor tubes and the steam reforming catalyst is packed inside. The pressure is usually at 20 *bar* and the steam to carbon ratio ranges from 2.5 to 3.0. Nickel-based catalysts have been favored, because of their sufficient activity and low cost. Consequently, the steps involved in the SMR process for the production of hydrogen can be divided into feed preparation, steam reforming, WGS conversion, and hydrogen purification [29].

3.1.2 Partial Oxidation

Noncatalytic partial oxidation (POX), autothermal reforming (ATR), and catalytic partial oxidation (CPO) of hydrocarbon containing feedstock share the same chemical mechanism, which is shown in Equation 3.2 for the example of methane.

$$\text{Partial oxidation} \qquad CH_4 + \frac{1}{2}O_2 \rightleftharpoons CO + 2H_2 \qquad \Delta H_R^0 = -36 \ \frac{kJ}{mol} \quad (3.2)$$
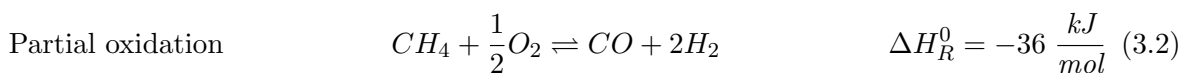
POX is the uncatalyzed reaction of natural gas or liquid hydrocarbons with oxygen at high temperature and high pressure to produce syngas. ATR is the reaction of natural gas or liquid hydrocarbons with steam and oxygen at high temperature and high pressure to produce

syngas. The reaction is exothermic and catalysts are used to improve hydrogen yield. CPO is the heterogeneous reaction of natural gas or liquid hydrocarbons with oxygen and steam at high space velocity over a solid catalyst to produce syngas [29].

Figure 3.3 illustrates those different partial oxidation processes, including further downstream process steps aiming for hydrogen production.
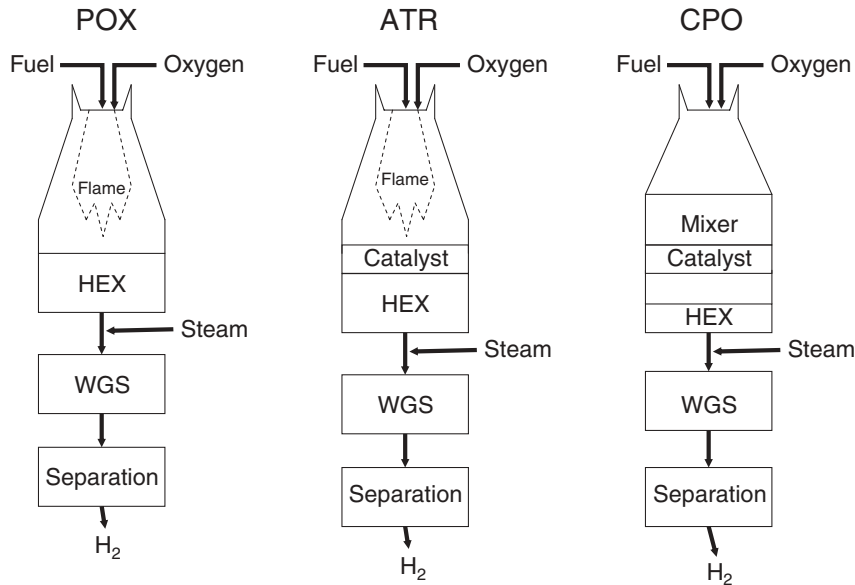

Figure 3.3: Schematic representation of noncatalytic partial oxidation (POX), autothermal reforming (ATR), and catalytic partial oxidation (CPO) reformers. Heat exchanger (HEX) [29].

In contrast to steam reforming, the partial oxidation reaction is slightly exothermic. The technological differentiation of reforming comes from the method by which the heat is generated and provided. For CPO or ATR, a portion of the fuel is oxidized within the reactor to generate the heat required to drive the endothermic steam reforming reaction occurring over the same catalyst bed. The main advantage of the partial oxidation process is that it will produce a synthesis gas with a favorable hydrogen to carbon monoxide ratio for downstream usage in chemical syntheses. In order to produce pure hydrogen the process will also include a WGS unit and a hydrogen purification step [29].

3.1.3 Coal Gasification

Coal gasification is a well established technology to convert coal with steam and oxygen to a synthesis gas which generally consists of CO, H_2, CO_2, CH_4, higher hydrocarbons, and impurities such as H_2S and NH_3. Coal gasifiers combust some of the coal with O_2 to provide the heat for the gasification reactions, this is refereed to as autothermal gasification. Steam or carbon dioxide is added to enhance gasification reactions [29]. Coal gasification with pure

oxygen as gasification agent can be seen as partial oxidation of a solid fuel. A schematic flow diagram of coal gasificiation and its main applications is shown in Figure 3.4.
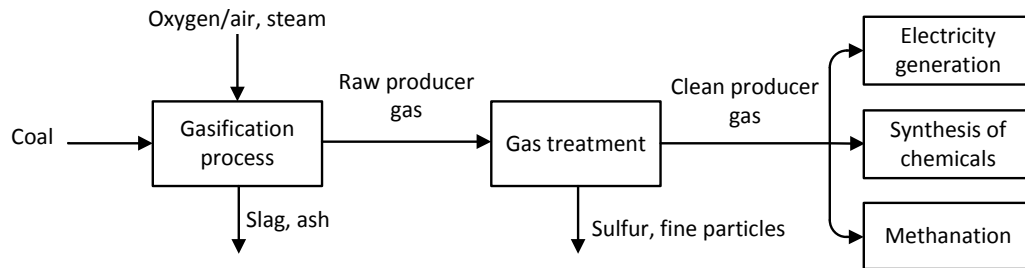

Figure 3.4: Basic process steps of coal gasification and its main applications [3].

3.1.4 Electrolysis

Hydrogen can be obtained from electrolysis of water by using electrical power. If electricity is from renewable sources, electrolysis could be a promising technology for future hydrogen production. However, electrolysis is currently used in a much smaller scale compared to steam reforming [29]. One benefit of electrolysis is the possible integration into a power-to-gas system used as energy storage. With power-to-gas, excess electricity is converted into hydrogen and oxygen by water electrolysis. The hydrogen can be stored and reconverted into electricity using fuel cells, or used as feedstock for further syntheses as well as secondary energy carrier. Also the oxygen should be brought to a commercial exploitation. Electrolyzer technologies can be divided into alkaline, proton exchange membrane (PEM) and solid oxide electrolysis cells, according to the electrolyte which is applied [10].

Figure 3.5 shows the main process steps of hydrogen production using electrolysis or even power-to-gas applications.
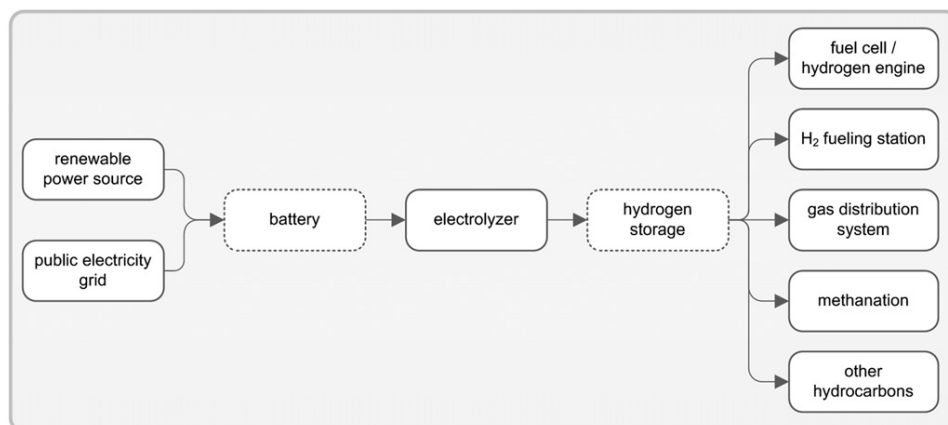

Figure 3.5: Process chain of the hydrogen production based on electrolysis [10].

3.2 Biomass Gasification

Biomass gasification is a thermochemical conversion of biomass. Biomass is converted to a gas which is referred to as wood gas. Other literature refers to as synthesis gas or syn gas, producer gas and product gas.
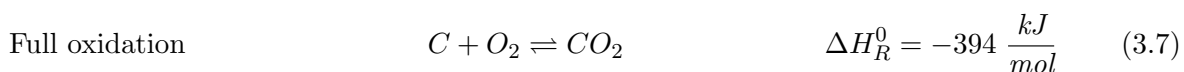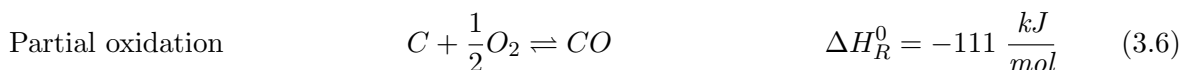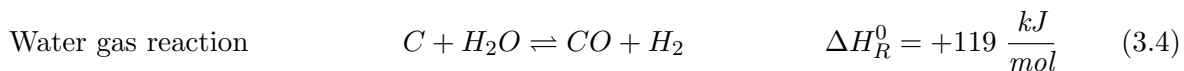
There are various gasification technologies available for solid biomass. The main differences are the way of heat supply, which is necessary because of the overall endothermic gasification reactions. This heat can be either added externally, in a so called allothermal gasification process, or generated internally by the full combustion of some biomass, referred to as autothermal gasification process. Another defining feature at different gasification processes is the reactor design, which distinguishes between fixed bed, fluidized bed, and entrained flow reactors and the used gasification agent.

One way of gasification is the autothermal gasification process with air as gasification agent. In this case a fraction of the biomass feed is fully combusted inside the gasification reactor. The resulting wood gas is highly diluted by nitrogen. In this case, the wood gas has only a low calorific value around 4 to 6 $\frac{MJ}{m^3_{N,db}}$, because of a high nitrogen content of 45 to 55 %. Wood gas with a calorific value of about 12 $\frac{MJ}{m^3_{N,db}}$ and nearly free of nitrogen can be produced with pure oxygen as gasification agent, but the costs for the pure oxygen production are high [15].
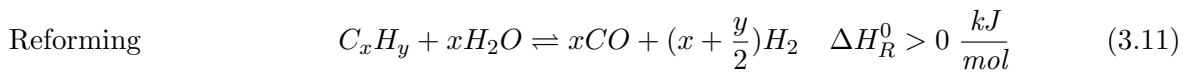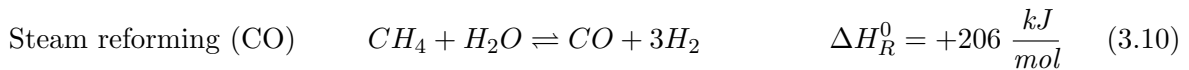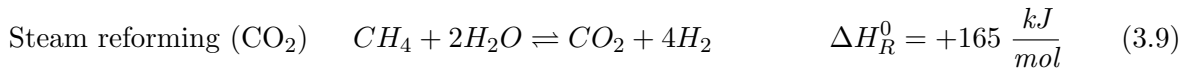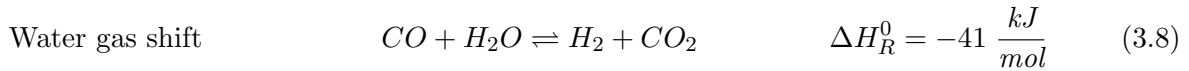
All these disadvantages can be avoided by using the innovative DFB system. The present work is based on steam gasification of solid wood chips by using the DFB steam gasification technology, which will be described in more detail in the next subsection.

The important heterogeneous gasification reactions are listed in Equations 3.3 to 3.7 and the important homogeneous gas phase reactions are listed in Equations 3.8 to 3.11 [19, 33].

Heterogeneous gasification reactions

$$\text{Boudouard reaction} \qquad C + CO_2 \rightleftharpoons 2CO \qquad \Delta H_R^0 = +160\ \frac{kJ}{mol} \qquad (3.3)$$

$$\text{Water gas reaction} \qquad C + H_2O \rightleftharpoons CO + H_2 \qquad \Delta H_R^0 = +119\ \frac{kJ}{mol} \qquad (3.4)$$

$$\text{Hydrogasification} \qquad C + 2H_2 \rightleftharpoons CH_4 \qquad \Delta H_R^0 = -88\ \frac{kJ}{mol} \qquad (3.5)$$

$$\text{Partial oxidation} \qquad C + \frac{1}{2}O_2 \rightleftharpoons CO \qquad \Delta H_R^0 = -111\ \frac{kJ}{mol} \qquad (3.6)$$

$$\text{Full oxidation} \qquad C + O_2 \rightleftharpoons CO_2 \qquad \Delta H_R^0 = -394\ \frac{kJ}{mol} \qquad (3.7)$$

Homogeneous gas phase reactions

Water gas shift $\quad\quad\quad\quad CO + H_2O \rightleftharpoons H_2 + CO_2 \quad\quad\quad\quad \Delta H_R^0 = -41\ \dfrac{kJ}{mol} \quad\quad$ (3.8)

Steam reforming (CO$_2$) $\quad CH_4 + 2H_2O \rightleftharpoons CO_2 + 4H_2 \quad\quad \Delta H_R^0 = +165\ \dfrac{kJ}{mol} \quad$ (3.9)

Steam reforming (CO) $\quad\quad CH_4 + H_2O \rightleftharpoons CO + 3H_2 \quad\quad\quad \Delta H_R^0 = +206\ \dfrac{kJ}{mol} \quad$ (3.10)

Reforming $\quad\quad\quad\quad C_xH_y + xH_2O \rightleftharpoons xCO + (x + \dfrac{y}{2})H_2 \quad \Delta H_R^0 > 0\ \dfrac{kJ}{mol} \quad$ (3.11)

During the gasification process the heterogeneous as well as homogeneous reactions occur. Figure 3.6 illustrates the influence of heat and a gasification agent to a wet wood particle. Depending on the temperature and time, three stages of thermochemical conversion are taking place.

First, up to 220 °C drying the wood particles, second 220 to 700 °C devolatilization, also called pyrolysis, and third, gasification occur, which takes place in the presence of a gasification agent and above 600 °C [19].

Tar is formed as undesired byproduct during the gasification process, and is predominantly formed during the devolatilization stage of the thermochemical conversion.

Tar is the collective term for a complex mixture of organic hydrocarbons, mainly aromatic components. There are many different definitions of tar in literature. Historically, tar was an operationally defined parameter, largely based on organics from gasification that condensed under operating conditions of boilers, transfer lines, and internal combustion engine inlet devices. In general, all components with a molecular weight above benzene ($78\frac{g}{mol}$) can be called tar [19, 31]. Tar is formed during the gasification process based on a series of complex thermochemical reactions. The reaction conditions are the main influence on tar formation. Tar consists of over 100 different substances. These substances can polymerize and condense in heat exchangers or on particle filters as well as in pipes which can lead to blockage and coking [34].
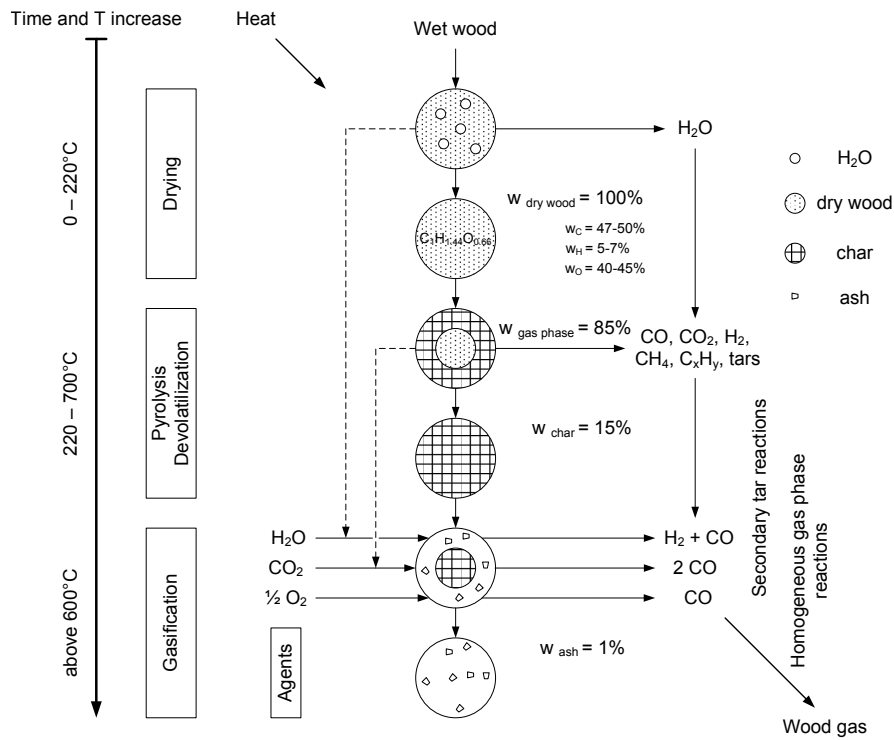
Figure 3.6: Conversion of a wet wood particle under the influence of the three stages of thermochemical conversion. [7] based on [19].

Evans et al. classified tar in [6] into three fractions: primary, secondary, and tertiary tar. Primary tar emerges from the devolatilization stage. Secondary tar occurs because of increasing temperature and the presence of a gasification agent during the gasification stage, a part of the primary tar reacts to small gaseous molecules or transforms into secondary tar by splitting off of small gaseous molecules. Above 800 °C tertiary tar can be found. Tertiary tar is also called recombination or high-temperature tar [34]. Figure 3.7 illustrates the formation of tertiary tar, depending on the gasifier temperature.
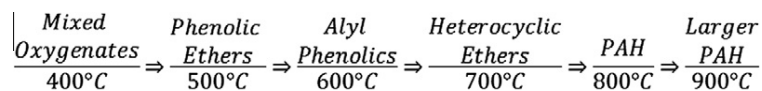

Figure 3.7: Tar transition as a function of process temperature from primary products to poly aromatic hydrocarbons (PAH) [31].

3.2.1 Dual Fluidized Bed Gasification Process

The basic idea of the dual fluidized bed (DFB) gasification concept, developed primarily at the Vienna University of Technology, is to divide the gasification process into two separated zones. One gasification zone, where the gasification with steam in the absence of oxygen

takes place and one combustion zone which provides the heat for the mostly endothermic gasification reactions. The gasification zone is operated as a bubbling fluidized bed and is fluidized with steam, which acts as well as gasification agent. The combustion zone is operated with air as a fast fluidized bed. A circulation loop of bed material between these two zones ensures that heat, which is needed for the gasification process, is transported from the combustion zone to the gasification zone and some remaining char coal is transported into the combustion zone. Fluidized loop seals ensure that wood gas from the gasification zone and flue gas from the combustion zone remain separated. This leads to a nearly nitrogen free wood gas with a calorific value of more than 12 $\frac{MJ}{m^3_{N,db}}$ [13, 19]. The principle of the DFB steam gasification process is shown in Figure 3.8.
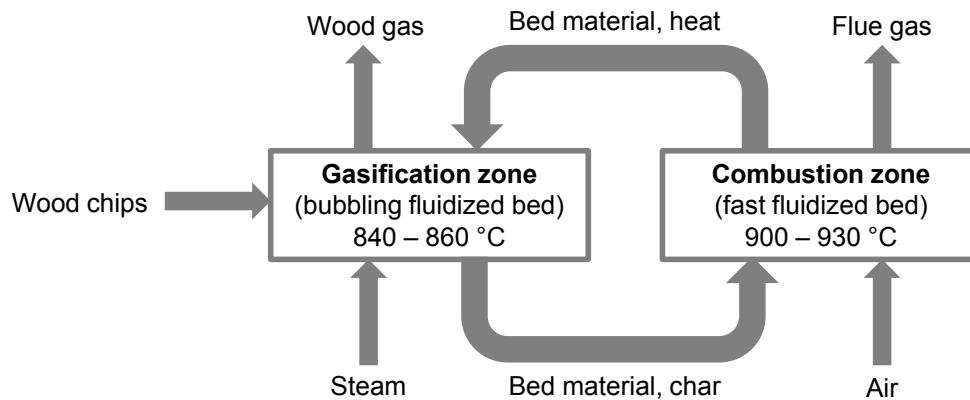

Figure 3.8: The functional principle of the DFB steam gasification process [7] based on [15].

Table 3.1 shows the typical wood gas composition range. The high H_2 content makes the wood gas a promising hydrogen source [3, 32]. Downstream gas conditioning, like the WGS reaction, can even increase the hydrogen yield.

Table 3.1: Typical wood gas composition ranges in the DFB steam gasification process [19].

Component	Value	Unit
H_2	35 - 40	$vol.\%_{db}$
CO	22 - 25	$vol.\%_{db}$
CO_2	20 - 25	$vol.\%_{db}$
CH_4	9 - 11	$vol.\%_{db}$
N_2	< 1	$vol.\%_{db}$
Calorific value	12 - 14	$\frac{MJ}{m^3_{N,db}}$

The DFB process successfully emerged from a first demonstration plant in Güssing, Austria and has reached commercialization [12, 19]. The combined heat and power (CHP) plant in Oberwart, Austria, was the first commercial facility using the DFB biomass steam gasification technology. The experimental test runs which are described in this thesis were conducted at the plant site of the DFB plant Oberwart. The plant Oberwart is described in detail in

Section 4.1. Today there are several commercial DFB biomass steam gasification plants in operation. Most DFB plants operate as CHP plants, a selection listed in Table 3.2 does not take the thermal output into account.

Table 3.2: A selection of demonstration and commercial DFB steam gasification plants, without thermal output. Organic Rankine cycle (ORC), Austrian Energy & Environment GmbH (AE&E), and Biomass synthetic natural gas (BioSNG), based on [17].

Location	Gas utilization	Fuel / Product in MW	Start up	Status	Supplier
Güssing, AT	Gas engine	$8_{fuel}/2.0_{el}$	2002	Operational	AE&E/Repotec
Oberwart, AT	Gas engine/ORC	$8.5_{fuel}/2.8_{el}$	2008	Operational	Ortner Anlagenbau
Villach, AT	Gas engine	$15_{fuel}/3.7_{el}$	2010	On hold	Ortner Anlagenbau
Senden/Ulm, DE	Gas engine/ORC	$14_{fuel}/5_{el}$	2011	Operational	Repotec
Burgeis, IT	Gas engine	$2_{fuel}/0.5_{el}$	2012	Operational	Repotec
Göteborg, SE	BioSNG	$32_{fuel}/20_{BioSNG}$	2013	Operational	Repotec/Valmet

3.3 Water Gas Shift Reaction

The water gas shift (WGS) reaction is a well established technology in industrial large scale plants producing hydrogen or setting the CO/H_2 ratio of synthesis gas. The WGS reaction, shown in Equation 3.8, is a reversible and moderately exothermic reaction between carbon monoxide and water (steam) to produce hydrogen and carbon dioxide. Its equilibrium constant decreases with temperature, therefore, high conversions are favored by low temperatures, as shown in Figure 3.9.
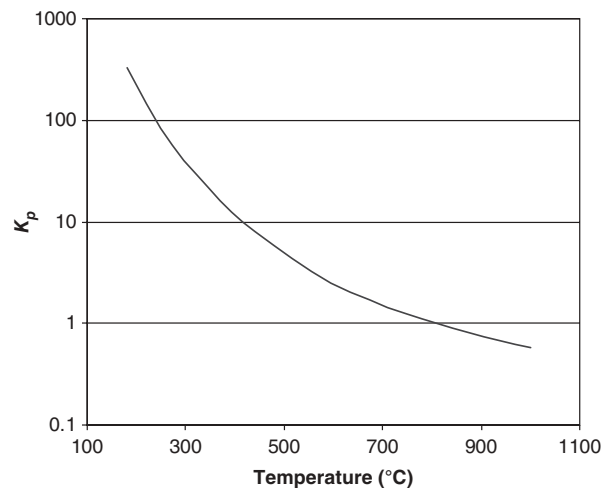

Figure 3.9: Variation of equilibrium constant (K_p) for the water gas shift reaction with temperature [29].

However, at low temperatures, reaction rates diminish and the reaction becomes kinetically controlled [29]. At adiabatic conditions conversion in a single bed of catalyst is thermodynamically limited, due to the increase of operating temperature, caused by the exothermic reaction. Because of the equimolar reaction, the equilibrium composition is virtually unaffected by pressure.

Industrial hydrogen production plants based on steam reforming, coal gasification, or partial oxidation, typically enhance the hydrogen yield by downstream WGS units. In most industrial implementations, the WGS reaction is carried out by a catalysis in two steps with a desulfurized feed.

First a high temperature shift (HTS) with a Fe/Cr based catalyst, which reduces the CO concentration down to 2 to 3 $vol.\%_{db}$ is applied. This HTS step is usually operated with a significant excess of steam and adiabatically with an inlet temperature of 350 to 550 °C, pressures above 20 bar, depending on the adjacent plant requirements, and a gas hourly space velocity ($GHSV$) of 400 to 1200 h^{-1}.

The second stage is a low temperature shift (LTS) stage with a Cu/Zn or Co/Mo based catalyst, which takes advantage of the favorable equilibrium below 250 °C in order to reduce the carbon monoxide concentration down to 0.2 to 0.4 $vol.\%_{db}$. The lower temperature limit for this LTS step is about 200 °C and is dictated by the water dew point under operating conditions which are typical pressures between 10 to 30 bar and a $GHSV$ of about 3600 h^{-1} [29, 33].

3.4   Hydrogen Production from Biomass

In this section, an overview of previous studies aiming at the hydrogen production from biomass using the DFB technology is given.

Hydrogen from biomass via the thermochemical routes is a promising technology for future hydrogen production, which is carbon dioxide neutral and independent of fossil fuels. Especially, the DFB steam gasification, with the high hydrogen content in the wood gas, seems to be ideally suited.

Müller et al. investigated in [32] the basic idea of a process design to produce hydrogen with biomass as feedstock. Therefore, a process chain was simulated using the software IPSEpro^{TM}. In the investigated case, the process chain was based on a DFB biomass steam gasification, a steam reformer, a WGS unit, and a gas permeation membrane.

Diaz demonstrated in [3] the technical viability of a simple process chain to separate hydrogen from wood gas generated by the DFB biomass steam gasification plant Oberwart, Austria. The design is based on a three-step process, illustrated in Figure 3.10.

First a gas cleaning step, performed in a low temperature RME gas scrubber is installed. This step is followed by a hydrogen enrichment step, using a membrane separation unit, and finally a hydrogen purification is performed in a pressure swing adsorption (PSA) unit. In

addition a PEM fuel cell was powered by the generated hydrogen in order to prove its quality.
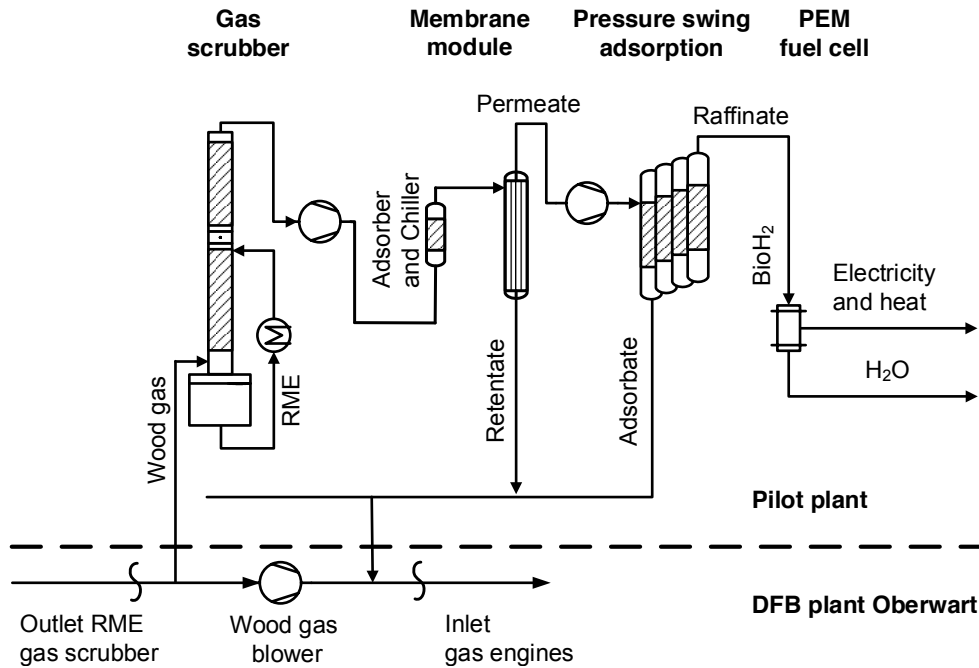

Figure 3.10: Process chain for the separation of pure hydrogen from wood gas, based on [3].

In order to increase the hydrogen yield, Fail et al. employed a process chain including a WGS unit, see [9]. This process chain is based on Diaz's work in [3] and adds a WGS unit upstream the gas scrubber. Figure 3.11 illustrates this process chain. High hydrogen yields were achieved resulting in an overall hydrogen recovery (H_2rec) of almost 70 %, which corresponds to 42 g of hydrogen per kg of dry biomass. The H_2rec is calculated towards the molar flow rate of hydrogen at the inlet and at the outlet, see Equation 4.6. The purity of the generated hydrogen was above 99.85 $\%vol._{db}$.

By removing the membrane module from the process chain Fail et al. demonstrated in [8] the feasibility of producing hydrogen with a purity of 99.97 $vol.\%_{db}$ and an overall H_2rec of 128 %. Figure 3.12 illustrates the improved process chain.

So far, all process chains were operated with wood gas extracted downstream of the DFB plant's RME gas scrubber. In order to reduce the heat demand for the steam production for the WGS reaction, the wood gas for the hydrogen production should be extracted upstream of the RME gas scrubber of the DFB plant, because of a significant higher water content and temperature upstream the RME gas scrubber. Consequently, the catalyst of the WGS unit would have to face a considerably higher load of impurities, mostly tar and ammonia.

This objective and its main question concerning the catalyst's performance when processing tar-rich wood gas lead to this present thesis.
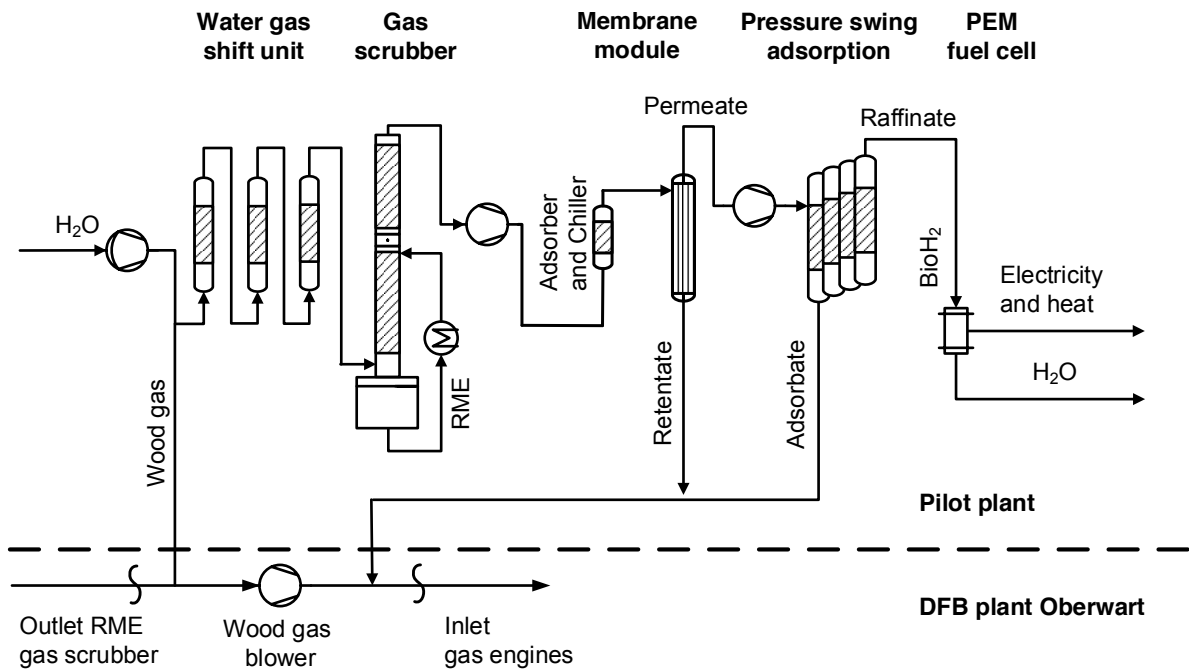
Figure 3.11: Process chain for the production of pure hydrogen from wood gas based on DFB steam gasification, based on [9].
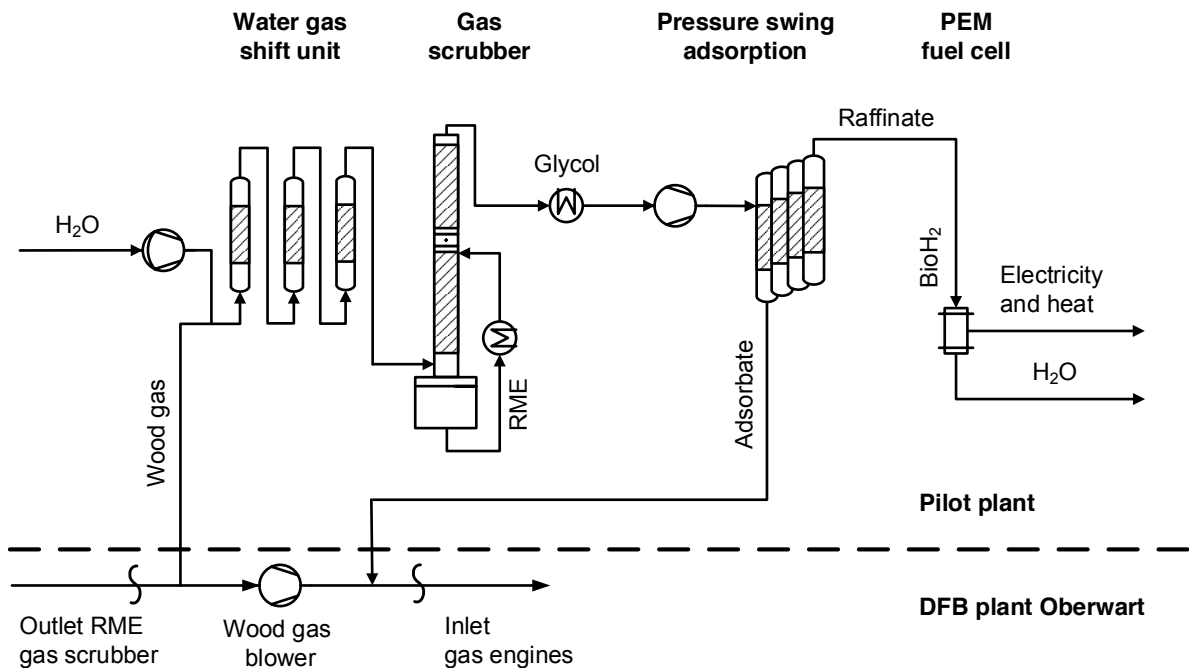

Figure 3.12: Improved process chain for the production of pure hydrogen from wood gas based on DFB steam gasification, based on [8].

Chapter 4

Experimental Setup and Methodology

This present experimental work was carried out with a WGS pilot unit, located at the plant site of the DFB biomass steam gasification plant in Oberwart, Austria. This CHP plant in Oberwart is an industrial scale DFB biomass steam gasification CHP plant, generating electricity and district heat. Figure 4.1 shows a picture of the DFB biomass steam gasification plant. The WGS pilot unit is part of a research facility, constructed in a 20 ft container which is directly connected to the CHP plant.

Figure 4.1: Picture of the DFB biomass steam gasification plant Oberwart, Austria in 2014 [7].

Apart from the WGS pilot unit, other pilot units like a low temperature RME gas scrubber, a membrane module, a PSA, and a PEM fuel cell are also parts of this research facility. This arrangement enabled the processing of real wood gas, produced by the commercial DFB gasification plant, in many different ways ([3, 8, 9] etc.).

The following sections give an overview about the DFB biomass steam gasification plant in Oberwart, the WGS pilot unit and the used sampling and analysis procedure, which were used during the experimental work for the investigation on the long term performance of the Fe/Cr based water gas shift catalyst processing tar-rich wood gas.

4.1 The Dual Fluidized Bed Biomass Steam Gasification Plant Oberwart, Austria

The biomass steam gasification plant in Oberwart, Austria, is based on the well documented plant in Güssing, Austria ([12, 13, 19] etc.). Both plants are characterized by the DFB steam gasification technology, explained in more detail in Subsection 3.2.1. In addition to the established system in Güssing, the DFB gasification plant in Oberwart has some modifications. A biomass dryer upstream of the gasifier, an organic Rankine cycle (ORC) process in order to increase the electrical output by using process heat and two gas engines instead of one. The main steps of the process remained the same. The wood gas is generated, cooled, filtered, cleaned, and finally used in power gas engines in order to generate electricity and district heat. Figure 4.2 shows a simplified flowchart of the applied process at the gasification plant in Oberwart.
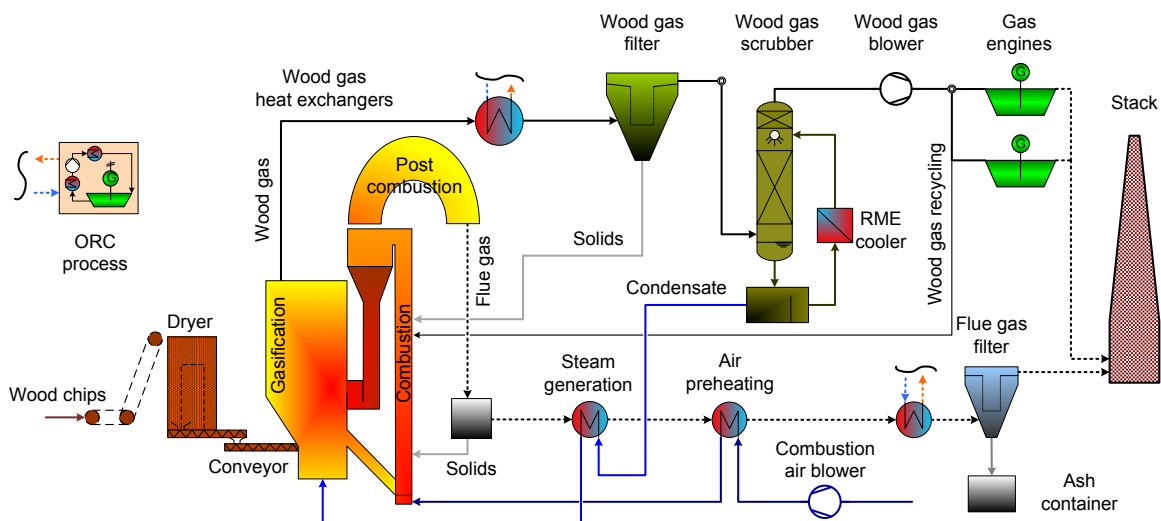

Figure 4.2: Simplified flowchart of the DFB biomass steam gasification plant Oberwart, Austria. [7] based on [3].

The gasification plant was commissioned successfully at the end of 2007. One year later, in 2008, regular operation started and has been improved continuously from that time on. This, by Energie Burgenland Biomasse GmbH Co & KG owned and operated, plant was the first commercial facility using the DFB gasification system [17, 20]. Table 4.1 shows the CHP plant's key figures.

The wood chips are transported from an intermediate storage into the biomass dryer and afterwards fed into the gasification zone of the DFB gasifier. A system of screw conveyors ensure that air does not enter the gasifier. Using olivine as bed material, which is a natural magnesium iron silicate, $(Mg,Fe)SiO_2$, is state of the art for DFB biomass steam gasifiers. Olivine, with its formed layer at the particle surface during usage, shows good results concerning tar reduction in the wood gas and enhances gasification properties significantly [21]. The circulating bed material ensures that heat, which is needed for the gasification process, is transported from the combustion zone to the gasification zone, which is fluidized with steam. This leads to a nearly nitrogen free wood gas. The generated wood gas is cooled in heat exchangers. Subsequently, a baghouse filter removes dust particles. Downstream a gas scrubber, operated with RME, cools the wood gas further down to a temperature of about 40 °C. Water, tar, and other impurities are condensed and discharged from the wood gas. A gas blower feeds the cleaned, cooled, and dried wood gas into the two gas engines to produce electricity. Process heat is transferred via a thermal oil circuit, in order to provide the heat for steam generating, district heat output, the ORC process and the biomass dryer.

Table 4.1: Operational key figures of the DFB biomass steam gasification plant Oberwart, Austria [20].

Fuel input		8.5	MW_{th}
Gas engines electrical output		2.4	MW_{el}
ORC process electrical output		0.35	MW_{el}
District heat output		3.5	MW_{th}
Wood chips fuel requirement		$\sim 23\,000$	$\frac{tons(air-dried)}{a}$
District heating transmission route		$\sim 5\,300$	m
District heating system temperatures	feed	~ 95	°C
	return	~ 65	°C

Figure 4.3 illustrates a simplified flowchart of the DFB plant in Oberwart, Austria, with the two wood gas extraction points for the WGS pilot unit investigations, one upstream of the RME scrubber and one downstream of the RME scrubber.
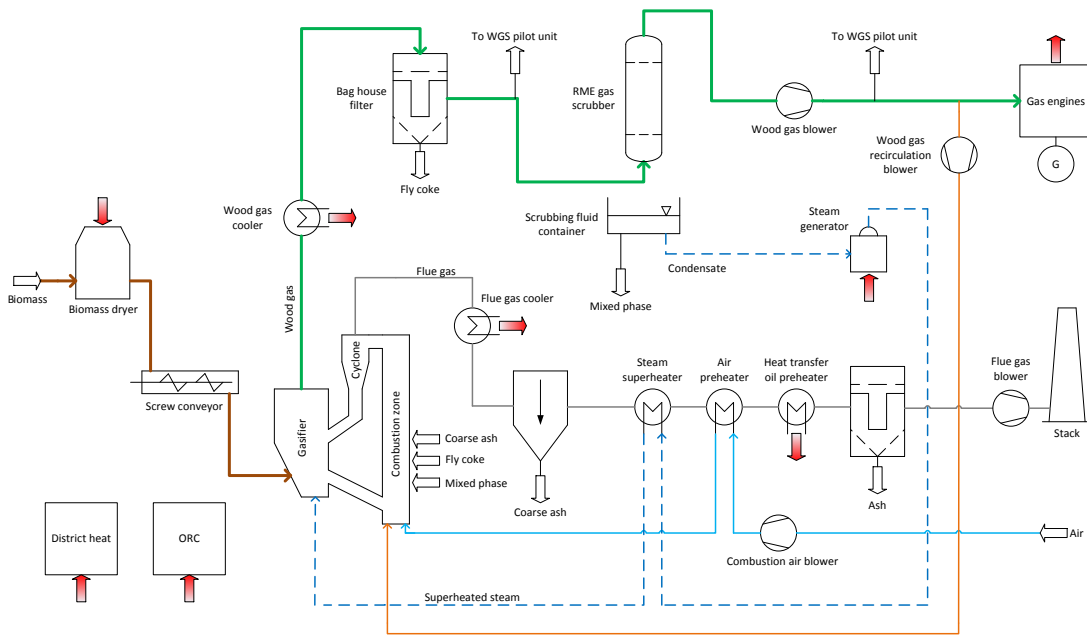
Figure 4.3: Simplified flowchart of the DFB biomass steam gasification plant in Oberwart, Austria. The two different extraction points, one upstream of the RME scrubber and one downstream of the RME scrubber are indicated by arrows [23].

Table 4.2 shows the wood gas conditions at those two extraction points, especially concerning temperature, water content and GCMS tar content.

Table 4.2: Wood gas conditions at the two extraction points (see Figure 4.3) along the DFB biomass steam gasification plant in Oberwart, Austria, at full load operation, based on [8].

	Upstream of the RME scrubber	Downstream of the RME scrubber	
Temperature	~ 150	~ 40	$^{\circ}$C
H_2O content	~ 35	~ 7	$mol.\%_{wb}$
GCMS tar content	~ 8200	~ 1100	$\frac{mg}{m^3_{N,db}}$

In the RME gas scrubber, the wood gas is cooled down to approximately 40 °C. The result is that water, tar, and most impurities are condensed and discharged from the wood gas.

Taking only the water content and the temperature into consideration it would be beneficial to extract the wood gas upstream of the RME gas scrubber for processing it in a WGS unit. In contrast, if the wood gas is extracted downstream of the RME scrubber, it has been suggested that, especially, the higher tar content as well as the other impurities negatively effect the WGS catalyst, which is investigated in this thesis.

4.2   The Water Gas Shift Pilot Unit

The WGS pilot unit was designed, built, and optimized by Silvester Fail during his dissertation, see [7]. Figure 4.4 shows the flowchart of the WGS pilot unit which consists of three fixed bed reactors in series, each equipped with 2.6 *L* of a commercial Fe/Cr based WGS catalyst. The catalyst was used in its original particle size.

The WGS pilot unit is connected to two different extraction points at the DFB gasification plant Oberwart, shown in Figure 4.3. These enable to process wood gas extracted upstream as well as downstream of the DFB gasification plant's RME gas scrubber. Figure 4.4 illustrates the possibility of choosing between the two different inlets and shows all the equipment geared to the WGS pilot unit. A membrane gas pump is installed upstream of the reactors in order to set the wood gas flow in terms of enabling steady operating conditions. Furthermore, a peristaltic pump in combination with an evaporator ensure the needed steam addition to achieve the aimed steam parameters at the inlet of the WGS pilot unit. Upstream each reactor, a heating section is located in order to enable constant temperature at each reactor inlet.
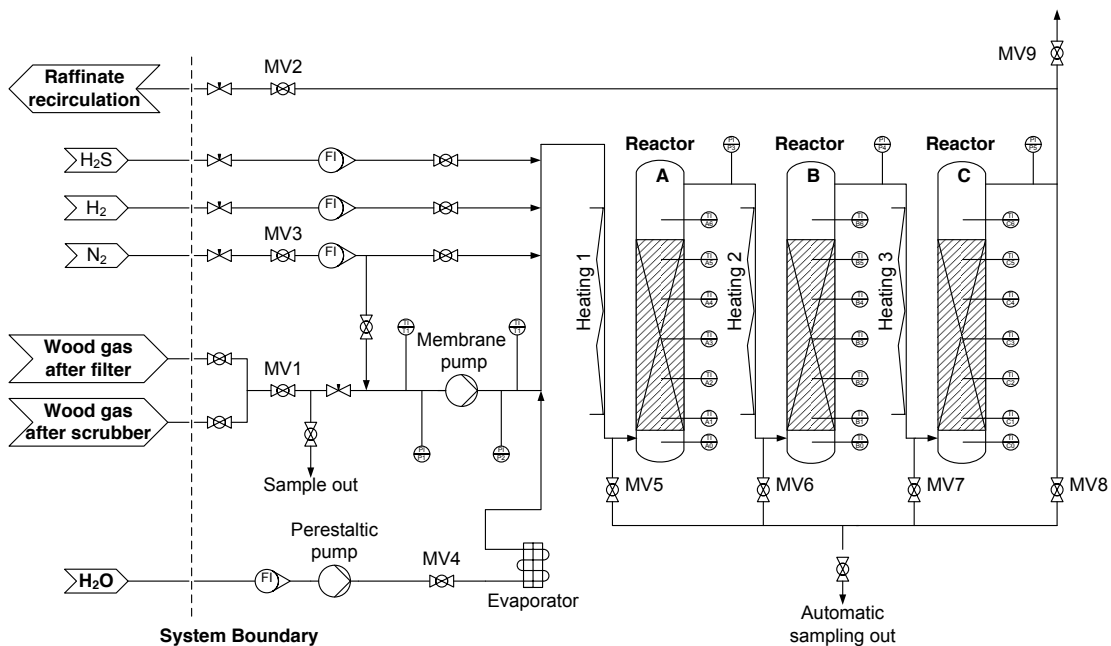

Figure 4.4: Detailed flowchart of the WGS pilot unit at the plant site of the DFB biomass steam gasification plant Oberwart, Austria [7].

A process control system (PCS), based on a system from the company Bernecker + Rainer Industrie-Elektronik GmbH (B&R), is used to operate the WGS pilot unit. Furthermore a

LabVIEW^{TM} program was used to visualize and register process data. A wide range of safety measures, like alarm limits and automatic shutdown procedures in the case of a shortfall in combination with many pilot-operated valves, led to an easy handling and high usability, even to a remote controlled operation.

Figure 4.5 shows two screenshots, one of the graphical user interface of the WGS pilot unit's PCS and one of the process data visualization using LabVIEW^{TM}. Figure 4.6 shows two pictures of the WGS pilot unit. Picture (a) was taken before the heat isolation was installed, picture (b) shows the actual pilot unit, ready-to-operate.
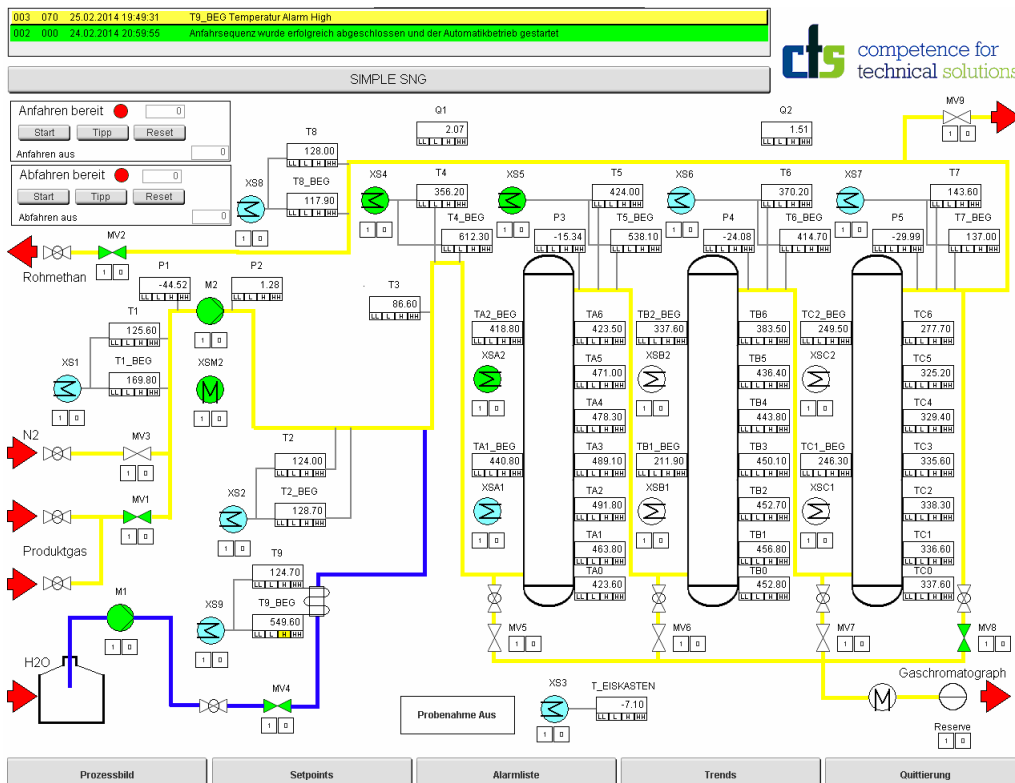
(a) PCS overview of the process control system.
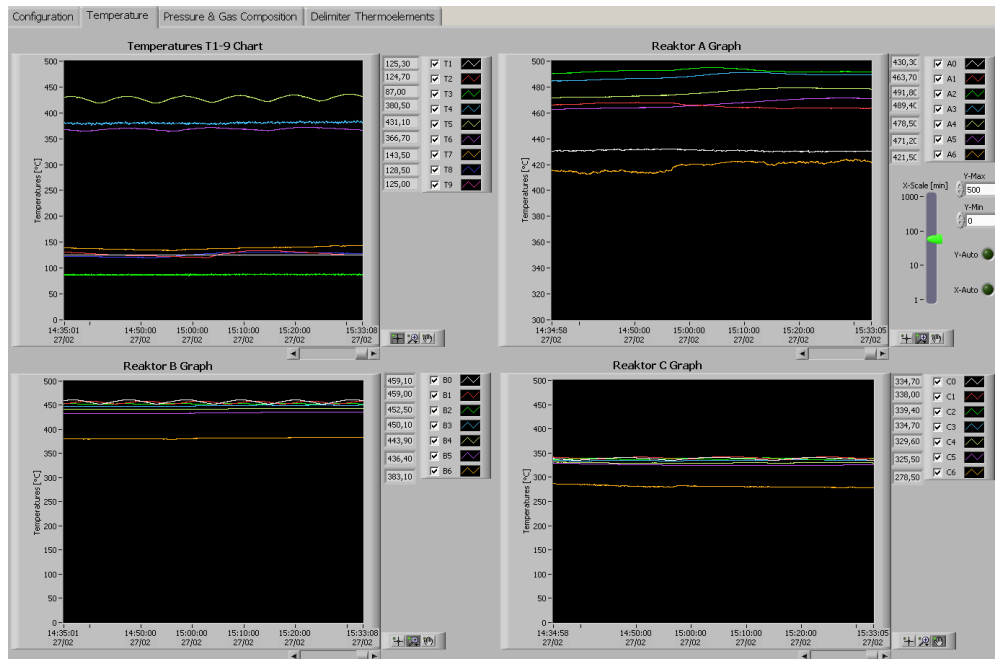
(b) Process visualization with LabVIEW™.

Figure 4.5: Screenshots of the graphical user interface of the WGS pilot unit [7].

(a) The WGS pilot unit during construction work, prior to heat isolation.

(b) Final setup of the WGS pilot unit, including all geared equipment.

Figure 4.6: Pictures of the WGS pilot unit, located in the research container on DFB biomass gasification plant's site in Oberwart, Austria [7].

4.3 Sampling and Analyses

During the experimental test runs, extensive analyses were carried out. The water content, the main gas and sulfur components, as well as the GCMS tar compounds and the ammonia content were measured. In addition, the catalyst's activity was observed by measuring the temperature profiles along the reactors due to the exothermic nature of the WGS reaction. The water content was determined gravimetrically. CO, CO_2, CH_4, N_2, O_2, C_2H_6, C_2H_4, C_2H_2, H_2S, COS, and C_4H_4S were measured by using a gas chromatograph (GC) on site, samples for GCMS tar compounds and ammonia content were taken and handed over to the Test Laboratory for Combustion Systems at the Vienna University of Technology for analyses.

In order to enable the different sampling and their gas conditioning, a sampling line was installed, which has two major ways of operation: First the "standard analysis line" through the bottom path in Figure 4.7 with a temperature from -5 to -3 °C in cooling box 2 for GC measurements and water content determinations. Second, the "tar analysis line", through the top path in Figure 4.7 with a temperature of 0 °C in cooling box 1 by using an ice bath and a temperature range from about -10 to -8 °C in cooling box 2 for taking GCMS tar samples.
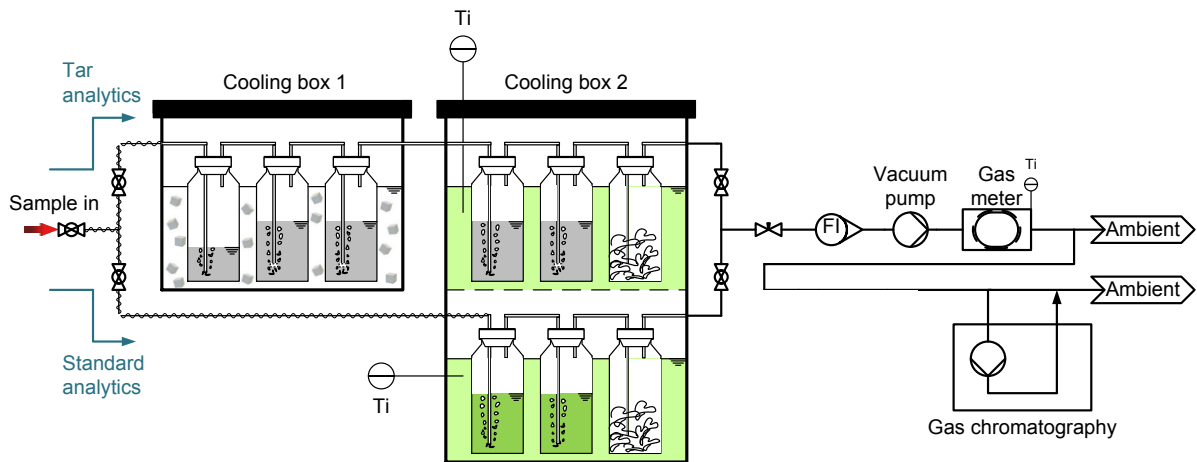

Figure 4.7: Flowchart of the installed sampling line. The "tar analysis line" trough the top path and the "standard analysis line" trough the bottom path, based on [7].

The cooling box 2 contained a glycol bath, which was placed inside an ordinary refrigerator. The refrigerator was integrated in the PCS, therefore, the temperature was regulated.

All sampling pipes upstream of the cooling boxes were heat-isolated and electrically trace heated in order to avoid condensation and blocking.

A two-channel gas chromatograph, Clarus 500$^{\text{TM}}$ from the company Perkin Elmer, was used to determine the main gas and sulfur components. The main gas components (CO, CO_2, CH_4, N_2, O_2, C_2H_6, C_2H_4, and C_2H_2) were quantified with a thermal conductivity detector (TCD). C_2H_6, C_2H_4, and C_2H_2 were summarized and refereed to as C_2H_y. The sulfur components (H_2S, COS, and C_4H_4S) were detected by a flame photometric detector (FPD). The amount of H_2 was calculated by closing the overall mass balance. This GC was also integrated in the PCS, which enabled in combination with pilot operated sampling valves and an analytic pump, an automated procedure of sampling. This led to one complete GC measurement with both channels in less than 30 minutes. Those pilot operated sampling valves are MV5, MV6, MV7, and MV8 as shown in Figure 4.4. More information regarding the GC and the sampling system can be found in [3].

The analysis gas stream was sent trough the "standard analysis line" before the sample stream entered the GC. The first two gas washing bottles were filled with water and glycol to prevent freezing. They were followed by a third gas washing bottle, filled with glass wool in order to remove aerosols. Those three gas washing bottles were located in a temperature controlled cooling bath inside the cooling box 2, shown in Figure 4.7. The temperature was adjusted from -5 to -3 °C.

The water content of the wood gas was measured gravimetrically. Therefore, the standard analysis line was used based on one assumption: all water is condensed in the gas washing bottles, which means that all additional weight in the gas washing bottles resulted by water condensing and the flow rate, registered in the flow meter downstream of the gas washing bottles was completely free of water. The additional weight of the gas washing bottles in combination with the dry gas flow rate enabled the calculation of the water content.

Those water content measurements were also the basis for the proven "water spike" method (see [7]), which was used for determining the mass balance of the system. In order to achieve the desired steam content at the inlet of the WGS pilot unit, water was added to the system. The steam and wood gas flow was mixed between the gas pump and the heating section upstream of the first reactor, as shown in Figure 4.4. This defined water addition and the water content measured downstream as well as upstream of the point of water addition enabled the calculation of the mass balance of the system and the $GHSV$.

The GCMS tar samples were taken using the "tar analysis line" (see Figure 4.7). Therefore six gas washing bottles at two different temperature levels were used. Five bottles were filled with a total of 500 mL of toluene, 100 mL each bottle, and one bottle filled with glass wool. Three of the toluene filled bottles were located at cooling box 1 at a temperature of 0 °C and two bottles of toluene and the one filled with glass wool were located downstream in cooling box 2 at a temperature range of -10 to -8 °C. The sampling stream of 2.0 to 2.5 $\frac{L_{N,db}}{min}$ was taken over about 3 hours to reach a gas sample volume of close to 0.5 $m^3_{N,db}$. After the tar samples were taken, the GCMS analysis were carried out by the Test Laboratory for Combustion Systems at the Vienna University of Technology. The analysis and the sampling

of the GCMS tar followed the method described in [14, 34].

The following list divides the detected GCMS tar, which have been measured above the detection limit, into GCMS tar substance groups according to [21]:

- **Aromatic compounds (AC)**
  Phenylacetylene, Indole, 1H-Indene, Mesitylene, Styrene

- **Naphthalenes**
  Naphthalene, 1-Methylnaphthalene, 2-Methylnaphthalene.

- **Others (Furans, Phenols, Thiophenes)**
  Benzofuran, Dibenzofuran, Phenol, 1-Benzothiophene

- **Polycyclic aromatic hydrocarbons (PAH)**
  Acenaphthene, Acenaphthylene, Anthracene, Biphenyl, Flouranthene, Flourene, Quinoline, Isoquinoline, Phenanthrene, 4,5-Methylphenenthrene, Pyrene

The ammonia samples were taken using a total of 200 mL of 0.05 $molar$ H_2SO_4 in two gas washing bottles, 100 mL in each bottle. Downstream the two gas washing bottles, a third gas washing bottle, filled with glass wool in order to remove aerosols, was installed. The bottles were located in cooling box 1 at a temperature of 0 °C. The sampling time for one sample was fifteen minutes with a gas sampling stream of 0.5 to 0.7 $\frac{L_{N,db}}{min}$. The ammonia analyses were carried out by the Test Laboratory for Combustion Systems at the Vienna University of Technology using column chromatography.

The temperature measurements along all three WGS reactors were performed with thermocouples (type J), seven thermocouples for each reactor. Those thermocouples were installed at equal distances along the reactors. Five thermocouples were placed inside the fixed bed WGS catalyst in order to record the temperature profile along the reactive zone. One thermocouple was placed upstream and one thermocouple was placed downstream of the catalyst fixed bed. Figure 4.4 shows the position of the thermocouples more detailed. All temperature measuring points served as a data input for the PCS and in addition were indicated and recorded by a LabVIEW$^{\text{TM}}$ program.

4.4   Key Figures

In order to characterize the WGS pilot unit operation, key figures are introduced. Besides the equilibrium and its dependence on temperature, discussed in Section 3.3, the following figures affected the WGS reaction and are important to describe the conditions along the WGS pilot unit.

The gas hourly space velocity on wet basis ($GHSV_{wb}$) is the ratio of wet gas flow rate to catalyst volume, calculated at standard conditions and consider water as an ideal gas. It indicates the stress of the catalyst, see Equation 4.1.

Gas hourly space velocity $$GHSV_{wb} = \frac{\dot{V}_{gas,wb}}{V_{catalyst}}$$ $[h^{-1}]$ (4.1)

The steam to dry gas ratio ($STDGR$), defined in Equation 4.2, gives information about the steam content in the gas mixture. Furthermore, the steam to carbon ratio ($STCR$), see Equation 4.3, and the steam to carbon monoxide ratio ($STCOR$) in Equation 4.4 are important figures which describe the risk of coking and carbon deposition on the surface of the catalyst.

Steam to dry gas ratio $$STDGR = \frac{\dot{n}_{H_2O}}{\dot{n}_{gas,db}}$$ $[-]$ (4.2)

Steam to carbon ratio $$STCR = \frac{\dot{n}_{H_2O}}{\dot{n}_C}$$ $[-]$ (4.3)

Steam to carbon monoxide ratio $$STCOR = \frac{\dot{n}_{H_2O}}{\dot{n}_{CO}}$$ $[-]$ (4.4)

In order to characterize the change in volumetric dry gas flow rate the delta dry gas flow rate ($\Delta\dot{V}_{db}$) was introduced. It was calculated according to Equation 4.5.

Delta dry gas flow rate $$\Delta\dot{V}_{db} = \frac{\dot{n}_{gas,db,out}}{\dot{n}_{gas,db,in}}$$ $[-]$ (4.5)

The hydrogen recovery (H_2rec), defined in Equation 4.6, is a key figure to describe if in the specific unit is hydrogen produced ($H_2rec > 1$), or if hydrogen is consumed or discharged ($H_2rec < 1$). The hydrogen recovery is suitable to evaluate the performance of single units within hydrogen production chains.

H$_2$ recovery
$$H_2rec = \frac{\dot{n}_{H_2,out}}{\dot{n}_{H_2,in}}$$
$[\,-\,]$ (4.6)

The carbon monoxide conversion rate (X_{CO}), according to Equation 4.7, was the key figure to evaluate the performance of the WGS pilot unit.

CO conversion rate
$$X_{CO} = \frac{\dot{n}_{CO,in} - \dot{n}_{CO,out}}{\dot{n}_{CO,in}}$$
$[\,-\,]$ (4.7)

To calculate the tar conversion rate (X_{tar}), defined in Equation 4.8 and the ammonia conversion rate (X_{NH_3}), defined in Equation 4.9 the concentration (c) was used. To take the effect of dilution into account the increase of the volumetric dry gas flow rate was considered. A negative value of the conversion rate indicates a production.

Tar conversion rate
$$X_{tar} = \frac{c_{tar,in} - (\Delta\dot{V}_{db} \cdot c_{tar,out})}{c_{tar,in}}$$
$[\,-\,]$ (4.8)

Ammonia conversion rate
$$X_{NH_3} = \frac{c_{NH_3,in} - (\Delta\dot{V}_{db} \cdot c_{NH_3,out})}{c_{NH_3,in}}$$
$[\,-\,]$ (4.9)

Chapter 5

Experimental Results and Discussion

This chapter describes the experiments which were carried out during this thesis in order to investigate the long term performance of a commercial Fe/Cr based WGS catalyst. After a longer resting period and through outside circumstances, the research facility on site the DFB biomass steam gasification plant Oberwart, Austria, was moved for some meters to a new location. Therefore, all cables and pipes which ensured the connection between the CHP plant and the research container had to be reinstalled and checked for proper function. This work was the main work load during the first months.

In order to ensure proper system operation and to facilitate a comparison to previous results, an already well documented operating point was chosen for the first test run. The wood gas, extracted downstream of the DFB gasification plant's RME gas scrubber, was processed for more than 100 hours.

Thereafter, the main research of this work, a WGS pilot unit long term test run processing tar-rich wood gas, extracted upstream of the DFB gasification plant's RME gas scrubber, was performed. During this long term test run, tar-rich wood gas was processed for more than 2330 hours.

The water content was determined and the main gas components (CO, CO_2, CH_4, N_2, O_2, C_2H_6, C_2H_4, and C_2H_2) as well as the sulfur components (H_2S, COS, and C_4H_4S) were measured. In addition GCMS tar and ammonia samples were taken and the temperature profiles along the reactors were recorded, in order to determine the catalyst's activity. Within this long term test run, about 100 hours of steady partial load operation of the DFB gasification plant as well as 320 hours of partial load operation of the WGS pilot unit were recorded.

This leads to overall four WGS pilot unit points of operation, which were investigated, the results are presented in the upcoming sections:

- **Operating point 1** Processing wood gas, extracted downstream of the DFB plant's RME scrubber. (Section 5.1)

- **Operating point 2** Processing tar-rich wood gas, extracted upstream of the DFB plant's RME scrubber. (Section 5.2)

- **Operating point 3** Processing tar-rich wood gas, extracted upstream of the DFB plant's RME scrubber, at partial load operation of the DFB biomass steam gasification plant. (Section 5.3)

- **Operating point 4** Processing tar-rich wood gas, extracted upstream of the DFB plant's RME scrubber, at partial load operation of the WGS pilot unit. (Section 5.4)

During the long term test run of the WGS pilot unit, processing tar-rich wood gas extracted upstream of the DFB gasification plant's RME scrubber, GCMS tar and ammonia measurements were performed. It was attempted to take one sample at each point of load condition, Table 5.22 in Section 5.5 shows the load conditions and the corresponding hours of operation. The samples were taken following the method described in Section 4.3. The samples were handed over to the Test Laboratory for Combustion Systems at the Vienna University of Technology for the follow up analysis. Finally, eight GCMS tar measurements, four times a pair of one sample from the WGS pilot unit's inlet and one sample from the WGS pilot unit's outlet were carried out. In addition six ammonia measurements, also as three pairs of one sample from the WGS pilot unit's inlet and one sample from the WGS pilot unit's outlet were performed.

Results regarding GCMS tar and ammonia measurements can also be reviewed in [28], which was carried out in collaboration with Kraussler et al.

5.1   Processing Wood Gas, Extracted Downstream of the DFB plant's RME Scrubber

In December 2014, when the reinstalling after the container movement was finished, a first WGS pilot unit test run with over 100 hours of operation was carried out. The wood gas for this test run was extracted downstream of the DFB biomass steam gasification plant's RME gas scrubber. The data and results from this experiment can also be reviewed in [23, 24]. The papers were carried out in collaboration with Kraussler et al.

Table 5.1 shows the key figures of operation for the WGS pilot unit processing wood gas, which was extracted downstream of the RME scrubber. This point of operation was defined

Table 5.1: Operating conditions of the WGS pilot unit processing wood gas, extracted downstream of the RME gas scrubber for 100 hours. All figures are given for the WGS pilot unit's inlet, based on [23].

Overall catalyst volume	7.8	L
Catalyst volume per reactor	2.6	L
Water content wood gas	7.6	$mol.\%_{wb}$
Water content inlet WGS pilot unit	54.06	$mol.\%_{wb}$
Volumetric flow rate dry	1.02	$\frac{m^3_{N,db}}{h}$
Volumetric flow rate wet	2.22	$\frac{m^3_{N,wb}}{h}$
$STDGR$	1.18	-
$STCR$	2.00	-
$STCOR$	5.05	-
Temperature setpoint inlet each reactor	350	$^\circ$C
$GHSV_{wb}$ overall	286	h^{-1}
$GHSV_{wb}$ per reactor	857	h^{-1}

as the "basic operation conditions" for the WGS pilot unit in [7]. The catalyst which was used was the same as in [7, 8] and has been activated before.

Furthermore, the catalyst was already operated for 800 hours, processing real wood gas on site the DFB gasification plant, before this test run [7, 8]. The main results of this test run are summarized in Table 5.2.

Table 5.2: Results of the WGS pilot unit operation processing wood gas, extracted downstream of the RME gas scrubber for 100 hours. Operating conditions according to Table 5.1, based on [23].

	$GHSV_{wb}$	$\Delta \dot{V}_{db}$	H_2rec	X_{CO}
Outlet reactor A	857 h^{-1}	1.20	1.52	0.85
Outlet reactor B	429 h^{-1}	1.21	1.54	0.88
Outlet WGS pilot unit	286 h^{-1}	1.21	1.56	0.92

Figures 5.1 to 5.3 show the temperature profiles and the change of concentrations (dry basis) of the reactive WGS components over each reactor, from reactor A to reactor C. All three reactors were operated with the same inlet temperature of 350 °C. Therefore, the change of temperature resulted from the heat of reaction of the WGS reaction. Especially Figure 5.1 indicates that the WGS reaction mainly took place in reactor A. There was a significant temperature increase, because of the moderately exothermic WGS reaction as well as the most significant change of the concentrations of the reactive components. The temperature decrease towards the outlet, which was observed at all three reactors, was caused by heat losses. The temperature profile's standard deviation is relatively small, because of the a steady water content of the processed wood gas downstream of the RME scrubber.

The temperature profiles in Figures 5.2 and 5.3 do not indicate a temperature increase, because of the predominate head losses. There was also only a very slight change of absolute

(a) Temperature profile of reactor A
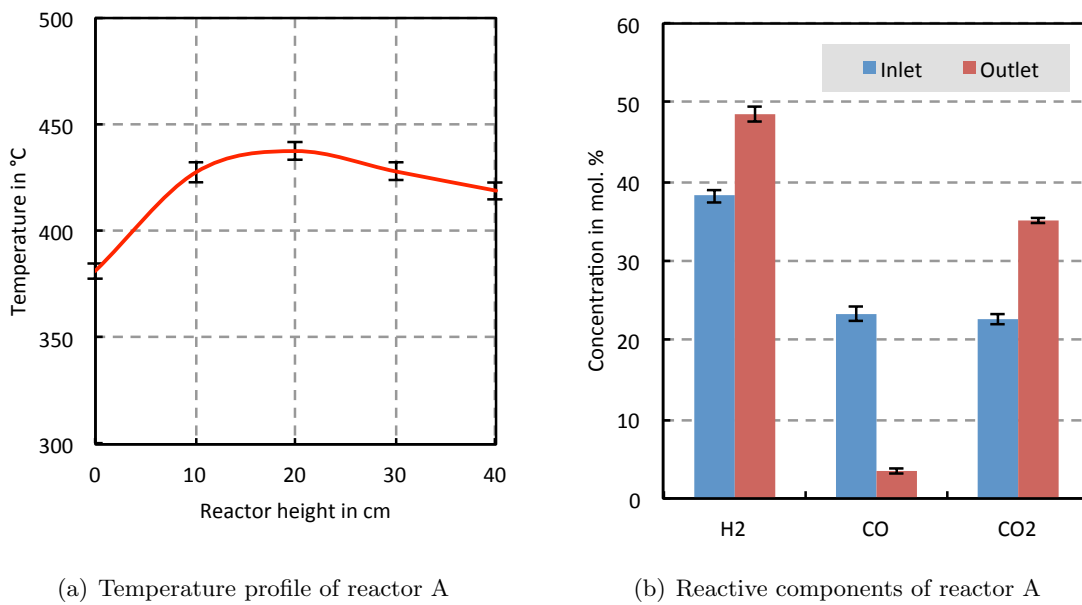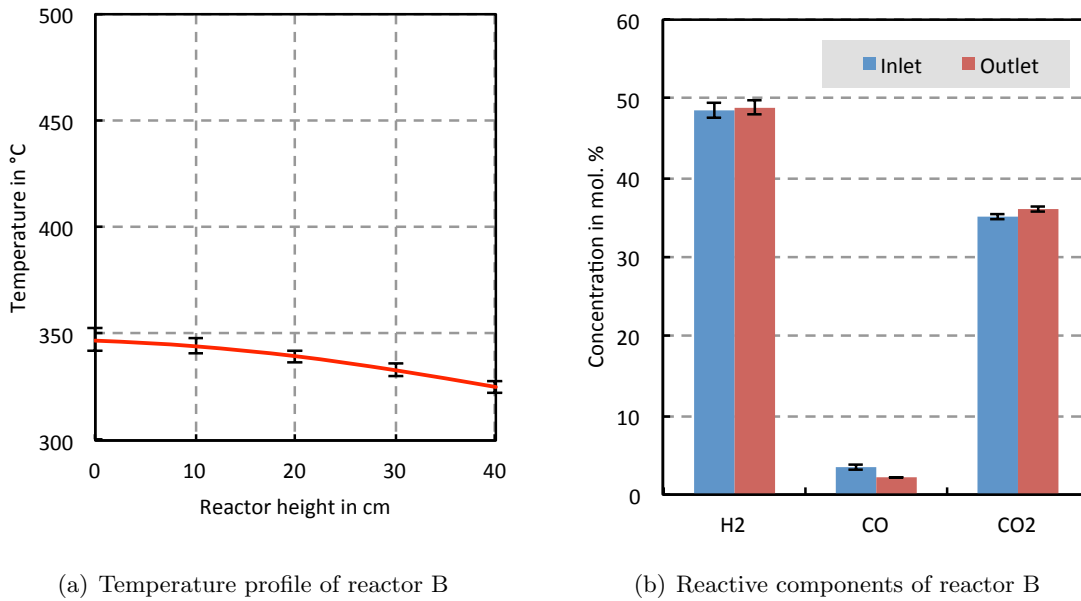
(b) Reactive components of reactor A

Figure 5.1: The average temperature profile and the average concentration (dry basis) of the reactive WGS components for reactor A processing wood gas, extracted downstream of the RME gas scrubber for 100 hours, based on [23].
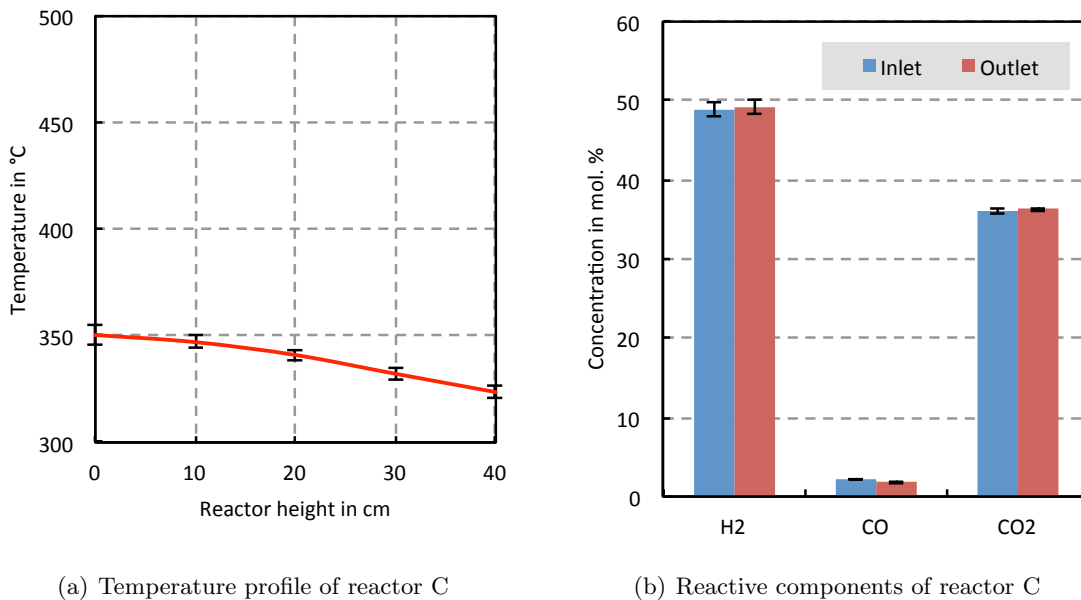
concentrations in the reactive components. In contrast, Table 5.2 shows that there was still a significant WGS reaction taking place, if taking the carbon monoxide conversion rate into account.

(a) Temperature profile of reactor B

(b) Reactive components of reactor B

Figure 5.2: The average temperature profile and the average concentration (dry basis) of the reactive WGS components for reactor B processing wood gas, extracted downstream of the RME gas scrubber for 100 hours, based on [23].

(a) Temperature profile of reactor C

(b) Reactive components of reactor C

Figure 5.3: The average temperature profile and the average concentration (dry basis) of the reactive WGS components for reactor C processing wood gas, extracted downstream of the RME gas scrubber for 100 hours, based on [23].

The detailed average gas composition of the 100 hours of operation is shown in Table 5.3. It summarizes the main gas components as well as the sulfur components. The values represent the composition on dry basis. In order to be able to state assumptions about the performance the increase of the volumetric dry gas flow rate, shown in Table 5.2, needs to be taken into consideration.

Table 5.3: The average concentrations of the main gas components and sulfur components along the WGS pilot unit processing wood gas, extracted downstream of the RME gas scrubber for 100 hours. Detection limit (DL) sulfur components: 0.3 mol.ppm$_{db}$, based on [23].

	H_2 mol.%$_{db}$	CO mol.%$_{db}$	CO_2 mol.%$_{db}$	CH_4 mol.%$_{db}$	C_2H_y mol.%$_{db}$
Inlet WGS pilot unit	38.2 ± 0.8	23.3 ± 0.9	22.7 ± 0.7	10.0 ± 0.4	2.8 ± 0.3
Outlet reactor A	48.5 ± 0.9	3.4 ± 0.3	35.1 ± 0.4	8.6 ± 0.3	2.2 ± 0.3
Outlet reactor B	48.9 ± 0.9	2.2 ± 0.1	36.0 ± 0.3	8.5 ± 0.3	2.2 ± 0.2
Outlet WGS pilot unit	49.2 ± 0.9	1.8 ± 0.1	36.3 ± 0.3	8.4 ± 0.3	2.2 ± 0.2
	N_2 mol.%$_{db}$	O_2 mol.%$_{db}$	H_2S mol.ppm$_{db}$	COS mol.ppm$_{db}$	C_4H_4S mol.ppm$_{db}$
Inlet WGS pilot unit	2.7 ± 0.3	0.30 ± 0.04	91 ± 13	3.8 ± 0.9	5.6 ± 1.6
Outlet reactor A	2.2 ± 0.2	0.03 ± 0.01	79 ± 12	BDL	5.1 ± 1.0
Outlet reactor B	2.1 ± 0.2	0.03 ± 0.01	59 ± 13	BDL	5.6 ± 0.9
Outlet WGS pilot unit	2.1 ± 0.2	0.03 ± 0.01	44 ± 9	BDL	5.7 ± 1.0

Compared with previous results of the WGS pilot unit in [7, 8, 9], no significant differences regarding the performance and operating behavior of the WGS pilot unit could be observed. This leads to the conclusion that the WGS pilot unit and its catalyst withstand all the research container movements and the period of rest unscathed. During this short term test run processing wood gas, extracted downstream of the RME gas scrubber, no GCMS tar and no ammonia measurements were performed.

5.2 Long Term Test Run Processing Tar-Rich Wood Gas, Extracted Upstream of the DFB plant's RME Scrubber

In order to investigate the long term performance of the Fe/Cr based catalyst, a long term test run processing tar-rich wood gas, which was extracted upstream of the DFB biomass steam gasification plant's RME gas scrubber was performed. The extraction point is illustrated in Figure 4.3 and the wood gas conditions can be seen in Table 4.2. The WGS pilot unit was operated for 2330 hours processing real, tar-rich wood gas from the DFB biomass gasification plant Oberwart, Austria from the end of December 2014 till the end of April 2015. In this period the WGS pilot unit showed a system availability of 85 %. The long term test run included 362 hours of rest, caused by a technical shortcoming and following servicing and maintenance work in the DFB biomass gasification plant. Without those 362 hours of downtime, the system availability could had even reached up to 97 %. 2293 hours of steady operating conditions were achieved.

Before the downtime, a significant decrease of pump capacity of the WGS pilot unit's membrane gas pump was observed. This resulted in a WGS pilot unit partial load operation for 320 hours with a reduced $GHSV_{wb}$. The following period of downtime was used to maintain the WGS pilot unit's membrane gas pump. After that, the originally aimed operating conditions were duly achieved.

Results from this long term test run served for journal and conference publications [23, 24, 25, 27], which were carried out in collaboration with Kraussler et al.

Table 5.4 shows the key figures of the operation of the WGS pilot unit processing tar-rich wood gas, extracted upstream of the RME scrubber and Table 5.5 summarizes the results of the long term operation.

Table 5.4: Operating conditions of the WGS pilot unit processing tar-rich wood gas, extracted upstream of the RME gas scrubber for 2293 hours. All figures are given for the WGS pilot unit's inlet, based on [27].

Overall catalyst volume	7.8	L
Catalyst volume per reactor	2.6	L
Water content wood gas	39.9	$mol.\%_{wb}$
Water content inlet WGS pilot unit	61.7	$mol.\%_{wb}$
Volumetric flow rate dry	1.24	$\frac{m^3_{N,db}}{h}$
Volumetric flow rate wet	3.24	$\frac{m^3_{N,wb}}{h}$
$STDGR$	1.61	-
$STCR$	2.68	-
$STCOR$	6.46	-
Temperature setpoint	350	°C
$GHSV_{wb}$ overall	415	h^{-1}
$GHSV_{wb}$ per reactor	1246	h^{-1}

Table 5.5: Results of the WGS pilot unit operation processing tar-rich wood gas, extracted upstream of the RME gas scrubber for 2293 hours. Operating conditions according to Table 5.4, based on [27]

	$GHSV_{wb}$	$\Delta \dot{V}_{db}$	$H_2 rec$	X_{CO}
Outlet reactor A	1246 h^{-1}	1.21	1.54	0.80
Outlet reactor B	623 h^{-1}	1.22	1.58	0.89
Outlet WGS pilot unit	415 h^{-1}	1.24	1.61	0.92

The operating conditions were charily chosen, to ensure a high $STDGR$ at the WGS inlet by adding excessively steam. This decision was taken because of fluctuations in the wood gas water content upstream of the RME scrubber. Observations showed that small technical malfunctions or inconsistent biomass quality led to upwards fluctuations.

The $GHSV_{wb}$ was close to the power limits with the present corresponding design points of evaporator and membrane gas pump.

Figures 5.4 to 5.6 show the temperature profiles and the change of concentrations (dry basis) of the reactive WGS components over each reactor, from reactor A to reactor C. All three reactors were operated with the same inlet temperature of 350 °C.

(a) Temperature profile of reactor A
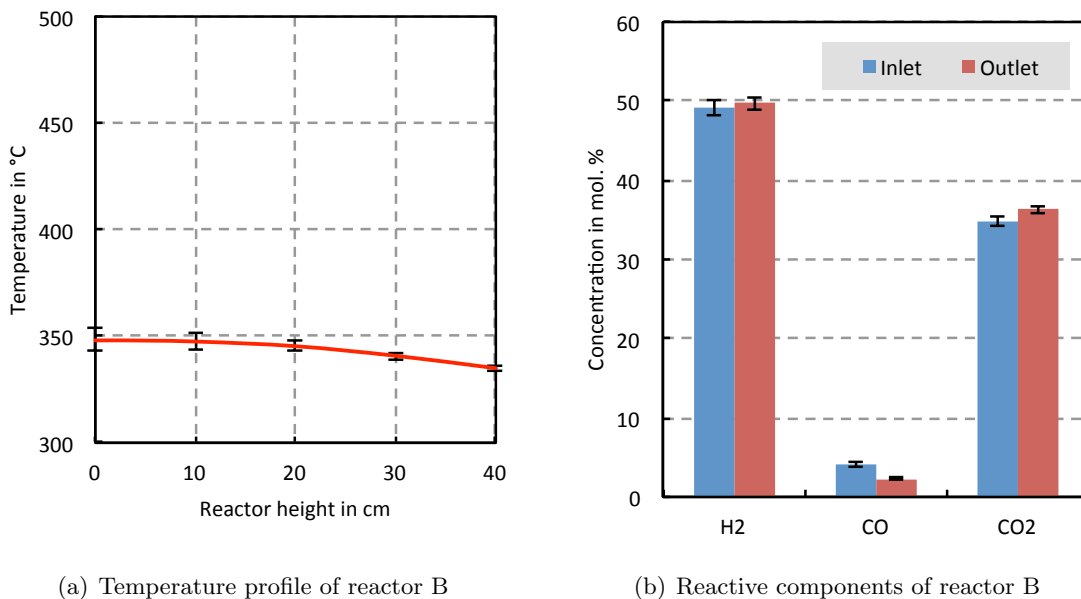
(b) Reactive components of reactor A
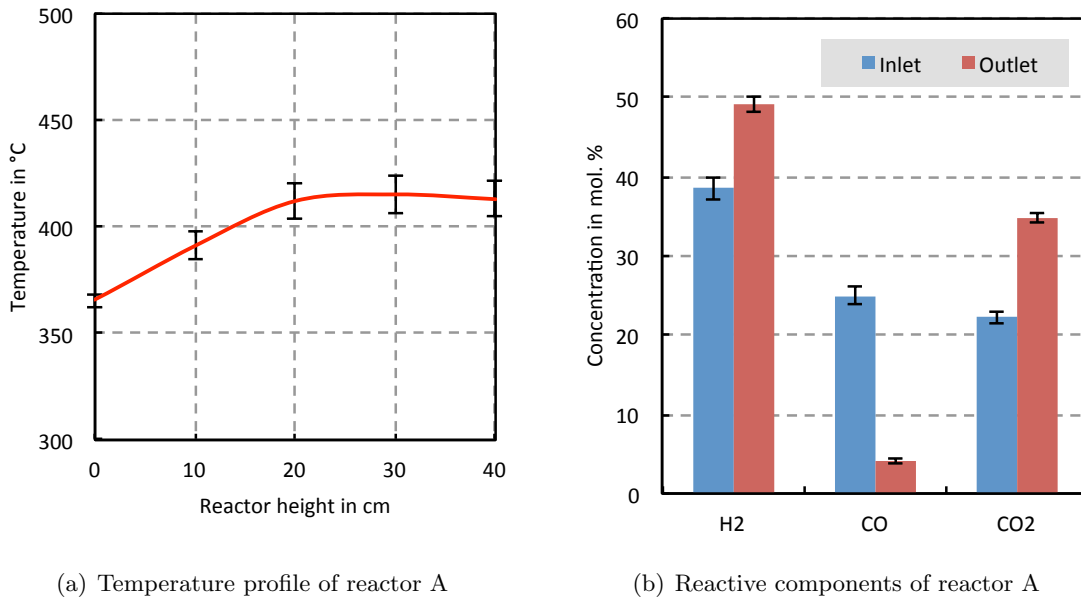
Figure 5.4: The average temperature profile and the average concentration (dry basis) of the reactive WGS components for reactor A processing tar-rich wood gas, extracted upstream of the RME gas scrubber for 2293 hours, excluding sections at partial load operation, based on [27].

The same pattern is seen as in Section 5.1. Figure 5.4 (a) indicates that the WGS reaction mainly took place in reactor A. It also shows a significant temperature increase because of the moderately exothermic WGS reaction. Subsequently, temperature decreases towards the outlet, which was observed at all reactors, because of heat losses. Also the most significant

change of the concentrations of the reactive components took place in reactor A.

In comparison to the results in Section 5.1, the shape of the temperature profile of reactor A from the operation with wood gas extracted upstream of the RME scrubber changed, caused by the different flow conditions and the the different water content. Also profiles from the operation with wood gas extracted upstream of the RME scrubber showed a higher standard deviation. This can especially be seen in the temperature profile of reactor A. This is primarily related to fluctuation in the wood gas water content upstream of the RME gas scrubber caused by changing operating conditions of the DFB gasification plant. If processing wood gas, extracted upstream of the RME scrubber, the WGS pilot unit is at the mercy of the effects of the wood gas water content.

In contrast, processing wood gas, extracted downstream of the RME scrubber, the wood gas water content has no direct impact on the WGS pilot unit's temperature profile because there is a steady water content downstream of the RME scrubber.

In reactor B and reactor C, the WGS reaction is diminished. Figures 5.5 (a) and 5.6 (a) do not indicate a temperature increase because of predominate head losses. There was also only a very slight change of absolute concentrations of the reactive components. Table 5.5 shows that there is still a significant WGS reaction taking place, if taking the carbon monoxide conversion rate into account.

(a) Temperature profile of reactor B   (b) Reactive components of reactor B

Figure 5.5: The average temperature profile and the average concentration (dry basis) of the reactive WGS components for reactor B processing tar-rich wood gas, extracted upstream of the RME gas scrubber for 2293 hours, excluding sections at partial load operation, based on [27].

(a) Temperature profile of reactor C

(b) Reactive components of reactor C
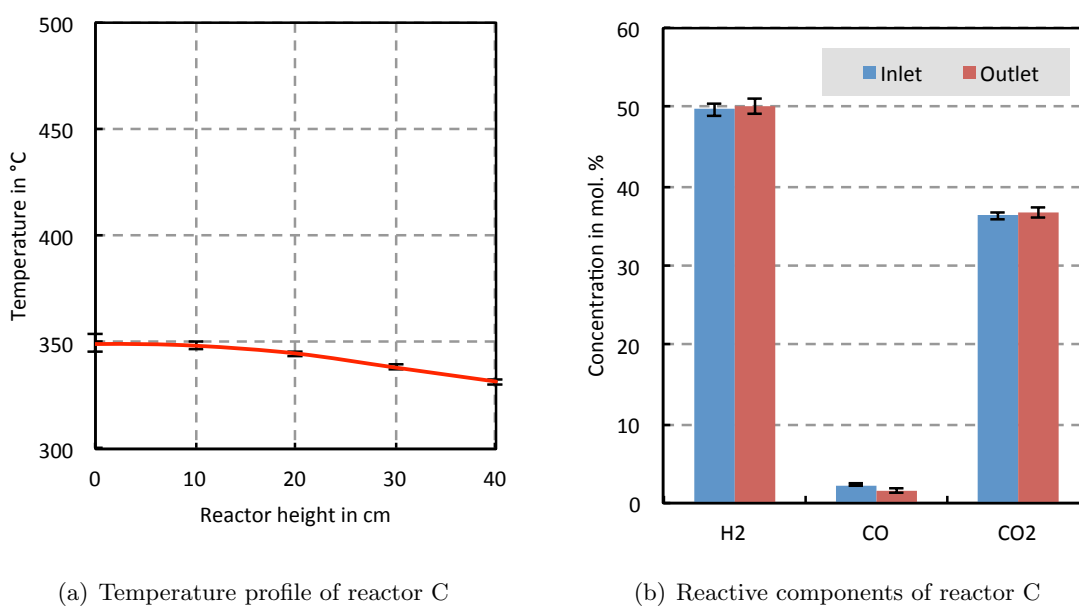
Figure 5.6: The average temperature profile and the average concentration (dry basis) of the reactive WGS components for reactor C processing tar-rich wood gas, extracted upstream of the RME gas scrubber for 2293 hours, excluding sections at partial load operation, based on [27].

The detailed average wood gas composition at the WGS pilot unit's inlet and also the gas composition at each reactor's outlet during the 2293 hours of operation processing wood gas, extracted upstream of the RME scrubber, is shown in Table 5.6. It summarizes the main gas components as well es the sulfur components.

Table 5.6: The average concentrations of the main gas components and sulfur components along the WGS pilot unit processing tar-rich wood gas, extracted upstream of the RME gas scrubber for 2293 hours. DL sulfur components: 0.3 mol.ppm$_{db}$, based on [27].

	H_2	CO	CO_2	CH_4	C_2H_y
	mol.%$_{db}$	mol.%$_{db}$	mol.%$_{db}$	mol.%$_{db}$	mol.%$_{db}$
Inlet WGS pilot unit	38.6 ± 1.5	24.9 ± 1.3	22.3 ± 1.2	10.1 ± 0.6	2.7 ± 0.3
Outlet reactor A	49.1 ± 1.3	4.1 ± 0.7	34.9 ± 1.0	8.6 ± 0.5	2.1 ± 0.2
Outlet reactor B	49.7 ± 1.3	2.3 ± 0.2	36.3 ± 0.8	8.4 ± 0.5	2.1 ± 0.2
Outlet WGS pilot unit	50.2 ± 1.3	1.6 ± 0.2	36.6 ± 0.8	8.3 ± 0.5	2.1 ± 0.2
	N_2	O_2	H_2S	COS	C_4H_4S
	mol.%$_{db}$	mol.%$_{db}$	mol.ppm$_{db}$	mol.ppm$_{db}$	mol.ppm$_{db}$
Inlet WGS pilot unit	1.4 ± 0.6	0.08 ± 0.04	93.5 ± 16.9	3.2 ± 1.2	5.8 ± 1.9
Outlet reactor A	1.1 ± 0.4	0.03 ± 0.02	94.6 ± 16.0	BDL	5.1 ± 1.6
Outlet reactor B	1.2 ± 0.6	0.03 ± 0.01	93.0 ± 15.6	BDL	5.1 ± 1.6
Outlet WGS pilot unit	1.1 ± 0.5	0.03 ± 0.02	90.9 ± 16.5	BDL	5.2 ± 1.7

Although the $GHSV_{wb}$ for this point of operation with tar-rich wood gas, which was extracted upstream of the RME gas scrubber is significantly higher as for the previous point of operation with wood gas, which was extracted downstream of the RME gas scrubber, a CO conversion of 92 % could be reached. The summarized results can be compared in Table 5.2 and Table 5.5. Especially, the dry flow rate should be highlighted, which was with a value of 1.24 $\frac{m^3_{N,db}}{h}$ the highest value measured within this work.

The main statement of the long term test run is summarized in Figure 5.7. It shows the temperature profiles along the first reactor (reactor A) after 500, 1000, 1500, and 2000 hours of operation processing tar-rich wood gas, extracted upstream of the RME gas scrubber. After the long term test run which lasted 2300 hours, the catalyst has faced more than 3200 hours of operation. No significant deactivation could be observed so far. Small variations in temperature could be explained by varying wood gas composition. Strong deviations of the temperature profiles could be explained by operating problems at the CHP plant. Frequently the temperature shows a slight under swinging of the referenced temperature profile, which was mainly caused by higher water content, or by the dilution with nitrogen. On the other hand strong over swinging of the temperature rarely occurs, due to the presence of oxygen in the wood gas.
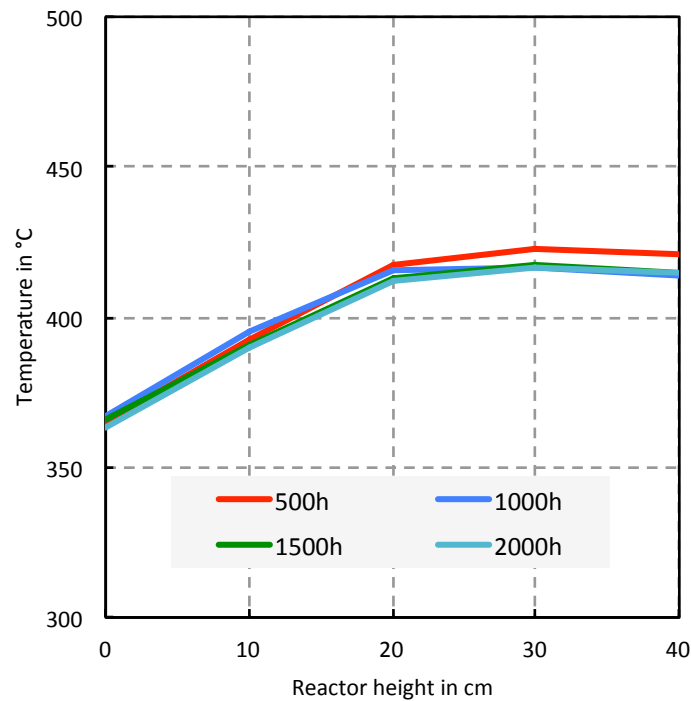
Figure 5.7: Temperature profiles of reactor A after 500, 1000, 1500, and 2000 hours of operation processing wood gas, extracted upstream of the DFB biomass steam gasification plant's RME gas scrubber, based on [27].

Figure 5.8 illustrates the main gas components and Figure 5.9 illustrates the sulfur components, each directly measured values (dry basis) over the time of operation. In order to be able to state assumptions about performance, the increase of the volumetric dry gas flow rate, shown in Table 5.5, needs to be taken into consideration.
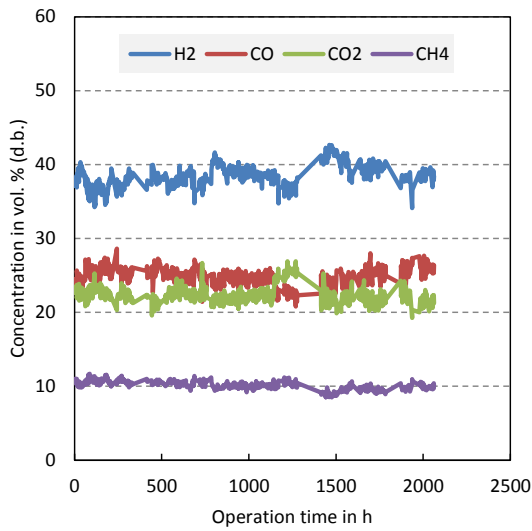
(a) Main gas composition at the inlet
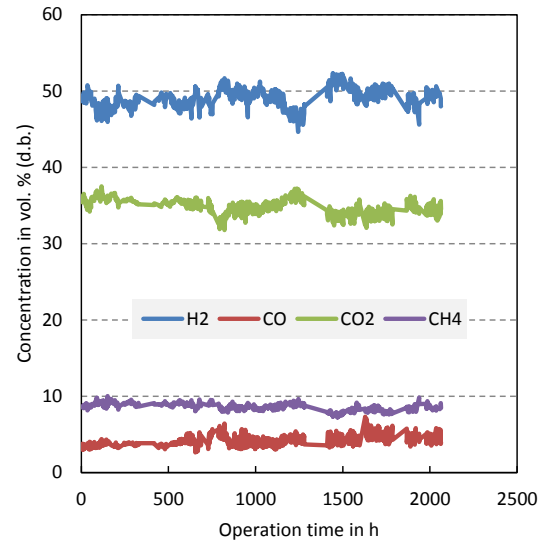
(b) Main gas composition at the outlet of reactor A
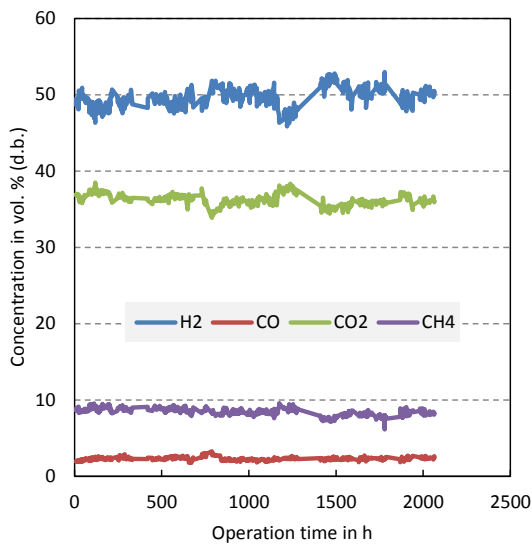
(c) Main gas composition at the outlet of reactor B
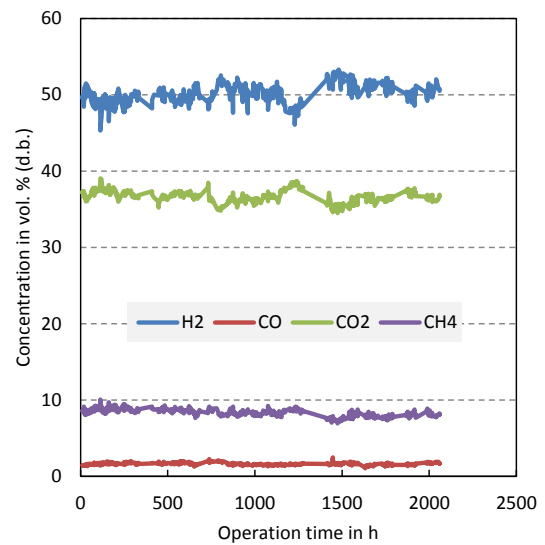
(d) Main gas composition at the outlet of reactor C

Figure 5.8: Main gas composition (dry basis) measured upstream and downstream at each of the three WGS pilot unit's reactors processing wood gas, extracted upstream of the RME gas scrubber during the long term test run [27].
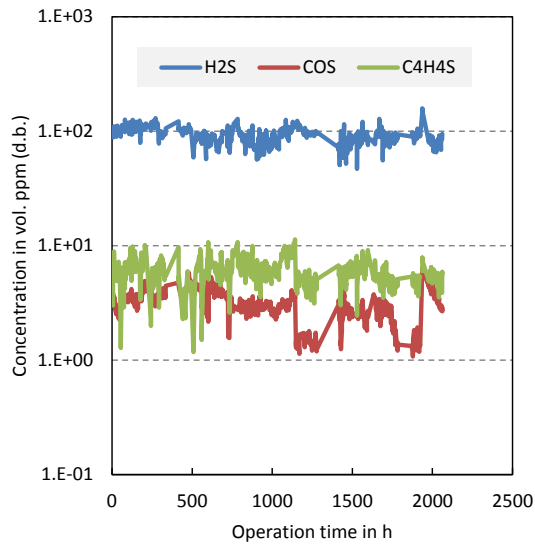
(a) Main sulfur components at the inlet
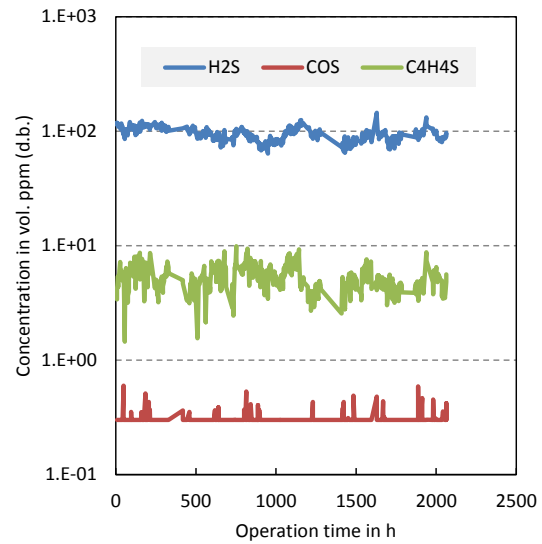
(b) Main sulfur components at the outlet of reactor A
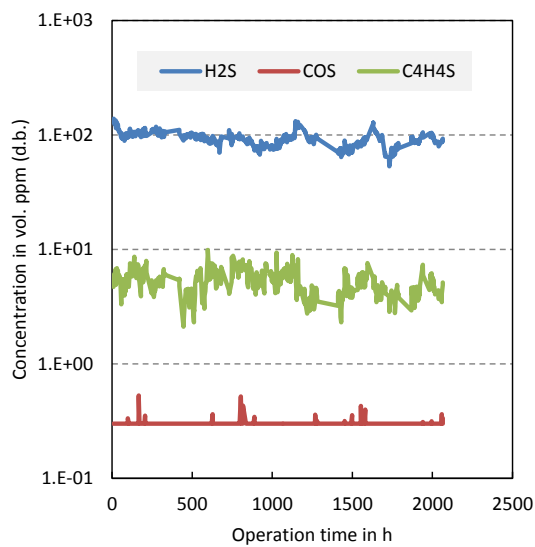
(c) Main sulfur components at the outlet of reactor B
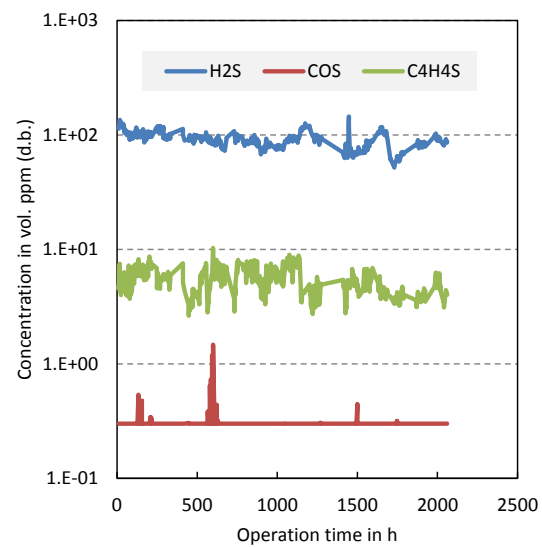
(d) Main sulfur components at the outlet of reactor C

Figure 5.9: Main sulfur components (dry basis) measured upstream and downstream at each of the three WGS pilot unit's reactors processing wood gas, extracted upstream of the RME gas scrubber during the long term test run [27].

During this long term test run processing tar-rich wood gas, extracted upstream of the DFB plant's RME scrubber, two GCMS tar measurements and one ammonia measurement, each time a WGS pilot unit's inlet/outlet pair of samples, were performed.

First, the ammonia measurement is presented. Table 5.7 shows the measured values for the inlet and the outlet concentration as well as the calculated ammonia conversion rate, defined in 4.9 which takes the increase of the volumetric dry gas flow rate (shown in Tables 5.5) into consideration. The measurement shows a decrease of the ammonia concentration along the WGS pilot unit caused by dilution. However, there was nearly no conversion of ammonia along the WGS pilot unit. Table 5.23 in Section 5.5 shows the results of all ammonia measurements carried out.

Table 5.7: Result of the ammonia measurement at the WGS pilot unit's inlet and outlet while processing tar-rich wood gas, extracted upstream of the DFB gasification plant's RME scrubber in $mol.ppm_{db}$, based on [28].

Date	Hours of Operation	Inlet	Outlet	X_{NH_3}
April 2015	$\sim 2050\ h$	2383	1869	0.03

Within this work, the influence of the WGS pilot unit on the amount of GCMS tar was investigated. Figure 5.10 and Table 5.8 show the results of the GCMS tar measurement performed after around 400 hours of the long term test run processing tar-rich wood gas, extracted upstream of the DFB plant's RME scrubber, in January 2015. Figure 5.10 illustrates the temperature profiles of the three WGS pilot unit's reactors at the time of sampling and the change of concentration of the three main GCMS tar substance groups without taking the dilution effect caused by the higher volumetric dry gas flow rate into account.

Table 5.8 shows the detected GCMS tar components and the classified GCMS tar substance groups in more detail. Measured values for the inlet and the outlet GCMS tar concentration are shown as well as the calculated tar conversion rate, defined in 4.8 which takes the increase of the volumetric dry gas flow rate (see Tables 5.5) into consideration. This GCMS tar measurement, performed in January 2015, was the measurement with the highest GCMS tar concentration. Table 5.8 indicates a conversion rate of the total GCMS tar of 11 %. The aromatic compounds showed a conversion rate of 75%. On the other hand, there was an increase of the amount of polycyclic aromatic hydrocarbons with a conversion rate of -7 %. This was the only pair of GCMS tar measurements which showed this increase in polycyclic aromatic hydrocarbons.
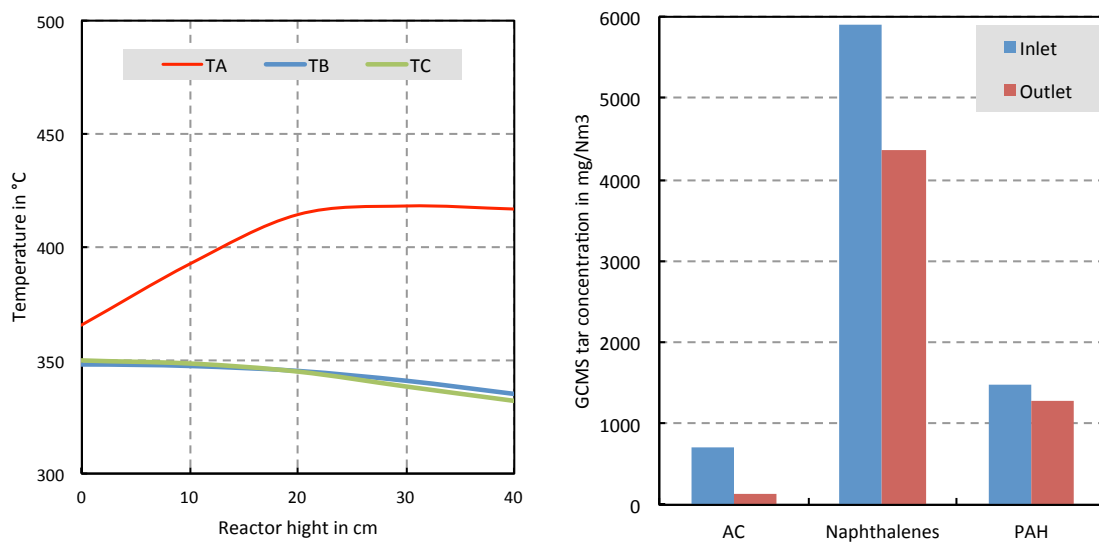
(a) Temperature profiles of the three WGS pilot unit reactors at the GCMS tar sampling.
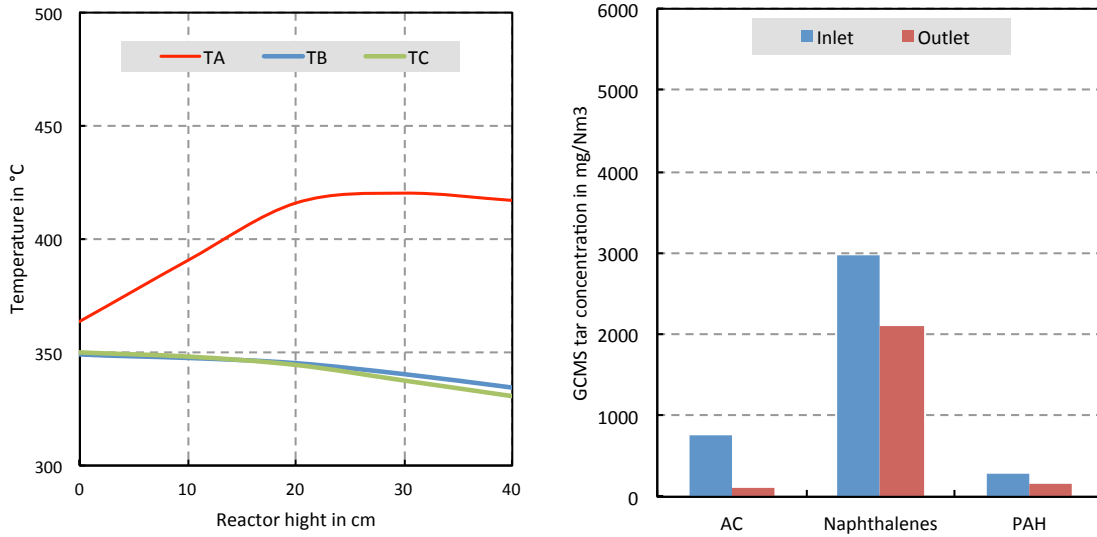
(b) Main GCMS tar substance groups.

Figure 5.10: Overview of the GCMS tar analysis (dry basis) in January 2015 during the long term test run, measured at the inlet and at the outlet of the WGS pilot unit after ∼400 hours of operation, based on [28].

Table 5.8: Detailed result of the GCMS tar measurement in January 2015 at the WGS pilot unit's inlet and outlet while processing wood gas, extracted upstream of the DFB gasification plant's RME scrubber in $\frac{mg}{m_{N,db}^3}$, GCMS tar DL 1 $\frac{mg}{m_{N,db}^3}$, based on [28].

January 2015	Inlet	Outlet	X_{tar}
Naphthalene	5804	4291	0.08
Styrene	272	32	0.85
1H-Indene	376	109	0.64
Phenylacetylene	47	BDL	0.96 to 1.00
Mesitylene	BDL	BDL	—
Benzofuran	2	BDL	0.38 to 1.00
Dibenzofuran	48	36	0.07
1-Benzothiophene	7	5	0.11
2-Methylnaphthalene	57	38	0.17
1-Methylnaphthalene	34	25	0.09
Biphenyl	57	44	0.04
Acenaphthylene	835	47	0.93
Acenaphthene	24	506	-25.14
Anthracene	375	467	-0.54
Flouranthene	38	56	-0.83
Pyrene	29	44	-0.88
Flourene	71	56	0.02
Quinoline	6	4	0.17
Phenol	2	BDL	0.38 to 1.00
Isoquinoline	1	BDL	0.24 to 1.00
Cresol	BDL	BDL	—
Phenanthrene	49	55	-0.39
4,5-Methylphenanthrene	11	14	-0.58
Indole	BDL	BDL	—
Sorted into GCMS tar substance groups, compare Section 4.3.			
Aromatic compounds	695	141	0.75
Naphthalenes	5895	4354	0.08
Others	59	41	0.14
Polycyclic aromatic hydrocarbons	1496	1293	-0.07
Total GCMS tar	8145	5829	0.11

Figure 5.11 and Table 5.9 show the results of the GCMS tar measurement performed after around 1700 hours of long term operation processing tar-rich wood gas, extracted upstream of the DFB plant's RME scrubber, in April 2015. The results of the GCMS tar measurements, carried out in February and in March 2015 are presented in the following sections, regarding the load conditions of operation at the time of sampling.

(a) Temperature profiles of the three WGS pilot unit reactors at the GCMS tar sampling.

(b) Main GCMS tar substance groups.

Figure 5.11: Overview of the GCMS tar analysis (dry basis) in April 2015 during the long term test run, measured at the inlet and at the outlet of the WGS pilot unit after ∼2050 hours of operation, based on [28].

Table 5.25 in Section 5.5 summarizes all results of a GCMS tar measurements at the WGS pilot unit's inlet and outlet while processing tar-rich wood gas, extracted upstream of the DFB gasification plant's RME scrubber.

Table 5.9: Detailed result of the GCMS tar measurement in April 2015 at the WGS pilot unit's inlet and outlet while processing wood gas, extracted upstream of the DFB gasification plant's RME scrubber in $\frac{mg}{m_{N,db}^3}$, GCMS tar DL 1 $\frac{mg}{m_{N,db}^3}$, based on [28].

April 2015	Inlet	Outlet	X_{tar}
Naphthalene	2925	2069	0.12
Styrene	253	31	0.85
1H-Indene	220	39	0.78
Phenylacetylene	25	BDL	0.95 to 1.00
Mesitylene	BDL	BDL	—
Benzofuran	2	2	-0.24
Dibenzofuran	6	4	0.17
1-Benzothiophene	5	3	0.26
2-Methylnaphthalene	28	15	0.34
1-Methylnaphthalene	19	10	0.35
Biphenyl	25	17	0.16
Acenaphthylene	196	3	0.98
Acenaphthene	26	122	-4.82
Anthracene	13	9	0.14
Flouranthene	3	4	-0.65
Pyrene	3	4	-0.65
Flourene	5	2	0.50
Quinoline	3	BDL	0.59 to 1.00
Phenol	BDL	BDL	—
Isoquinoline	BDL	BDL	—
Cresol	BDL	BDL	—
Phenanthrene	1	1	-0.24
4,5-Methylphenanthrene	BDL	BDL	—
Indole	4	BDL	0.69 to 1.00
Sorted into GCMS tar substance groups, compare Section 4.3.			
Aromatic compounds	502	70	0.83
Naphthalenes	2972	2094	0.13
Others	13	9	0.14
Polycyclic aromatic hydrocarbons	275	162	0.14
Total GCMS tar	3762	2335	0.23

5.3 DFB Biomass Steam Gasification Plant at Partial Load Operation

This section provides the results of about 100 hours of steady partial load operation of the DFB plant and the results of operation of the WGS pilot unit processing tar-rich wood gas, extracted upstream the RME scrubber at this steady partial load operation of the DFB plant.

The partial load condition of the DFB steam gasification plant was caused by a technical shortcoming in one of the two CHP plant's gas engines. Consequently the wood gas production was reduced to power only one gas engine. As a result, the amount of produced wood gas was decreased form $2299.5 \pm 78.3 \; \frac{m^3_{N,db}}{h}$ to $1325.6 \pm 90.3 \; \frac{m^3_{N,db}}{h}$. Furthermore, the water content in the wood gas increased. This was caused by feeding the same amount of steam, used as fluidization medium, and less biomass into the gasifier. During the full load operation the wood gas water content was $39.9 \; mol.\%_{wb}$. During the partial load operation the water content of the wood gas increased to $46.3 \; mol.\%_{wb}$. These values were calculated using the the DFB plant's data of the amount of condensate, which occurs at the DFB gasification plant's RME scrubber.

In this thesis, 100 hours of steady DFB biomass gasification plant's operation at full load conditions, Figure 5.12(a) and 100 hours of it's partial load conditions, Figure 5.12(b) were analyzed. Figure 5.12 illustrates the change in the main gas composition during the partial load operation. The detailed average gas composition of both points of operation are shown in Table 5.10.

(a) Full load operation. (b) Partial load operation.
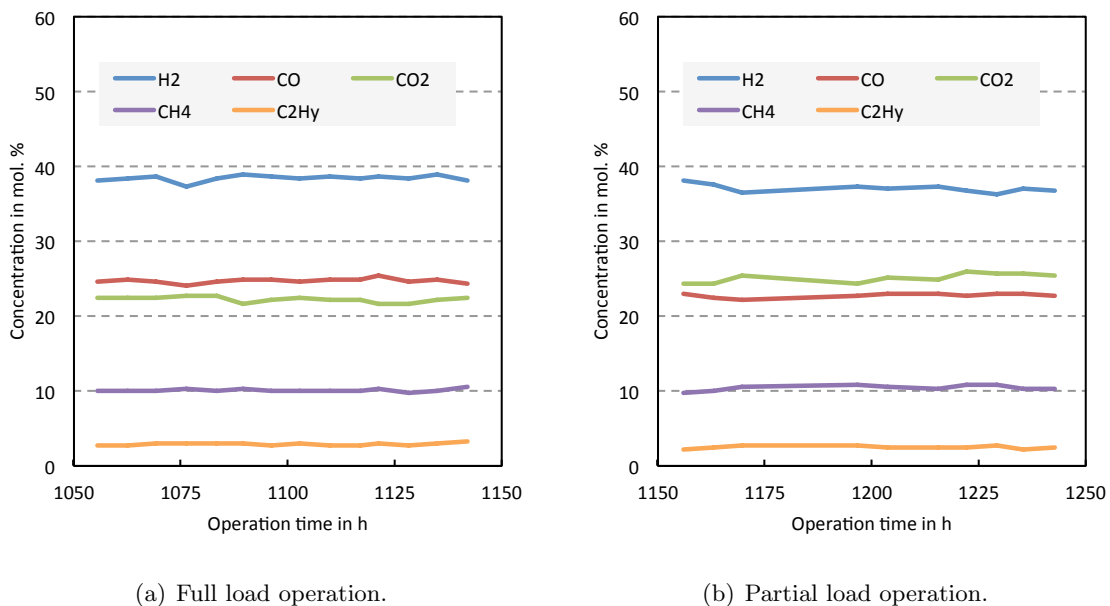
Figure 5.12: Main wood gas composition (dry basis) at full load operation of the DFB biomass steam gasification plant (a) and at partial load operation of the DFB biomass steam gasification plant (b).

Table 5.10: The average concentrations of the main gas components and sulfur components during 100 hours of full load operation and 100 hours of partial load operation of the DFB biomass steam gasification plant Oberwart, Austria, based on [26].

	H_2	CO	CO_2	CH_4	C_2H_y
	mol.%$_{db}$	mol.%$_{db}$	mol.%$_{db}$	mol.%$_{db}$	mol.%$_{db}$
Full load	38.4 ± 0.5	24.8 ± 0.6	22.3 ± 0.6	10.1 ± 0.2	2.9 ± 0.2
Partial load	37.1 ± 0.9	22.7 ± 0.6	25.2 ± 0.7	10.4 ± 0.4	2.5 ± 0.3
	N_2	O_2	H_2S	COS	C_4H_4S
	mol.%$_{db}$	mol.%$_{db}$	mol.ppm$_{db}$	mol.ppm$_{db}$	mol.ppm$_{db}$
Full load	1.5 ± 0.7	0.08 ± 0.01	103 ± 09	3.3 ± 0.3	8.5 ± 1.0
Partial load	2.0 ± 0.7	0.08 ± 0.02	101 ± 09	1.5 ± 0.5	4.7 ± 0.8

The data, generated during the DFB biomass gasification plant's partial load operation, serves as a basis for a conference publication which has been carried out in collaboration with Kraussler et al. [26].

During the examined period, the average gasifier temperature was 867 °C at full load operation and 876 °C at partial load operation. Even though the gasifier temperature is higher during partial load, the change of wood gas composition is quite the opposite, which can be found in literature [11, 19].

In Figure 5.13, the influence of the gasifier temperature on the wood gas composition is shown. On the one hand, with increasing gasifier temperature, hydrogen and carbon monoxide concentrations are increasing. On the other hand carbon, dioxide and methane are decreasing.
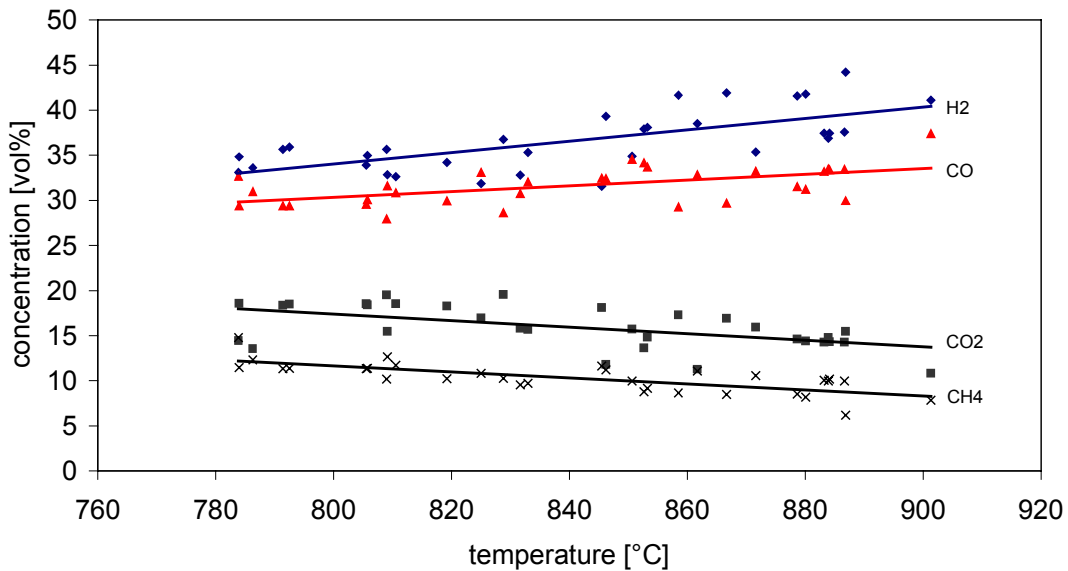
Figure 5.13: Dependency of the wood gas composition on the gasifier's temperature using the DFB biomass steam gasification technology [11].

Another impact on the wood gas composition is the water content. During partial load operation, the water content in the wood gas is higher, which leads to a higher steam to fuel ratio. In Figure 5.14, the dependency of the gas composition on the steam to fuel ratio for a temperature range between 850 to 900 °C is shown.
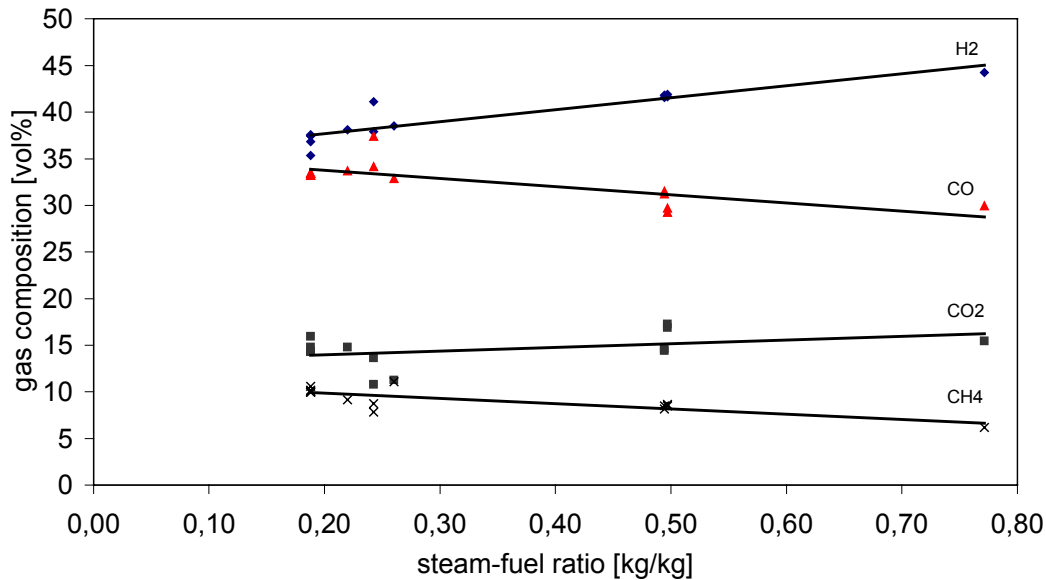
Figure 5.14: Dependency of the wood gas composition on the steam to fuel ration using the DFB biomass steam gasification technology [11].

Those tendencies show more consistency with the wood gas composition, recorded during the partial load operation. This leads to the conclusion that the change of the wood gas composition during the partial load operation is mainly caused by the higher water content, respectively the higher steam ratio.

During this DFB biomass steam gasification plant's partial load operation the WGS pilot unit was operated with the same settings as for the long term test run. The constant water addition in combination with the higher wood gas water content, led to a $STDGR$ of more than 1.9, shown in Table 5.11.

In addition, also caused by the lower amount of carbon monoxide in the wood gas, the $STCOR$ even increased to 8.45. The performance of the WGS pilot unit, expressed by using the carbon monoxide conversion, is in the same range as operating at full load operation and therefore, not affected by the higher steam content. Table 5.12 shows the carbon monoxide conversion and other results of this point of operation.

Table 5.11: Operating conditions of the WGS pilot unit processing tar-rich wood gas, extracted upstream of the RME gas scrubber, at partial load operation of the DFB biomass steam gasification plant for 100 hours. All figures are given for the WGS pilot unit's inlet, based on [26].

Overall catalyst volume	7.8	L
Catalyst volume per reactor	2.6	L
Water content wood gas	46.3	$mol.\%_{wb}$
Water content inlet WGS pilot unit	65.7	$mol.\%_{wb}$
Volumetric flow rate dry	1.11	$\frac{m^3_{N,db}}{h}$
Volumetric flow rate wet	3.24	$\frac{m^3_{N,wb}}{h}$
STDGR	1.92	-
STCR	3.15	-
STCOR	8.45	-
Temperature setpoint inlet each reactor	350	$^{\circ}C$
$GHSV_{wb}$ overall	415	h^{-1}
$GHSV_{wb}$ per reactor	1246	h^{-1}

Table 5.12: Results of the WGS pilot unit operation processing tar-rich wood gas, extracted upstream of the RME gas scrubber, at partial load operation of the DFB biomass steam gasification plant for 100 hours. Operating conditions according to Table 5.4, based on [26]

	$GHSV_{wb}$	$\Delta\dot{V}_{db}$	H_2rec	X_{CO}
Outlet reactor A	1246 h^{-1}	1.19	1.50	0.78
Outlet reactor B	623 h^{-1}	1.21	1.56	0.88
Outlet WGS pilot unit	415 h^{-1}	1.21	1.68	0.92

By taking a closer look at the temperature profile of reactor A, illustrated in Figure 5.15(a), it can be seen that the temperature increased to 400 °C. In comparison, at full load operation, the temperature in reactor A increased significantly higher caused by the higher CO amount and consequently more heat of WGS reaction.

Figures 5.16 and 5.17 show the temperature profiles of reactor B and reactor C as well as the changes of the reactive WGS components in reactor B and reactor C. Again, caused of the already low carbon monoxide content downstream reactor A, there is no noticeable temperature increase in reactor B and reactor C. Also the changes in the reactive WGS components along those two reactors are insignificant.

The detailed average wood gas composition at the WGS pilot unit's inlet and at each reactor's outlet, processing wood gas, extracted upstream of the RME scrubber during partial load operation of the DFB gasification plant, is shown in Table 5.18.

(a) Temperature profile of reactor A

(b) Reactive components of reactor A
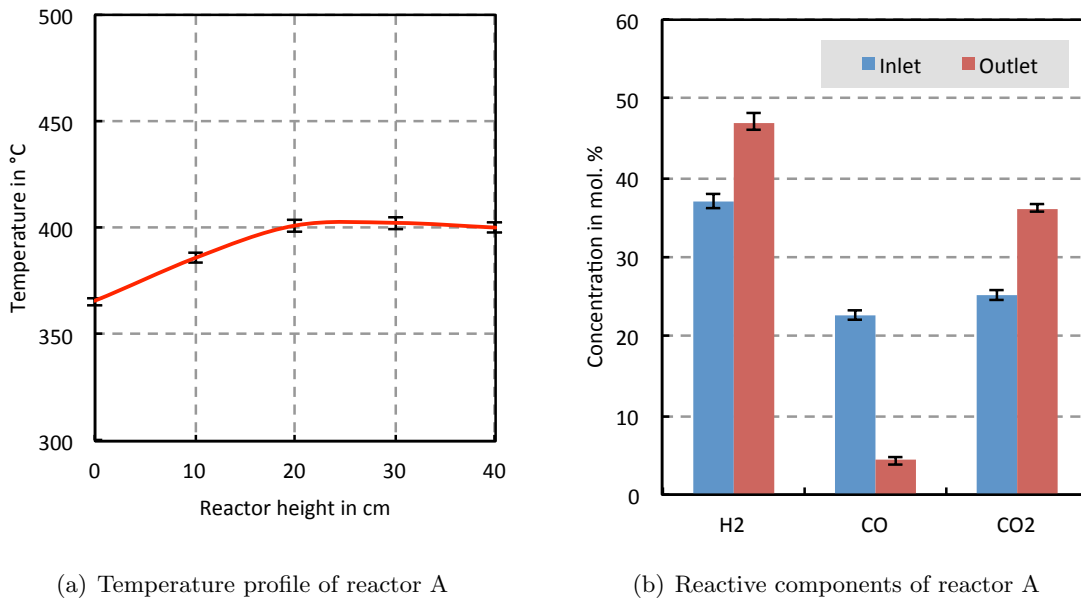
Figure 5.15: The average temperature profile and the average concentration (dry basis) of the reactive WGS components for reactor A processing tar-rich wood gas, extracted upstream of the RME gas scrubber, at partial load operation of the DFB biomass steam gasification plant for 100 hours, based on [26].

(a) Temperature profile of reactor B

(b) Reactive components of reactor B
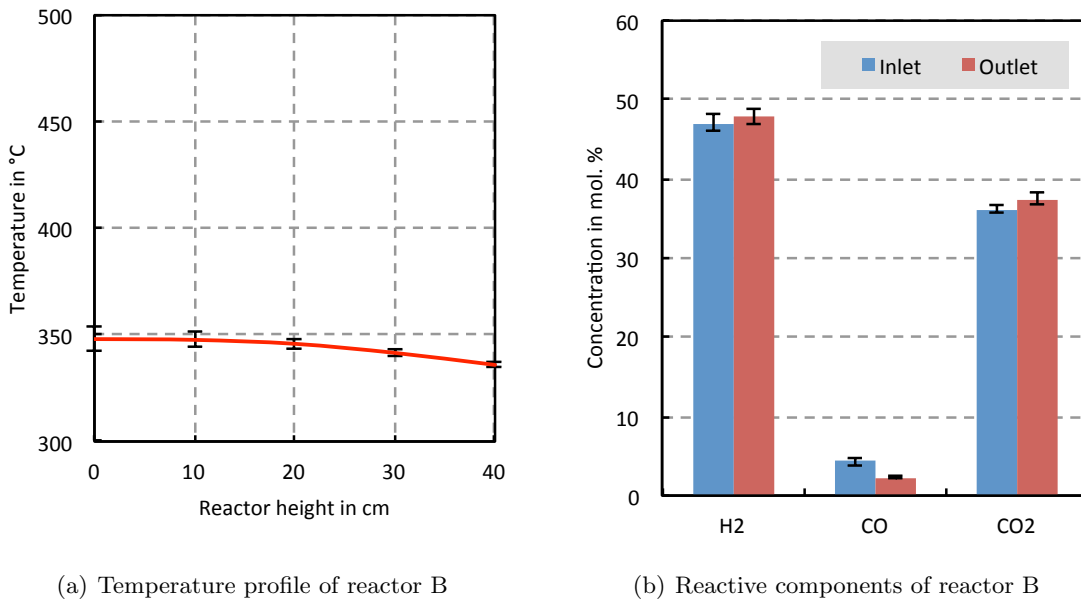
Figure 5.16: The average temperature profile and the average concentration (dry basis) of the reactive WGS components for reactor B processing tar-rich wood gas, extracted upstream of the RME gas scrubber, at partial load operation of the DFB biomass steam gasification plant for 100 hours, based on [26].

(a) Temperature profile of reactor C

(b) Reactive components of reactor C
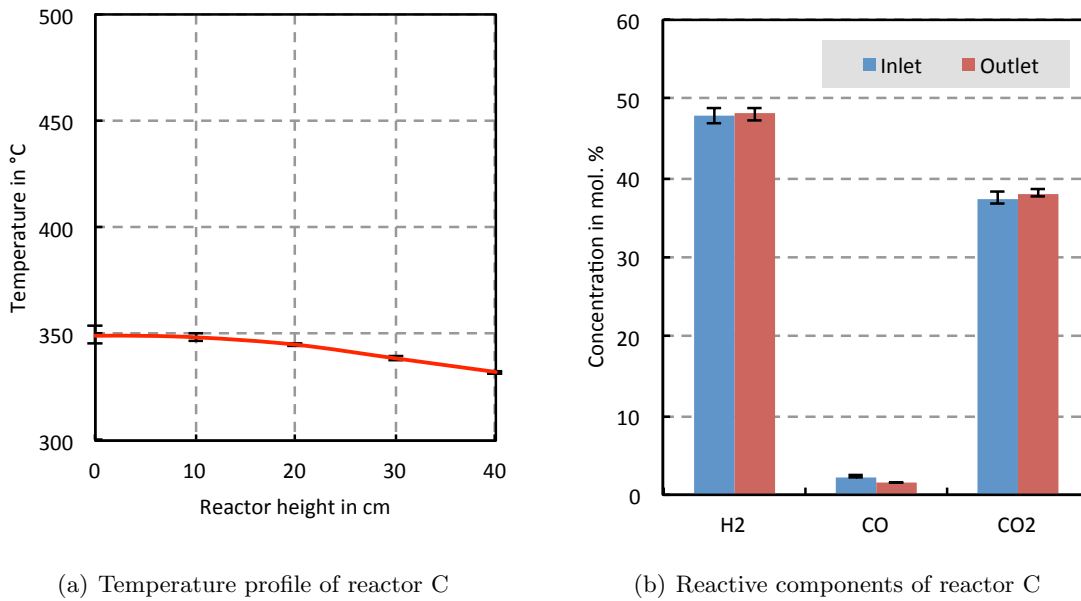
Figure 5.17: The average temperature profile and the average concentration (dry basis) of the reactive WGS components for reactor C processing tar-rich wood gas, extracted upstream of the RME gas scrubber, at partial load operation of the DFB biomass steam gasification plant for 100 hours, based on [26].

Table 5.13: The average concentrations of the main gas components and sulfur components along the WGS pilot unit processing tar-rich wood gas, extracted upstream of the RME gas scrubber, at partial load operation of the DFB biomass steam gasification plant for 100 hours. DL sulfur components: 0.3 mol.ppm$_{db}$, based on [26].

	H_2 mol.%$_{db}$	CO mol.%$_{db}$	CO_2 mol.%$_{db}$	CH_4 mol.%$_{db}$	C_2H_y mol.%$_{db}$
Inlet WGS pilot unit	37.1 ± 0.9	22.7 ± 0.6	25.2 ± 0.7	10.4 ± 0.4	2.5 ± 0.3
Outlet reactor A	47.1 ± 1.0	4.3 ± 0.5	36.2 ± 0.6	8.9 ± 0.3	2.0 ± 0.2
Outlet reactor B	47.9 ± 1.0	2.3 ± 0.1	37.5 ± 0.7	8.7 ± 0.3	2.0 ± 0.2
Outlet WGS pilot unit	48.1 ± 0.8	1.5 ± 0.1	38.1 ± 0.4	8.7 ± 0.3	1.9 ± 0.2
	N_2 mol.%$_{db}$	O_2 mol.%$_{db}$	H_2S mol.ppm$_{db}$	COS mol.ppm$_{db}$	C_4H_4S mol.ppm$_{db}$
Inlet WGS pilot unit	2.0 ± 0.7	0.08 ± 0.02	101 ± 09	1.5 ± 0.5	4.7 ± 0.8
Outlet reactor A	1.5 ± 0.5	0.03 ± 0.01	104 ± 11	BDL	4.0 ± 0.7
Outlet reactor B	1.6 ± 0.7	0.03 ± 0.01	101 ± 18	BDL	3.8 ± 1.2
Outlet WGS pilot unit	1.6 ± 0.5	0.03 ± 0.01	106 ± 10	BDL	3.9 ± 0.7

One GCMS tar measurement and one ammonia measurement, each time a WGS pilot unit's inlet/outlet pair of samples, was performed during the DFB plant operated at partial load operation.

Table 5.14 shows the result and the conversion rate of the ammonia measurements carried out at partial load operation of the DFB biomass steam gasification plant. The calculated ammonia conversion rate considers the increase of the volumetric dry gas flow rate shown in Table 5.12. Ammonia was not converted in the WGS pilot unit.

Table 5.14: Result of the ammonia measurement at the WGS pilot unit's inlet and outlet while processing tar-rich wood gas, extracted upstream of the DFB gasification plant's RME scrubber, at partial load operation of the DFB biomass steam gasification plant in $mol.ppm_{db}$, based on [28].

Date	Hours of Operation	Inlet	Outlet	X_{NH_3}
February 2015	$\sim 1200\ h$	3395	2840	-0.01

Figure 5.18 and Table 5.15 show the results of the GCMS tar measurement performed after around 1200 hours of long term operation at partial load operation of the DFB biomass steam gasification plant, in February 2015.
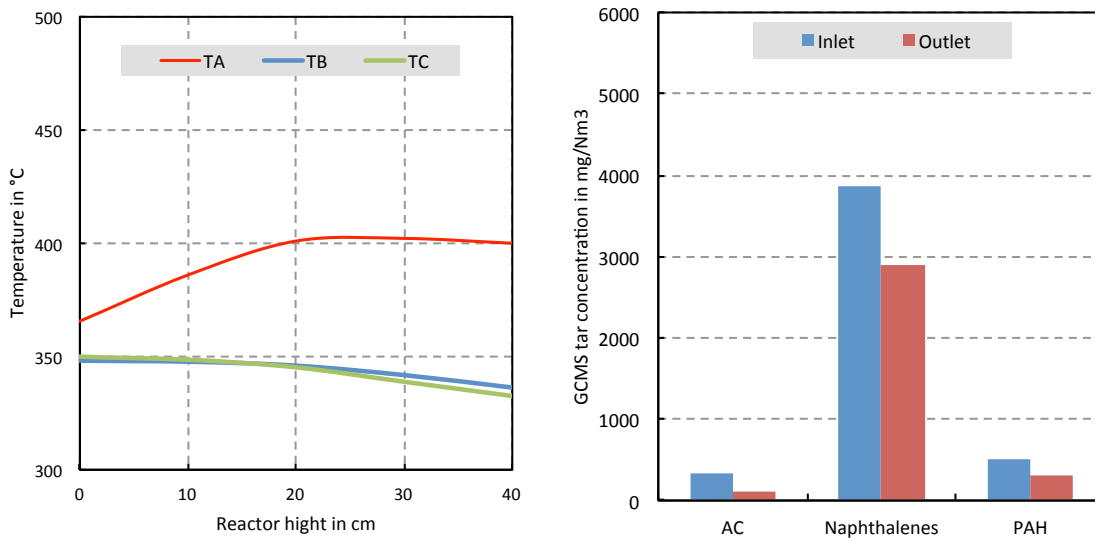
(a) Temperature profiles of the three WGS pilot unit reactors at the GCMS tar sampling.

(b) Main GCMS tar substance groups.

Figure 5.18: Overview of the GCMS tar analysis (dry basis) in February 2015 during the long term test run, measured at the inlet and at the outlet of the WGS pilot unit after ~1200 hours of operation, based on [28].

The GCMS tar analysis for the tar sample at partial load operation of the DFB biomass steam gasification plant showed a comparative low amount of Styrene and 1H-Indene. In general, it seems that the partial load operation condition of the DFB plant did not affect the amount of total GCMS tar.

Table 5.15: Detailed result of the GCMS tar measurement in February 2015 at the WGS pilot unit's inlet and outlet while processing wood gas, extracted upstream of the DFB gasification plant's RME scrubber in $\frac{mg}{m^3_{N,db}}$, GCMS tar DL 1 $\frac{mg}{m^3_{N,db}}$, based on [28].

February 2015	Inlet	Outlet	X_{tar}
Naphthalene	3822	2870	0.09
Styrene	166	38	0.72
1H-Indene	138	65	0.43
Phenylacetylene	25	BDL	0.95 to 1.00
Mesitylene	BDL	BDL	—
Benzofuran	BDL	BDL	—
Dibenzofuran	8	7	-0.06
1-Benzothiophene	7	5	0.14
2-Methylnaphthalene	26	21	0.02
1-Methylnaphthalene	18	15	-0.01
Biphenyl	24	21	-0.06
Acenaphthylene	233	6	0.97
Acenaphthene	37	190	-5.21
Anthracene	118	46	0.53
Flouranthene	33	18	0.34
Pyrene	30	17	0.31
Flourene	9	6	0.19
Quinoline	1	BDL	—
Phenol	BDL	BDL	—
Isoquinoline	BDL	BDL	—
Cresol	BDL	BDL	—
Phenanthrene	11	4	0.56
4,5-Methylphenanthrene	4	2	0.40
Indole	BDL	BDL	—
Sorted into GCMS tar substance groups, compare Section 4.3.			
Aromatic compounds	329	103	0.62
Naphthalenes	3866	2906	0.09
Others	15	12	0.03
Polycyclic aromatic hydrocarbons	500	310	0.25
Total GCMS tar	4710	3331	0.14

5.4 WGS Pilot Unit at Partial Load Operation

Within this section, the results of 320 hours of WGS partial load operation are presented. This period, characterized by a reduced wood gas flow rate through the WGS pilot unit, took place during the long term test run, described in detail in Section 5.2.

The reduced wood gas flow rate through the WGS pilot unit was caused by a technical defect in the WGS pilot unit's gas membrane pump. During this period, the amount of added steam was reduced, in order to set the same $STDGR$ as during the long term test run (compare Table 5.4 and Table 5.16). This results in a lower $GHSV_{wb}$.

Table 5.16: Operating conditions of the WGS pilot unit processing wood gas, extracted upstream of the RME gas scrubber, at partial load operation of the WGS pilot unit for 320 hours. All figures are given for the WGS pilot unit's inlet.

Overall catalyst volume	7.8	L
Catalyst volume per reactor	2.6	L
Water content wood gas	39.9	$mol.\%_{wb}$
Water content inlet WGS pilot unit	61.4	$mol.\%_{wb}$
Volumetric flow rate dry	0.81	$\frac{m^3_{N,db}}{h}$
Volumetric flow rate wet	2.11	$\frac{m^3_{N,wb}}{h}$
$STDGR$	1.59	-
$STCR$	2.68	-
$STCOR$	6.27	-
Temperature setpoint	350	$°C$
$GHSV_{wb}$ overall	271	h^{-1}
$GHSV_{wb}$ per reactor	812	h^{-1}

The results of the WGS pilot unit operation processing wood gas with this low $GHSV_{wb}$ are summarized in Table 5.17. Even though the $GHSV_{wb}$ is significantly lower, the performance of the WGS pilot unit is nearly the same, as shown in Table 5.5 and Table 5.17.

Table 5.17: Results of the WGS pilot unit operation processing tar-rich wood gas, extracted upstream of the RME gas scrubber, at partial load operation of the WGS pilot unit for 320 hours. Operating conditions according to Table 5.16.

	$GHSV_{wb}$	$\Delta\dot{V}_{db}$	H_2rec	X_{CO}
Outlet reactor A	812 h^{-1}	1.20	1.52	0.78
Outlet reactor B	541 h^{-1}	1.22	1.57	0.89
Outlet WGS pilot unit	271 h^{-1}	1.23	1.60	0.93

The majority of the WGS reaction takes place in reactor A, as illustrated in Figure 5.19. There is a significant increase of the reactor temperature which indicates the presence of the WGS reaction, as observed in the points of operation described in the previous sections. Because of the lower CO amount and the associated less heat of reaction, the temperature

increase is considerably less than at full load operation of the WGS pilot unit (compare Figure 5.4). Furthermore, the heat losses become the majority and temperature distinctly decreases with reactor height. Especially the temperature profiles of reactor B, Figure 5.20, and reactor C, Figure 5.21, show a fast decrease of temperature, caused by the predominant heat losses.

(a) Temperature profile of reactor A

(b) Reactive components of reactor A
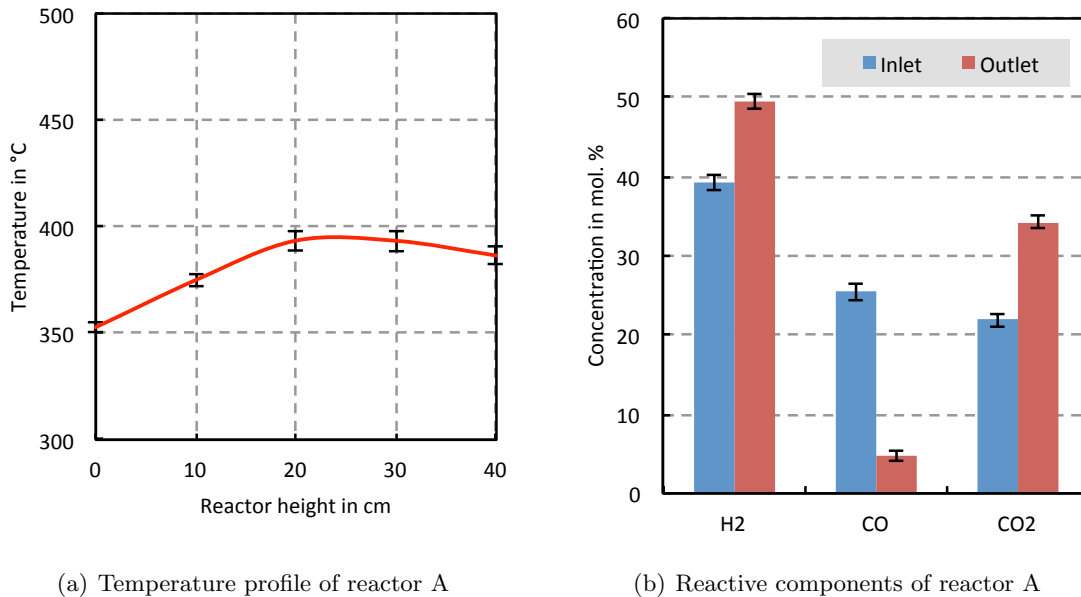
Figure 5.19: The average temperature profile and the average concentration (dry basis) of the reactive WGS components for reactor A processing tar-rich wood gas, extracted upstream of the RME gas scrubber, at partial load operation of the WGS pilot unit for 320 hours.

If the results from Section 5.1 and the results from the current section are compared, it can be seen that the $GHSV_{wb}$ is nearly the same. On the other hand, the $STDGR$ is at WGS pilot unit's partial load operation higher. This leads to a reduced dry gas flow rate and consequently less CO amount and the resulting less heat of reaction, even if the carbon monoxide conversion rates in Table 5.17 are slightly higher compared to the results in Table 5.2. Therefore, the maximum temperatures in Figures 5.19 to 5.21 are lower, because the heat losses were more dominant than at the operating conditions found in Section 5.1.

Table 5.18 shows the detailed average wood gas composition at the WGS pilot unit's inlet and also the gas composition at each reactor's outlet during the WGS pilot unit's partial load operation.

Comparing the WGS plant's results from different load operation, no significant differences regarding the performance and operating behavior could be observed. Consequently, nearly the same carbon monoxide conversion was reached. This leads to the conclusion that the WGS pilot unit and its Fe/Cr based catalyst performed well with a steady CO conversion above 91 %, even at partial load operation of the WGS pilot unit. Those results should

(a) Temperature profile of reactor B

(b) Reactive components of reactor B
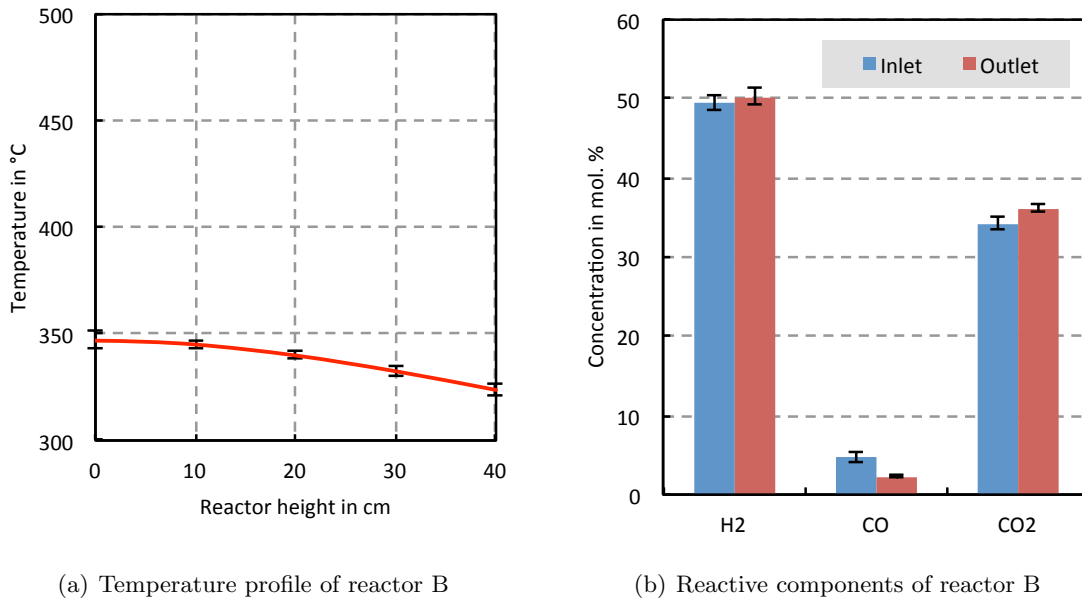
Figure 5.20: The average temperature profile and the average concentration (dry basis) of the reactive WGS components for reactor B processing tar-rich wood gas, extracted upstream of the RME gas scrubber, at partial load operation of the WGS pilot unit for 320 hours.

(a) Temperature profile of reactor C

(b) Reactive components of reactor C
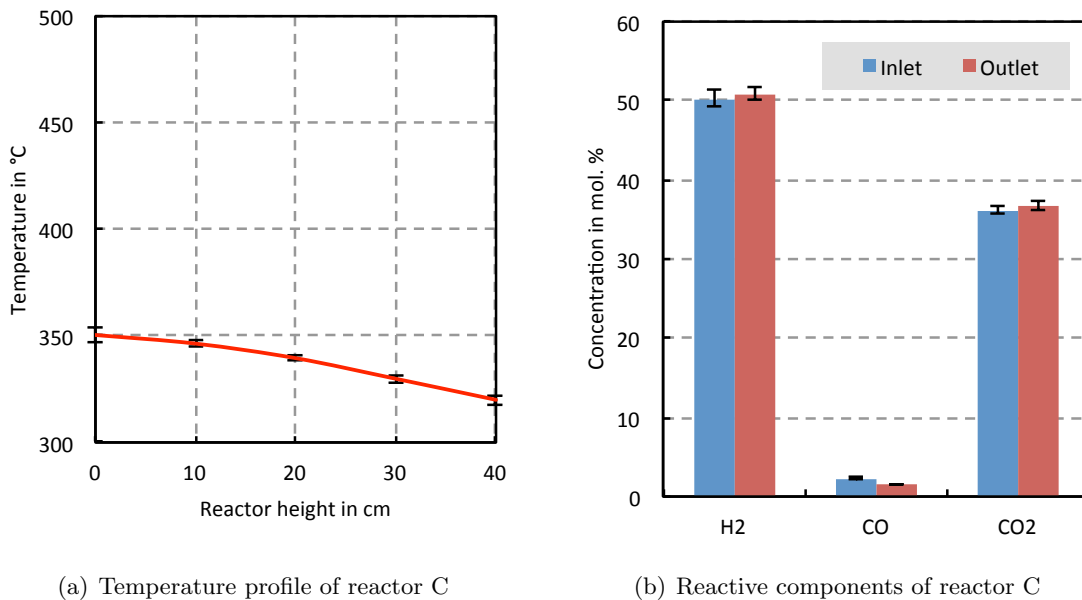
Figure 5.21: The average temperature profile and the average concentration (dry basis) of the reactive WGS components for reactor C processing tar-rich wood gas, extracted upstream of the RME gas scrubber, at partial load operation of the WGS pilot unit for 320 hours.

Table 5.18: The average concentrations of the main gas components and sulfur components along the WGS pilot unit processing tar-rich wood gas, extracted upstream of the RME gas scrubber, at partial load operation of the WGS pilot unit for 320 hours. DL sulfur components: 0.3 mol.ppm$_{db}$

	H_2 mol.%$_{db}$	CO mol.%$_{db}$	CO_2 mol.%$_{db}$	CH_4 mol.%$_{db}$	C_2H_y mol.%$_{db}$
Inlet WGS pilot unit	39.2 ± 0.9	25.4 ± 1.0	21.9 ± 0.9	9.6 ± 0.3	2.6 ± 0.2
Outlet reactor A	49.5 ± 0.9	4.7 ± 0.7	34.4 ± 0.9	8.2 ± 0.3	2.2 ± 0.2
Outlet reactor B	50.3 ± 1.0	2.3 ± 0.2	36.2 ± 0.5	8.0 ± 0.4	2.1 ± 0.2
Outlet WGS pilot unit	50.8 ± 0.8	1.5 ± 0.1	36.7 ± 0.5	7.9 ± 0.5	2.1 ± 0.2
	N_2 mol.%$_{db}$	O_2 mol.%$_{db}$	H_2S mol.ppm$_{db}$	COS mol.ppm$_{db}$	C_4H_4S mol.ppm$_{db}$
Inlet WGS pilot unit	1.2 ± 0.6	0.06 ± 0.01	90.6 ± 8.8	2.2 ± 0.7	4.9 ± 0.9
Outlet reactor A	1.0 ± 0.4	0.03 ± 0.04	89.5 ± 7.8	BDL	4.3 ± 0.6
Outlet reactor B	1.1 ± 0.5	0.02 ± 0.01	85.2 ± 12.2	BDL	4.0 ± 0.5
Outlet WGS pilot unit	1.0 ± 0.5	0.02 ± 0.00	83.4 ± 18.2	BDL	4.0 ± 0.5

provide the basis for further research activity in future aiming for a higher $GHSV_{wb}$ and less steam excess.

Table 5.19 shows the result of the ammonia measurement carried out at partial load operation of the WGS pilot unit. In addition, the ammonia conversion rate, based on the increase of the volumetric dry gas flow rate (see Table 5.17), through the WGS pilot unit is shown.

Table 5.19: Result of the ammonia measurement at the WGS pilot unit's inlet and outlet while processing tar-rich wood gas, extracted upstream of the DFB gasification plant's RME scrubber, at partial load operation of the WGS pilot unit in *mol.ppm$_{db}$*, based on [28].

Date	Hours of Operation	Inlet	Outlet	X_{NH_3}
March 2015	$\sim 1700\ h$	1924	1460	0.07

Figure 5.22 and Table 5.20 show the results of the GCMS tar measurement performed after around 1700 hours of long term operation at partial load operation of the WGS pilot unit, in March 2015.

This GCMS tar measurement of tar-rich wood gas, extracted upstream of the DFB gasification plant's RME scrubber showed the lowest value. The correlation between measured total amount of GCMS tar and time of nonstop operation of the DFB biomass steam gasification plant is discussed in Section 5.5. Table 5.24 in Section 5.5 shows the results of all GCMS tar measurements carried out (January 2015 to April 2015) and results from previous measurements. All those tar samples were taken from tar-rich wood gas upstream of the DFB plant's gas scrubber.

The conversion rate of total GCMS tar was 15 % at partial load operation of the WGS pilot unit. Compared to full load operation of the WGS pilot unit, which showed a conversion rate of total GCMS tar of 11 % to 23 %, it seems that the lower $GHSV_{wb}$ at partial load operation of the WGS pilot unit did not significant affect the GCMS tar reduction.
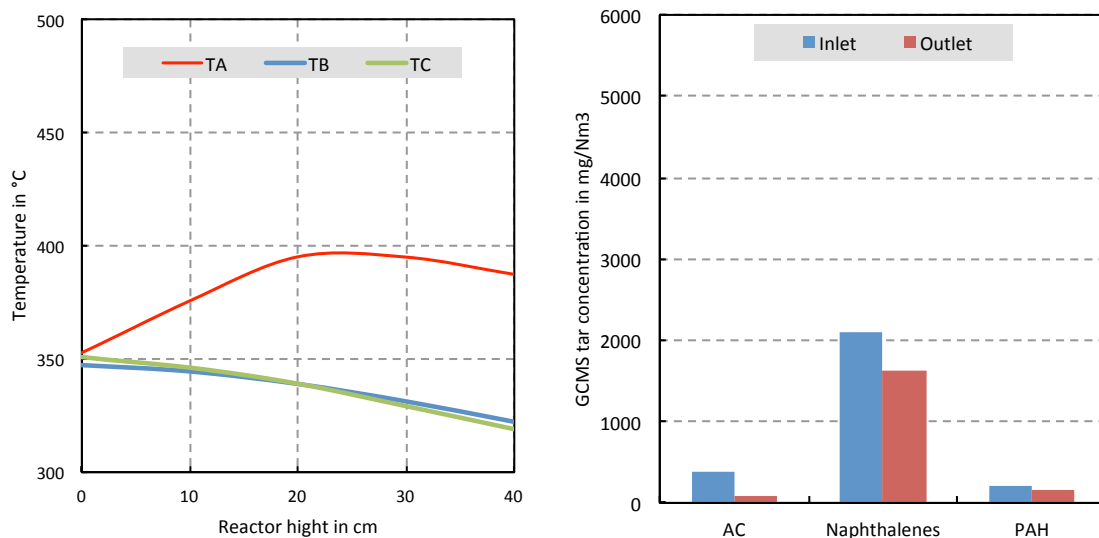
(a) Temperature profiles of the three WGS pilot unit reactors at the GCMS tar sampling.

(b) Main GCMS tar substance groups.

Figure 5.22: Overview of the GCMS tar analysis (dry basis) in March 2015 during the long term test, measured run at the inlet and at the outlet of the WGS pilot unit after ~1700 hours of operation, based on [28].

Table 5.20: Detailed result of the GCMS tar measurement in March 2015 at the WGS pilot unit's inlet and outlet while processing wood gas, extracted upstream of the DFB gasification plant's RME scrubber in $\frac{mg}{m^3_{N,db}}$, GCMS tar DL 1 $\frac{mg}{m^3_{N,db}}$, based on [28].

March 2015	Inlet	Outlet	X_{tar}
Naphthalene	2060	1595	0.05
Styrene	190	20	0.87
1H-Indene	165	47	0.65
Phenylacetylene	24	BDL	0.95 to 1.00
Mesitylene	1	7	-7.61
Benzofuran	2	2	-0.23
Dibenzofuran	5	5	-0.23
1-Benzothiophene	5	3	0.26
2-Methylnaphthalene	22	19	-0.06
1-Methylnaphthalene	15	13	-0.07
Biphenyl	15	12	0.02
Acenaphthylene	128	7	0.93
Acenaphthene	17	103	-6.45
Anthracene	19	15	0.03
Flouranthene	8	6	0.08
Pyrene	7	6	-0.05
Flourene	5	5	-0.23
Quinoline	1	1	-0.23
Phenol	2	2	-0.23
Isoquinoline	BDL	BDL	—
Cresol	BDL	BDL	—
Phenanthrene	4	3	0.08
4,5-Methylphenanthrene	2	2	-0.23
Indole	BDL	BDL	—
Sorted into GCMS tar substance groups, compare Section 4.3.			
Aromatic compounds	380	74	0.76
Naphthalenes	2097	1627	0.05
Others	14	12	-0.05
Polycyclic aromatic hydrocarbons	206	160	0.04
Total GCMS tar	2697	1873	0.15

5.5   Summary of the Experimental Results

This section provides an overview of the four WGS pilot unit points of operation, which were investigated and discussed in detail in the previous sections:

- **Operating point 1** Processing wood gas, extracted downstream of the DFB plant's RME scrubber. (Section 5.1)

- **Operating point 2** Processing tar-rich wood gas, extracted upstream of the DFB plant's RME scrubber. (Section 5.2)

- **Operating point 3** Processing tar-rich wood gas, extracted upstream of the DFB plant's RME scrubber, at partial load operation of the DFB biomass steam gasification plant. (Section 5.3)

- **Operating point 4** Processing tar-rich wood gas, extracted upstream of the DFB plant's RME scrubber, at partial load operation of the WGS pilot unit. (Section 5.4)

Table 5.21 gives a summary of the WGS pilot unit operating points. In operating point 1 wood gas, extracted downstream of the DFB plant's RME scrubber was processed. In operation points 2 to 4 tar-rich wood gas, extracted upstream of the DFB plant's RME scrubber was processed. To minimize the possibility of coking and carbon deposition on the surface of the catalyst, the WGS pilot unit was operated with a significant excess of steam. Because of this, the $STDGR$ for operating points 2 to 4 was significantly higher, than for operating point 1. The WGS pilot unit has proven to be reliable and robust, even partial load operation did not affect the performance in a negative way.

Table 5.21: Overview of the results and operation conditions of the WGS pilot unit for each point of operation, based on [23, 26, 27].

Operating point	1	2	3	4	
$GHSV_{wb}$	286	415	415	271	h^{-1}
$\dot{V}_{db}$	1.02	1.24	1.11	0.81	$\frac{m^3_{N,db}}{h}$
$STDGR$	1.18	1.61	1.92	1.59	-
$STCOR$	5.05	6.46	8.45	6.27	-
$\Delta\dot{V}_{db}$	1.21	1.24	1.21	1.23	-
H_2rec	1.56	1.61	1.68	1.60	-
X_{CO}	0.92	0.92	0.92	0.93	-

Figure 5.23 shows the temperature profiles of reactor A at each operating point. The temperature profile of operating point 1 showed the most significant difference, caused by different flow conditions and the comparatively low $STDGR$. The temperature profiles of operation points 2 to 4 showed the same shape. The maximum temperature varied, depending on the volumetric dry gas flow rate and, consequently, on the amount of carbon monoxide and the related heat of the exothermic WGS reaction.
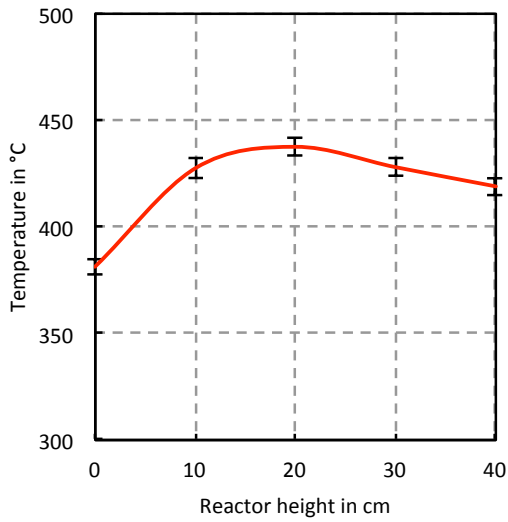
(a) Operating point 1
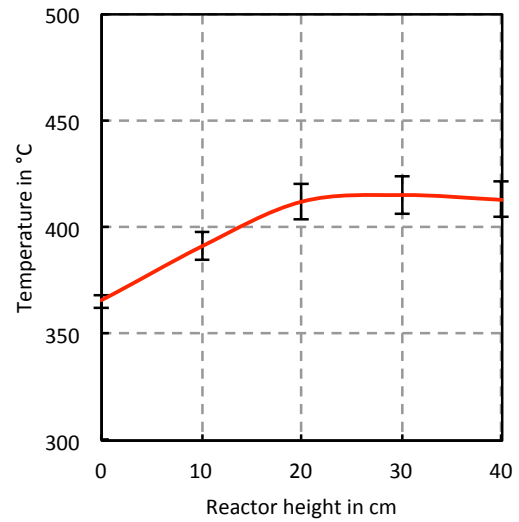
(b) Operating point 2
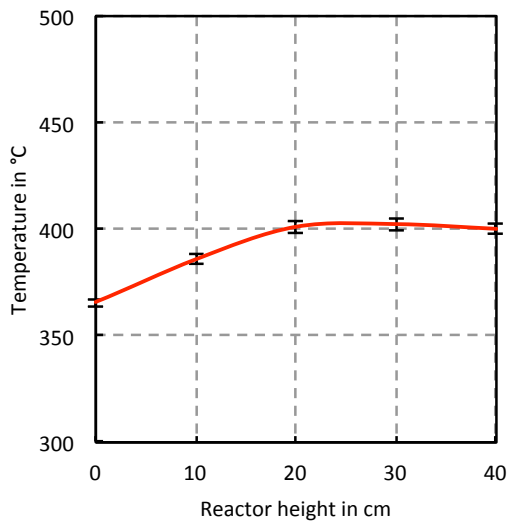
(c) Operating point 3
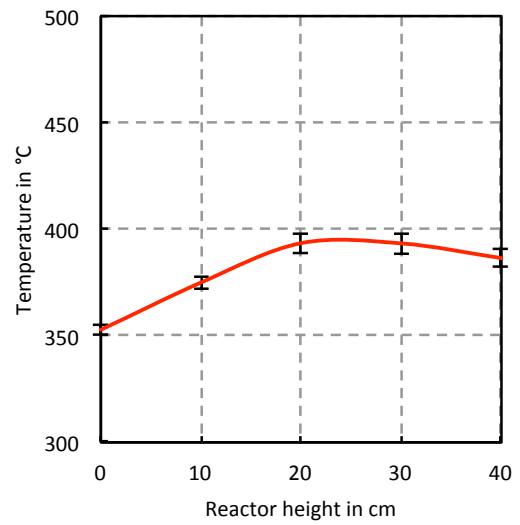
(d) Operating point 4

Figure 5.23: Overview of the average temperature profiles for reactor A at each point of operation, based on [23, 26, 27].

During the long term test run of the WGS pilot unit, processing tar-rich wood gas extracted upstream of the DFB gasification plant's RME scrubber, GCMS tar and ammonia measurements were performed. Table 5.22 shows the load conditions and the corresponding hours of operation.

Table 5.22: Load conditions of operation and approximate hours of operation of the long term test run processing tar-rich wood gas extracted upstream of the DFB plant's RME gas scrubber, based on [28].

Sample	Date	Hours of operation	Operating point	Load conditions DFB plant	Load conditions WGS pilot unit
GCMS Tar	January 2015	$\sim 400\ h$	2	full	full
GCMS Tar and NH$_3$	February 2015	$\sim 1200\ h$	3	partial	full
GCMS Tar and NH$_3$	March 2015	$\sim 1700\ h$	4	full	partial
GCMS Tar and NH$_3$	April 2015	$\sim 2050\ h$	2	full	full

Table 5.23 illustrates the results of the ammonia measurements which were carried out. The calculated ammonia conversion rate is based on the increase of the volumetric dry gas flow rate shown in Table 5.21. The measurement showed a decrease of the ammonia concentration along the WGS pilot unit caused by dilution, but there was no significant conversion of ammonia along the WGS pilot unit.

Table 5.23: Results of the ammonia measurements at the WGS pilot unit's inlet and outlet, while processing tar-rich wood gas, extracted upstream of the DFB gasification plant's RME scrubber in $mol.ppm_{db}$, based on [28].

Date	Hours of operation	Operating point	Inlet	Outlet	X_{NH_3}
February 2015	$\sim 1200\ h$	3	3395	2840	-0.01
March 2015	$\sim 1700\ h$	4	1924	1460	0.07
April 2015	$\sim 2050\ h$	2	2383	1869	0.03

Table 5.24 shows the results of the GCMS tar measurements which were carried out (January 2015 to April 2015) and results from previous measurements. All those tar samples were taken from tar-rich wood gas upstream of the DFB plant's RME gas scrubber.

If taking a closer look at the total GCMS tar value from the measurements of January 2015, February 2015 and March 2015 it can be seen, that the amount of total GCMS tar continuously decreased. In December 2014, the DFB biomass steam gasification plant did not operate for a couple of days. After restarting the DFB plant at the end of December 2014, also the long term test run was started.

The tar sample, taken in January 2015, shows the highest amount of GCMS tar. The amount of GCMS tar successively decreased in the samples taken in February 2015 and March 2015. This is closely associated with the operating time of the DFB gasification plant. In the end of March 2015, again the DFB biomass steam gasification plant did not operate for a couple of days. The next GCMS tar measurement performed in April 2015 shows again

a higher value than the measurement before the plant's stop. This values suggest that the amount of GCMS tar is related to the DFB biomass steam gasification plant's non stop operating time, or to some acting of the plant operator during the period of non-operation.

Kirnbauer et al. showed in [22] the catalytic effects of fresh olivine and used olivine on tar reduction. This GCMS tar behavior, in combination with the DFB gasification plant's start-up and shutdown operations and, consequently, bed material handling should be investigated in more detail in the future.

Table 5.25 summarizes the results of the GCMS tar measurements at the WGS pilot unit's inlet and outlet while processing tar-rich wood gas, extracted upstream of the DFB gasification plant's RME scrubber. The results indicate a hydrogenation of some tar species. Particularly, the hydrogenation of acenaphthylene to acenaphthene. Acenaphthylene is reduced from 835 to 47 $\frac{mg}{m^3_{N,db}}$, which corresponds to a conversion rate of 93 % and on the other hand the amount of acenaphthene increased from 24 to 506 $\frac{mg}{m^3_{N,db}}$, which corresponds to a conversion rate of -2514 %. The aspect of hydrogenation of some tar species can be seen at all GCMS tar measurements carried out.

Table 5.24: Detailed results of the GCMS tar measurements of tar-rich wood gas extracted upstream of the DFB gasification plant's RME scrubber in $\frac{mg}{m^3_{N,db}}$, GCMS tar DL 1 $\frac{mg}{m^3_{N,db}}$, including results from [7, 28], and Robert Bardolf.

Operating point	—	—	—	2	3	4	2
Date	Aug 2013	Feb 2014	Apr 2014	Jan 2015	Feb 2015	Mar 2015	Apr 2015
Naphthalene	6999	2855	6209	5804	3822	2060	2925
Styrene	401	202	249	272	166	190	253
1H-Indene	403	292	147	376	138	165	220
Phenylacetylene	29	32	31	47	25	24	25
Mesitylene	BDL	BDL	BDL	BDL	BDL	1	BDL
Benzofuran	6	BDL	BDL	2	BDL	2	2
Dibenzofuran	56	14	8	48	8	5	6
1-Benzothiophene	7	6	9	7	7	5	5
2-Methylnaphthalene	84	62	28	57	26	22	28
1-Methylnaphthalene	49	40	20	34	18	15	19
Biphenyl	105	41	34	57	24	15	25
Acenaphthylene	1570	383	320	835	233	128	196
Acenaphthene	68	32	35	24	37	17	26
Anthracene	527	60	11	375	118	19	13
Flouranthene	46	6	BDL	38	33	8	3
Pyrene	40	6	BDL	29	30	7	3
Flourene	118	31	8	71	9	5	5
Quinoline	11	3	BDL	6	1	1	3
Phenol	2	2	BDL	2	BDL	2	BDL
Isoquinoline	3	BDL	BDL	1	BDL	BDL	BDL
Cresol	BDL	BDL	BDL	BDL	BDL	BDL	BDL
Phenanthrene	45	4	1	49	11	4	1
4,5-Methylphenanthrene	14	2	BDL	11	4	2	BDL
Indole	5	1	BDL	BDL	BDL	BDL	4
Sorted into GCMS tar substance groups, compare Section 4.3.							
Aromatic compounds	838	527	427	695	329	380	502
Naphthalenes	7132	2957	6257	5895	3866	2097	2972
Others	71	22	17	59	15	14	13
Polycyclic aromatic hydrocarbons	2547	568	409	1496	500	206	275
Total GCMS tar	10588	4074	7110	8145	4710	2697	3762

Table 5.25: Detailed results of the GCMS tar measurements at the WGS pilot unit's inlet and outlet while processing tar-rich wood gas, extracted upstream of the DFB gasification plant's RME scrubber in $\frac{mg}{m_{N,db}^3}$, GCMS tar DL 1 $\frac{mg}{m_{N,db}^3}$, based on [28].

	January 2015, Operating point 2			February 2015, Operating point 3			March 2015, Operating point 4			April 2015, Operating point 2		
	Inlet	Outlet	X_{tar}	Inlet	Outlet	X_{tar}	Inlet	Outlet	X_{tar}	Inlet	Outlet	X_{tar}
Naphthalene	5804	4291	0.08	3822	2870	0.09	2060	1595	0.05	2925	2069	0.12
Styrene	272	32	0.85	166	38	0.72	190	20	0.87	253	31	0.85
1H-Indene	376	109	0.64	138	65	0.43	165	47	0.65	220	39	0.78
Phenylacetylene	47	BDL	0.96 to 1.00	25	BDL	0.95 to 1.00	24	BDL	0.95 to 1.00	25	BDL	0.95 to 1.00
Mesitylene	BDL	BDL	—	BDL	BDL	—	1	7	-7.61	BDL	BDL	—
Benzofuran	2	BDL	0.38 to 1.00	BDL	BDL	—	2	2	-0.23	2	2	-0.24
Dibenzofuran	48	36	0.07	8	7	-0.06	5	5	-0.23	6	4	0.17
1-Benzothiophene	7	5	0.11	7	5	0.14	5	3	0.26	5	3	0.26
2-Methylnaphthalene	57	38	0.17	26	21	0.02	22	19	-0.06	28	15	0.34
1-Methylnaphthalene	34	25	0.09	18	15	-0.01	15	13	-0.07	19	10	0.35
Biphenyl	57	44	0.04	24	21	-0.06	15	12	0.02	25	17	0.16
Acenaphthylene	835	47	0.93	233	6	0.97	128	7	0.93	196	3	0.98
Acenaphthene	24	506	-25.14	37	190	-5.21	17	103	-6.45	26	122	-4.82
Anthracene	375	467	-0.54	118	46	0.53	19	15	0.03	13	9	0.14
Flouranthene	38	56	-0.83	33	18	0.34	8	6	0.08	3	4	-0.65
Pyrene	29	44	-0.88	30	17	0.31	7	6	-0.05	3	4	-0.65
Flourene	71	56	0.02	9	6	0.19	5	5	-0.23	5	2	0.50
Quinoline	6	4	0.17	1	BDL	—	1	1	-0.23	3	BDL	0.59 to 1.00
Phenol	2	BDL	0.38 to 1.00	BDL	BDL	—	2	2	-0.23	BDL	BDL	—
Isoquinoline	1	BDL	0.24 to 1.00	BDL	BDL	—	BDL	BDL	—	BDL	BDL	—
Cresol	BDL	BDL	—	BDL	BDL	—	BDL	BDL	—	BDL	BDL	—
Phenanthrene	49	55	-0.39	11	4	0.56	4	3	0.08	1	1	-0.24
4,5-Methylphenanthrene	11	14	-0.58	4	2	0.40	2	2	-0.23	BDL	BDL	—
Indole	BDL	BDL	—	BDL	BDL	—	BDL	BDL	—	4	BDL	0.69 to 1.00
Sorted into GCMS tar substance groups, compare Section 4.3.												
Aromatic compounds	695	141	0.75	329	103	0.62	380	74	0.76	502	70	0.83
Naphthalenes	5895	4354	0.08	3866	2906	0.09	2097	1627	0.05	2972	2094	0.13
Others	59	41	0.14	15	12	0.03	14	12	-0.05	13	9	0.14
Polycyclic aromatic hydrocarbons	1496	1293	-0.07	500	310	0.25	206	160	0.04	275	162	0.14
Total GCMS tar	8145	5829	0.11	4710	3331	0.14	2697	1873	0.15	3762	2335	0.23

Chapter 6

Conclusions and Outlook

Producing hydrogen from biomass via thermochemical route is a promising technology for future decarbonized applications. Especially the DFB steam gasification, using wood chips or other biomass as feedstock and generating a high calorific wood gas with about 40 $mol.\%_{db}$ hydrogen content seems to be an ideal basis for further gas conditioning using a WGS unit in order to increase the hydrogen yield.

Within this thesis, a WGS pilot unit which employed a commercial Fe/Cr based catalyst was investigated. The pilot unit was processing wood gas from an industrial scale DFB biomass steam gasification plant. Therefore, two test runs, one short term test run for about 100 hours with wood gas, extracted downstream of the DFB gasification plant's RME gas scrubber and one long term test run for 2337 hours with wood gas extracted upstream of the DFB gasification plant's RME gas scrubber, were performed.

No significant differences regarding the performance of the WGS pilot unit could be observed. Even a partial load operation of the DFB biomass steam gasification plant did not negatively affect the performance of the WGS pilot unit. A technically immaculate functionality and a steady long term operation could be achieved.

The WGS pilot unit, equipped with a commercial Fe/Cr based catalyst, in its original size, was operated with a significant excess of steam in order to avoid possible coking and carbon deposition on the surface of the catalyst. Observations showed that small technical malfunctions or inconsistent biomass quality led to fluctuations upwards of the steam content in the wood gas. Future test runs processing tar-rich wood gas, extracted upstream of the DFB biomass gasification plant's RME scrubber can truly aim for a lower $STDGR$.

At these operating conditions, a carbon monoxide conversion rate between 91 and 93 % and, consequently, less than 1.5 to 1.8 mol.$\%_{db}$ carbon monoxide at the WGS pilot unit's outlet was obtained. The hydrogen yield was even increased to 156 to 161 % by the WGS reaction. In addition it could be assumed that the total GCMS tar load was significantly affected and reduced by the WGS pilot unit. The total GCMS tar conversion rate was between 11 and 23 %. The ammonia measurements carried out made no significant statement, it seems

that ammonia is not converted along the WGS pilot unit.

With the present experimental layout, no catalyst deactivation could be observed. This indicates that, in fact, the commercial WGS Fe/Cr based catalyst can handle tar-rich wood gas which is produced from a DFB biomass steam gasification plant. Therefore, it can be a promising technology for a future renewable and carbon dioxide neutral hydrogen production based on biomass.

An aspect for future work should be to investigate the catalyst deactivation or poisoning in detail. Analyses on the catalyst itself could verify if a mechanism of catalyst deactivation or poisoning took place.

Future work should focus on lowering the steam excess. If the catalyst can handle a lower $STDGR$, a future use of this technology would be more efficient and more simple to implement. Therefore, the catalyst's performance at lower steam content seems to be an important approach for future research.

List of Publications

Below, a list of journal and conference publications is given which were carried out in collaboration with Kraussler et al. based on results from this thesis:

- Michael Kraussler, Matthias Binder, Silvester Fail, Klaus Bosch, Marius Hackel, and Hermann Hofbauer. Performance of a water gas shift pilot plant processing product gas from an industrial scale biomass steam gasification plant. unpublished, 2015

- Michael Kraussler, Matthias Binder, Silvester Fail, Klaus Bosch, Marius Hackel, and Hermann Hofbauer. Performance of a water gas shift unit processing product gas from biomass steam gasification. In *Proceedings of the 23rd European Biomass Conference*, pages 668–678, 06 2015

- Michael Kraussler, Matthias Binder, Silvester Fail, Antonio Plaza, Alberto Cortes, and Hermann Hofbauer. Validation of a kinetic model for the catalyzed water gas shift reaction applying a Fe/Cr catalyst processing product gas from biomass steam gasification. In *Proceedings of the 23rd European Biomass Conference*, pages 810–818, 06 2015

- Michael Kraussler, Matthias Binder, and Hermann Hofbauer. Performance of a water gas shift pilot plant processing tar-rich product gas from a commercial biomass steam gasification plant operating at partial load conditions. unpublished, International Bioenergy (Shanghai) Exhibition ad Asian Bioenergy Conference , 10 2015

- Michael Kraussler, Matthias Binder, and Hermann Hofbauer. 2250-hour long term operation of a water gas shift pilot plant processing tar-rich product gas from an industrial scale biomass steam gasification plant. unpublished, 2015

- Michael Kraussler, Matthias Binder, and Hermann Hofbauer. Behavior of GCMS tar components along a water gas shift pilot plant operated with tar-rich product gas from an industrial scale biomass steam gasification plant. unpublished, 2015

List of Figures

List of Tables

Nomenclature

Abbreviations & Acronyms

AC   Aromatic compounds

AE&E   Austrian Energy & Environment GmbH

AT   Austria

ATR   Autothermal reforming

BDL   Below detection limit

BioSNG   Biomass synthetic natural gas

B&R   Bernecker + Rainer Industrie-Elektronik GmbH

CHP   Combined heat and power

CPO   Catalytic partial oxidation

DE   Germany

DFB   Dual fluidized bed

DL   Detection limit

DME   Dimethyl ether

FI   Flow indicator

FPD   Flame photometric detector

GC   Gas chromatograph

GCMS   Gas chromatograph coupled with a mass spectrometer

HTS   High temperature shift

IT   Italy

LTS	Low temperature shift
MCFC	Molten carbonate fuel cell
MV	Pilot operated valve
ORC	Organic Rankine cycle
PAH	Polycyclic aromatic hydrocarbons
PCS	Process control system
PEMFC	Proton exchange membrane fuel cell
PEM	Proton exchange membrane
PI	Pressure indicator
POX	Noncatalytic partial oxidation
PROX	Preferential oxidation
PSA	Pressure swing adsorption
RME	Rapeseed oil methyl ester
SE	Sweden
SMR	Steam methane reforming
SOFC	Solid oxide fuel cell
TCD	Thermal conducticity detector
WGS	Water gas shift

Indices

C	Carbon
CO	Carbon monoxide
db	Dry basis
el	Electric
gas	Gaseous components
H_2	Hydrogen
in	Inlet

N   At standard conditions (0 °C and 101.325 kPa)

out   Outlet

th   Thermal

wb   Wet basis

Symbols

c_{NH_3} Ammonia concentration in $mol.ppm_{db}$

c_{tar} Tar concentration in $\frac{mg}{m_{N,db}^3}$

ΔH_R^0 Enthalpy of reaction at standard conditions (0 °C and 101.325 kPa) in $\frac{kJ}{mol}$

$\Delta \dot{V}_{db}$ Delta volumetric dry gas flow rate in -

$GHSV$ Gas hourly space velocity in h^{-1}

H_2rec Hydrogen recovery in -

K_p Equilibrium constant in -

$\dot{n}$ Molar flow rate in $\frac{mole}{h}$

$STCOR$ Steam to carbon monoxide ratio in -

$STCR$ Steam to carbon ratio in -

$STDGR$ Steam to dry gas ratio in -

V Volume in m^3

$\dot{V}$ Volumetric flow rate in $\frac{m_N^3}{h}$

$V_{catalyst}$ Bulk volume of the catalyst in m^3

X_{CO} Carbon monoxide conversion rate in -

X_{NH_3} Ammonia conversion rate in -

X_{tar} Tar conversion rate in -

Bibliography

[1] Havva Balat and Elif Kirtay. Hydrogen from biomass - present scenario and future prospects. *International Journal of Hydrogen Energy*, 35(14):7416–7426, 2010.

[2] Michael Ball and Martin Wietschel. The future of hydrogen - opportunities and challenges. *International Journal of Hydrogen Energy*, 34:615–627, 2009.

[3] Nicolas Diaz. *Hydrogen Separation from Producer Gas Generated by Biomass Steam Gasification*. PhD thesis, Vienna University of Technology, 2013.

[4] Axel Düker. Hydrogen Production and Application in Industry. In *Presentation Süd - Chemie*. Süd - Chemie AG, 2011.

[5] Seth Dunn. Hydrogen futures: toward a sustainable energy system. *International Journal of Hydrogen Energy*, 27(3):235–264, 2002.

[6] Robert J. Evans and Thomas A. Milne. Molecular characterization of the pyrolysis of biomass. *Energy and Fuels*, 1(2):123–138, 1987.

[7] Silvester Fail. *Biohydrogen Production Based on the Catalyzed Water Gas Shift Reaction in Wood Gas*. PhD thesis, Vienna University of Technology, 2014.

[8] Silvester Fail, Nicolas Diaz, Florian Benedikt, Michael Kraussler, Julian Hinteregger, Klaus Bosch, Marius Hackel, Reinhard Rauch, and Hermann Hofbauer. Wood gas processing to generate pure hydrogen suitable for PEM fuel cells. *American Chemical Society, Sustainable Chemistry and Engineering*, 2:2690–2698, 2014.

[9] Silvester Fail, Nicolas Diaz, David Konlechner, Marius Hackel, Ed Sanders, Reinhard Rauch, Michael Harasek, Klaus Bosch, Franz Schwenninger, Petr Zapletal, Zdenek Schee, and Hermann Hofbauer. An experimental approach for the production of pure hydrogen based on wood gasification. In *Proceedings of the ICPS 2013*, pages 109–126. Vienna University of Technology, September 2013.

[10] Gerda Gahleitner. Hydrogen from renewable electricity: An international review of power-to-gas pilot plants for stationary applications. *International Journal of Hydrogen Energy*, 38(5):2039 – 2061, 2013.

[11] Hermann Hofbauer and Reinhard Rauch. Stoichiometric water consumption of steam gasification by the FICFB-gasification process. In *Progress in Thermochemical Biomass Conversion*, 2000.

[12] Hermann Hofbauer, Reinhard Rauch, Klaus Bosch, Reinhard Koch, and Christian Aicherning. *Biomass CHP Plant Güssing A Success Story*. CPL Press, 2003.

[13] Hermann Hofbauer, Reinhard Rauch, and Gerhard Löffler. Six years of experience with the FICFB-gasification process. In *12th European Conference on Biomass and Bioenergy*, 2002.

[14] Hermann Hofbauer, Reinhard Rauch, and Ingmar Siefert. Analytik III, Messung von organischen Inhaltsstoffen, Partikeln und Wasser in Produktgasen von Biomassevergasern. Technical report, Vienna University of Technology, Institute of Chemical Engineering, 2003.

[15] Hermann Hofbauer, Günter Veronik, Thomas Fleck, and Reinhard Rauch. The FICFB - gasification process. *Developments in Thermochemical Biomass Conversion*, 2:1016–1025, 1997.

[16] Jamelyn D. Holladay, Jianli Hu, David L. King, and Yong Wang. An overview of hydrogen production technologies. *Catalysis Today*, 139(4):244–260, 2009.

[17] http://www.ficfb.at/aims.htm. Overview about commercial gasifiers, July 2015. Last update on 29th December 2014 by Webmaster.

[18] Robert A. Hefner III. The age of energy gases. *International Journal of Hydrogen Energy*, 27(1):1 – 9, 2002.

[19] Martin Kaltschmitt, Hans Hartmann, and Hermann Hofbauer. *Energie aus Biomasse*. Springer Verlag, 2009.

[20] Energie Burgenland Biomasse GmbH&Co KG. Biomasse Vergasungskraftwerk Oberwart. Booklet, April 2014.

[21] Friedrich Kirnbauer, Veronika Wilk, and Hermann Hofbauer. Performance improvement of dual fluidized bed gasifiers by temperature reduction: The behavior of tar species in the product gas. *Fuel*, 108(0):534–542, 2013.

[22] Friedrich Kirnbauer, Veronika Wilk, Hannes Kitzler, Stefan Kern, and Hermann Hofbauer. The positive effects of bed material coating on tar reduction in a dual fluidized bed gasifier. *Fuel*, 95(0):553–562, 2012.

[23] Michael Kraussler, Matthias Binder, Silvester Fail, Klaus Bosch, Marius Hackel, and Hermann Hofbauer. Performance of a water gas shift pilot plant processing product gas from an industrial scale biomass steam gasification plant. unpublished, 2015.

[24] Michael Kraussler, Matthias Binder, Silvester Fail, Klaus Bosch, Marius Hackel, and Hermann Hofbauer. Performance of a water gas shift unit processing product gas from biomass steam gasification. In *Proceedings of the 23rd European Biomass Conference*, pages 668–678, 06 2015.

[25] Michael Kraussler, Matthias Binder, Silvester Fail, Antonio Plaza, Alberto Cortes, and Hermann Hofbauer. Validation of a kinetic model for the catalyzed water gas shift reaction applying a Fe/Cr catalyst processing product gas from biomass steam gasification. In *Proceedings of the 23rd European Biomass Conference*, pages 810–818, 06 2015.

[26] Michael Kraussler, Matthias Binder, and Hermann Hofbauer. Performance of a water gas shift pilot plant processing tar-rich product gas from a commercial biomass steam gasification plant operating at partial load conditions. unpublished, International Bioenergy (Shanghai) Exhibition ad Asian Bioenergy Conference , 10 2015.

[27] Michael Kraussler, Matthias Binder, and Hermann Hofbauer. 2250-hour long term operation of a water gas shift pilot plant processing tar-rich product gas from an industrial scale biomass steam gasification plant. unpublished, 2015.

[28] Michael Kraussler, Matthias Binder, and Hermann Hofbauer. Behavior of GCMS tar components along a water gas shift pilot plant operated with tar-rich product gas from an industrial scale biomass steam gasification plant. unpublished, 2015.

[29] Ke Liu, Chunshan Song, and Velu Subramani. *Hydrogen and Syngas Production and Purification Technologies*. Wiley, 2010.

[30] Fanhua Ma, Nashay Naeve, Mingyue Wang, Long Jiang, Renzhe Chen, and Shuli Zhao. Hydrogen-enriched compressed natural gas as a fuel for engines. *Natural Gas*, 2010.

[31] Thomas A. Milne, Robert J. Evans, and Nicolas Abatzoglou. Biomass gasifier tars: their nature, formation, and conversion. Technical report, National Renewable Energy Laboratory, US Department of Energy, November 1998.

[32] Stefan Müller, Martin Stidl, Tobias Pröll, Reinhard Rauch, and Hermann Hofbauer. Hydrogen from biomass: large-scale hydrogen production based on a dual fluidized bed steam gasification system. *Biomass Conversion and Biorefinery*, 1(1):55–61, 2011.

[33] Martyn V. Twigg. *Catalyst Handbook-Chapter 6: The Water-gas Shift Reaction*. Manson Publishing, 1989.

[34] Ute Wolfesberger, Isabella Aigner, and Hermann Hofbauer. Tar content and composition in producer gas of fluidized bed gasification of wood - Influence of temperature and pressure. *Environmental Progress & Sustainable Energy*, 28(3):372–379, OCT 2009.

Michael Kraussler, Matthias Binder, Silvester Fail, Klaus Bosch, Marius Hackel, and Hermann Hofbauer.

Performance of a water gas shift unit processing product gas from biomass steam gasification.

In *Proceedings of the 23rd European Biomass Conference*, pages 668-678, 06 2015

PERFORMANCE OF A WATER GAS SHIFT UNIT PROCESSING PRODUCT GAS FROM BIOMASS STEAM GASIFICATION

Kraussler M.[1], Binder M.[2], Fail S.[2], Bosch K.[3], Hackel M.[4], Hofbauer H.[1,2]
[1]Bioenergy2020+ GmbH, Wienerstrasse 49, 7540 Guessing, Austria
[2]Vienna University of Technology, Institute of Chemical Engineering, Getreidemarkt 9, 1060 Vienna, Austria
[3]Energie Burgenland AG, Kasernenstraße 9, 7000 Eisenstadt, Austria
[4]Air Liquide[TM], Forschung und Entwicklung GmbH, Frankfurt Research and Technology Center (FRTC),
Gwinnerstrasse 27-33, 60388 Frankfurt am Main, Germany

ABSTRACT: In this present paper, the performance of a commercial Fe/Cr based catalyst for the water gas shift reaction was investigated. The catalyst was applied in a water gas shift pilot plant which processed product gas from a commercial biomass steam gasification plant for combined heat and power. The water gas shift pilot plant successively processed product gas upstream and downstream a rapeseed methyl ester gas scrubber. During the investigations, extensive chemical analyses were carried out. The main components (CO, CO_2, CH_4, N_2, O_2, C_2H_6, C_2H_4, and C_2H_2) and sulfur components (H_2S, COS, and C_4H_4S) were measured. In addition, tar and NH_3 analyses were performed. Furthermore, the catalyst's activity was observed by measuring the temperature profiles along the reactors of the water gas shift pilot plant. During the operation, no catalyst deactivation could be observed. A CO conversion up to 94 % was reached. The results showed that the application of a Fe/Cr based catalyst in a water gas shift unit seems to be a suitable way for increasing the hydrogen content in the product gas which was generated by biomass steam gasification. Furthermore, with such a technique it is possible to adjust the required CO/H_2 ratio for several syntheses reactions (e.g. methanation, Fischer Tropsch) in an optimal way.
Keywords: Biomass, Gasification, Hydrogen, Product Gas, Water Gas Shift

1 INTRODUCTION

Today, hydrogen is an important resource for a wide range of applications in chemical industry [1]. Steam reforming of natural gas and other processes with fossil fuels as feedstock produces more than 95 % of the hydrogen for the industry. With the background of the climate change, a CO_2 neutral method for hydrogen production should be established [2]. Biomass steam gasification is a proven technology and a CO_2 neutral alternative to steam reforming of natural gas [3].

A promising technology for biomass steam gasification is the dual fluidized bed (DFB) process [4,5]. The commercial biomass steam gasification plants in Guessing and Oberwart have been using this technology for several years. Both plants generate a product gas with a H_2 content of about 40 vol. %. Other main components are about 25 vol. % CO, 20 vol. % CO_2, and 10 vol. % CH_4. In addition, small amounts of N_2, O_2, higher hydrocarbons, and about 100 vol. ppm H_2S and other sulfur components are contained in minor amounts. The high H_2 content makes the product gas a promising CO_2 neutral H_2 source [6]. A process which can further increase the hydrogen content in the product gas is the water gas shift (WGS) reaction (see Equation 1).

$$CO + H_2O \overset{-\Delta H}{\longleftrightarrow} H_2 + CO_2 \qquad (1)$$
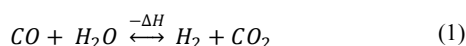
It converts carbon monoxide and steam to hydrogen and carbon dioxide. In order to reach economic reaction rates, catalysts are necessary. A suitable catalyst is a Fe/Cr based catalyst. Fe/Cr based catalysts seem to be robust against sulfur poisoning at H_2S amounts which are contained in the product gas of biomass steam gasification [7,8].

For this work, a WGS pilot plant applying a commercial Fe/Cr based catalyst was operated with product gas from the commercial biomass steam gasification plant in Oberwart, Austria.

The WGS pilot plant was operated with product gas upstream a rapeseed methyl ester (RME) gas scrubber for more than 100 hours as well as with product gas downstream a RME gas scrubber for more than 100 hours again. [11] and [12] showed that an operation with product gas downstream a RME gas scrubber is possible. The performance of a WGS pilot plant applying a Fe/Cr based catalyst which was processing product gas upstream the RME gas scrubber with a high content of tar is compared with the operation of the WGS pilot plant with product gas downstream the RME gas scrubber with a low content of tar.

2 MATERIALS AND METHODS

The experimental work was carried out at the plant site of the biomass steam gasification plant in Oberwart, Austria, where the WGS pilot plant is located. The pilot plant consisted of three reactors in series which applied a Fe/Cr based catalyst. The gas composition and the steam content were measured upstream and downstream each reactor. Tar and NH_3 analyses were performed by the Test Laboratory for Combustion Systems at Vienna University of Technology. The temperature profile along each reactor was recorded. This allowed a judgement on the activity of the Fe/Cr based catalyst.

2.1 The Biomass Steam Gasification Plant in Oberwart

The WGS pilot plant processed product gas from the combined heat and power (CHP) plant in Oberwart. Figure 1 shows a simplified flowchart of the applied process.

The plant is based on the DFB steam gasification technology which is described in detail in [4] and [5]. The CHP plant generates district heat and electricity with biomass (woodchips) as feedstock. Table I shows the main operation parameters of the CHP plant.
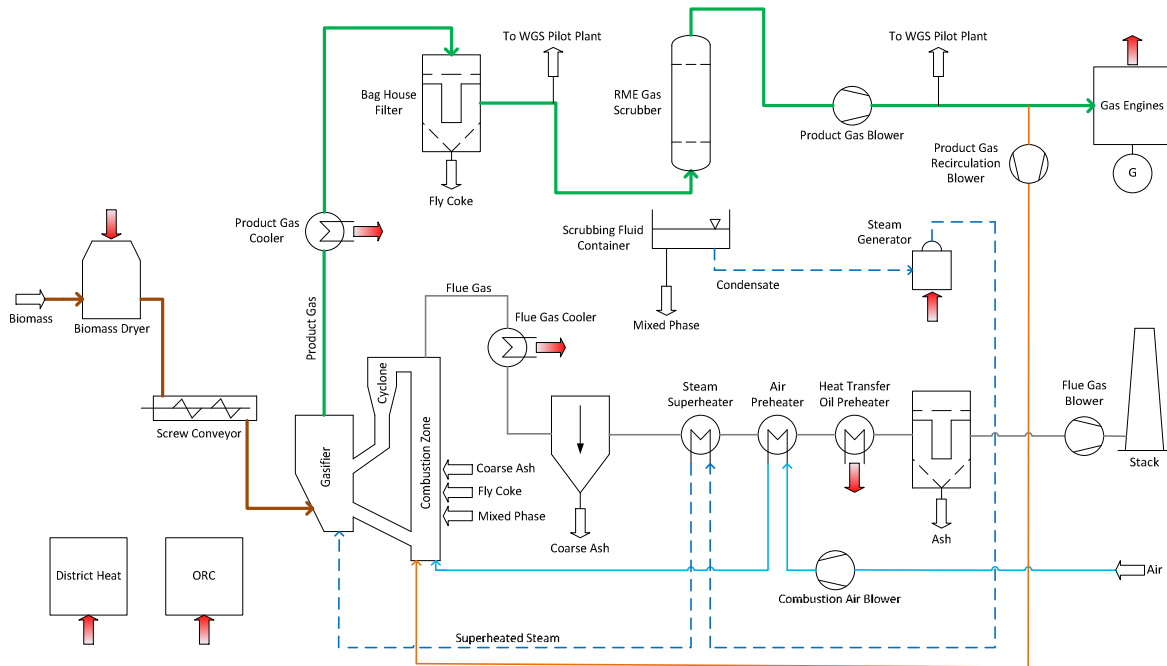
Figure 1: Simplified flowchart of the CHP plant in Oberwart, Austria. Heat sources and heat sinks of the process are indicated by arrows.

Table I: Main operation parameters of the CHP plant in Oberwart, Austria [6].

Parameter	Value	Unit
Fuel Power	8.7	MW
District Heat Power	4.0	MW
Electrical Power	2.8	MW

Biomass is fed into the biomass dryer. Afterwards, a screw conveyor transports the biomass into the gasifier. In the gasifier the biomass is in contact with steam and the bed material (olivine) at about 850 °C. Result is a product gas with a high hydrogen content (about 40 vol. %). The product gas is cooled, passes through a bag house filter, and a RME gas scrubber. In the RME gas scrubber, tar, NH_3, and other condensable fractions of the product gas are removed before the product gas is fed into gas engines for electricity generation. Heat from the flue gas line is mainly recovered for the process. Fly ash is removed before the flue gas is released to the atmosphere.

It is possible to take a partial flow of the product gas for experimental work from two different extraction points along the product gas line (see Figure 4). The first extraction point is upstream the RME gas scrubber and the second extraction point is downstream the RME gas scrubber. Table II shows the conditions at the two different extraction points.

Table II: Operation conditions at the experimental extraction points (see Figure 1) at the CHP plant in Oberwart, Austria, under full load operation of the CHP plant [12].

Parameter	Upstream Scrubber	Downstream Scrubber	Unit
Temperature	~ 150	~ 40	°C
H_2O Content	~ 35	~ 7	vol. %
Tar Content	~ 8.2	~ 1.1	g/Nm^3

During the investigations, the product gas was successively taken from both extraction points for about 100 hours. The water content and the temperature of the product gas at the extraction point upstream the RME gas scrubber is significantly higher than at the extraction point downstream the RME gas scrubber. Therefore, from an energy efficiency point of view, it is useful to take the product gas from the extraction point upstream the RME gas scrubber as the temperature and the water content is more suitable for a WGS reaction compared to the extraction point downstream the RME gas scrubber. Furthermore, the tar content upstream the RME gas scrubber is much higher which is a challenge for a reliable operation.

A detailed description of the process and the power plant can be found in [4], [6], and [8].

2.2 The WGS Pilot Plant
The experimental work was carried out at a WGS pilot plant located at the plant site of the CHP plant in Oberwart. Figure 2 shows a simplified flowchart of the WGS pilot plant.
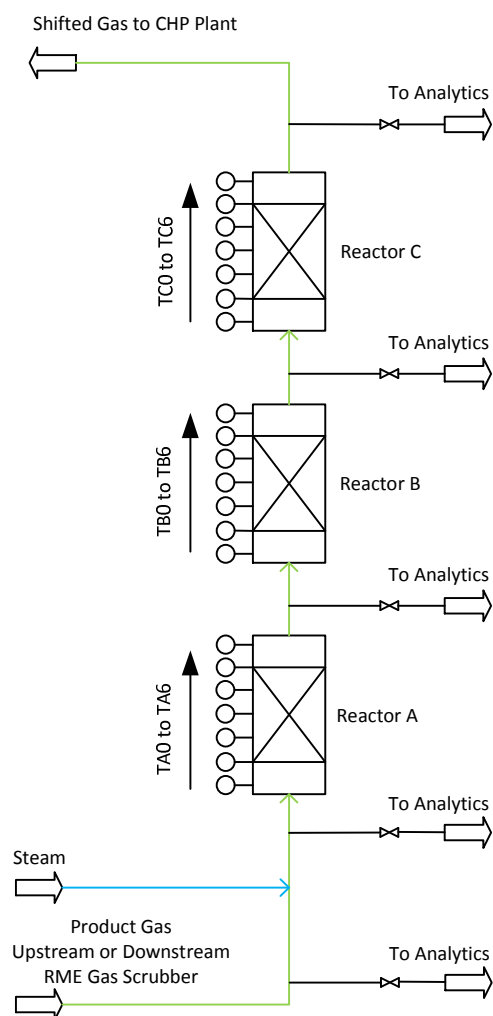
Figure 2: Simplified flowchart of the WGS pilot plant located at the plant site of the CHP plant in Oberwart.

The WGS pilot plant consisted of three fixed bed reactors (A, B, and C) in series filled with a commercial Fe/Cr based catalyst. Each catalyst bed had a diameter of about 9 cm and a bed height of about 40 cm resulting in a Fe/Cr based catalyst volume of about 2.5 L for each reactor.

Along the reactor height of each reactor seven type J thermocouples (TA0 to TA6, TB0 to TB6, and TC0 to TC6) were installed in order to record the temperature profile along the reactors. At the inlet and outlet of reactors A and B, the gas stream could be heated or cooled in order to achieve the desired gas inlet temperature.

Upstream and downstream each reactor, a partial flow of the processed gas was sent to the analytical line were the gas composition measurements, water measurements, tar samplings, and NH_3 samplings were done.

Upstream the inlet of the first reactor, the product gas was mixed with steam to assure the desired steam content in the processed gas along the WGS pilot plant.

The WGS pilot plant was operated at ambient pressure.

2.3 Temperature Measurement Along the WGS Reactors

Figure 2 shows the position of the thermocouples (Type J) along the studied WGS reactors. Thermocouple T0 was positioned before the fixed bed Fe/Cr based catalyst. Therefore, it was not in the reactive zone. T1 to T5 were positioned along the catalyst bed with a distance of 10 cm to each other. T1 was positioned directly at the beginning of the catalyst bed and T5 was positioned directly at the end of the catalyst bed. T6 was outside the catalyst bed. This arrangement was the same in each of the three reactors. A Labview^{TM} program recorded the temperature profiles.

2.4 Measurement of the Gas Composition

A gas chromatograph (Clarus 500^{TM} from Perkin Elmer^{TM}) measured the gas composition upstream and downstream each WGS reactor. Figure 3 shows the setup of the gas conditioning for the gas chromatograph (GC).
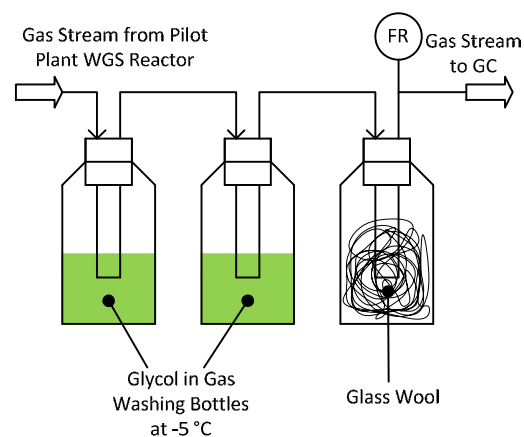
Figure 3: Sampling line for the gas composition analytics upstream the gas chromatograph (GC).

The analytical gas stream was led through two gas washing bottles filled with glycol at a temperature of about -5 °C in order to condense the steam. Therefore, a dry gas stream could be assumed after the two gas washing bottles. The dry gas stream passed another gas washing bottle filled with glass wool in order to prevent aerosols from entering the GC. After the glass wool a gas meter recorded the volumetric dry gas flow.

In the GC, a thermal conductivity detector (TCD) enabled the quantification of CO, CO_2, CH_4, N_2, O_2, C_2H_6, C_2H_4, and C_2H_2. The C_2 species were summarized and referred to as C_2H_y. A flame photometric detector (FPD) was used to detect H_2S, COS, and C_4H_4S.

2.5 Measurement of the Steam Content in the Gas

Figure 3 also shows the flowchart for the gravimetrical steam content determination. The gas passed through the glycol gas washing bottles at -5 °C for a certain time. Subsequently, the volumetric dry gas flow was recorded with a gas meter.

By weighing the gas washing bottles, the water content before steam addition, at the inlet, and at the outlet of each reactor was determined. Volumetric flow rates were calculated with the water balance.

2.6 Tar Sampling Method

During both experimental runs, tar measurements at the inlet and outlet of the WGS pilot plant were performed. Additional information about the method is available in [13]. Figure 4 shows the principle of the tar sampling.
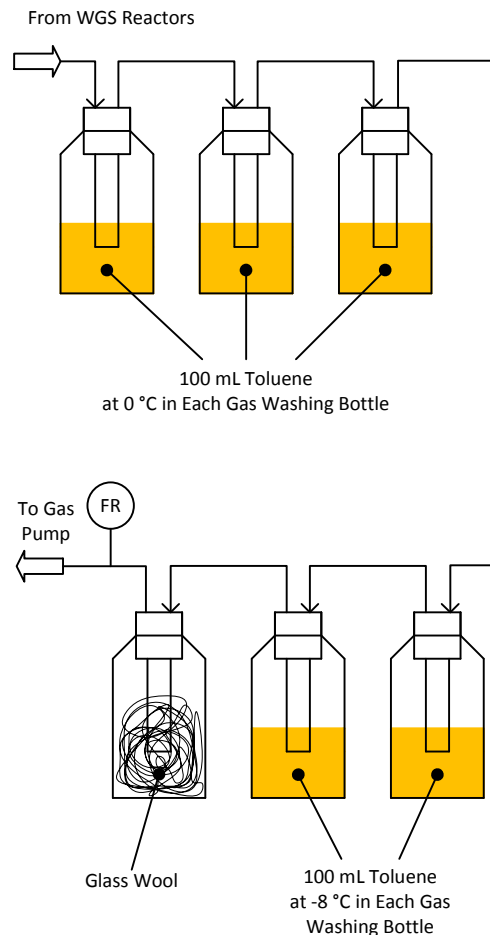
Figure 4: Flowchart of the tar sampling line.

A partial flow of the product gas passed through the tar sampling line. The product gas passed five gas washing bottles filled with overall 500 mL toluene and one gas washing bottle filled with glass wool in order to prevent aerosols to enter the analytical gas pump. Tar shows a good solubility in toluene [13]. The first three gas washing bottles were cooled to about 0 °C. Consequently, tar was dissolved and steam condensed. The next two gas washing bottles were cooled to -8 °C to make sure that all other remaining tar components were finally dissolved in toluene. The gas was sent through the sampling line for about three hours. In addition, the volumetric dry gas flow was recorded by a gas meter. The dry gas sampling flow rate was set to 2 to 2.5 NL/min.

After the sampling, the content of the gas washing bottles was mixed and so were the toluene phase with dissolved tar and the condensate phase. The samples were handed over to the Test Laboratory for Combustion Systems at Vienna University of Technology. The test laboratory determined the gravimetrical amount of tar as well as the amount of GC/MS tar components.
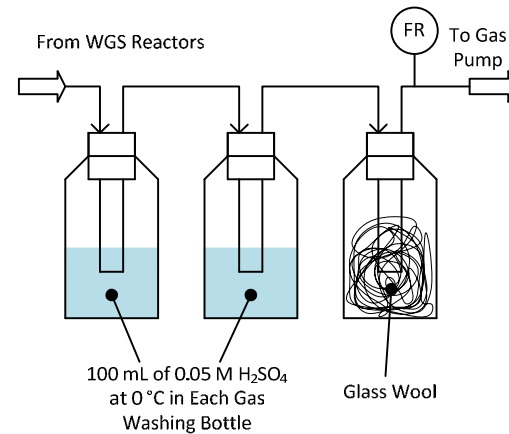
2.7 NH$_3$ Sampling Method

The NH$_3$ sampling was carried out according to the instructions of the Test Laboratory for Combustion Systems at Vienna University of Technology. Figure 5 shows the principle in a flowchart.

Figure 5: Flowchart of the NH$_3$ sampling line.

A partial flow of the processed gas at the inlet and outlet of the WGS pilot plant was led through the NH$_3$ sampling line. The gas passed through two gas washing bottles filled with overall 200 mL of 0.05 M sulfuric acid. The sampling time for one sample was about fifteen minutes. The volumetric dry gas flow was recorded by a gas meter. The dry gas sampling flow rate was set to 0.5 to 0.7 NL/min.

After the sampling, the content of the two gas washing bottles was mixed and the sample volume was filled up to a certain volume with sulfuric acid in order to obtain the volumetric NH$_3$ content of the product gas.

The analyses were carried out with column chromatography by the Test Laboratory for Combustion Systems at Vienna University of Technology.

2.8 Characteristic Figures of the WGS Pilot Plant

The WGS reactors were described by characteristic figures. The first figure (Equation 2) was the gas hourly space velocity (GHSV). It was calculated as quotient of the volumetric dry gas flow rate (standard conditions) at the inlet of the reactor and the catalyst volume of the reactor. It indicated the stress of the catalyst.

$$GHSV = \frac{\dot{V}_{Dry}}{V_{Catalyst}} \qquad (2)$$

The second figure (Equation 3) was the steam to dry gas ratio (STDGR). This figure is the ratio of the volumetric steam flow rate to the volumetric dry gas flow rate in the feed of the WGS reactor.

$$STDGR = \frac{\dot{V}_{H2O}}{\dot{V}_{Dry}} \qquad (3)$$

The third figure (Equation 4) was the steam to carbon ratio (STCR). This figure is the ratio of the volumetric steam flow rate and the volumetric flow rate of all gas components which included at least one carbon atom. The value of the STCR must not be too low in order to

671

avoid coking and carbon deposition on the surface of the catalyst.

$$STCR = \frac{\dot{V}_{H2O}}{\dot{V}_{Dry} \cdot (c_{CO} + c_{CO2} + c_{CH4} + c_{C2Hy})} \quad (4)$$

Another typical figure of the WGS pilot plant was the CO conversion in Equation 5.

$$X_{CO} = \frac{c_{CO,IN} - c_{CO,OUT}}{c_{CO,IN}} \quad (5)$$

It was calculated with the CO concentrations at the inlet and the outlet of a WGS reactor.

All four figures described the conditions in the WGS reactors. In addition, those figures make different WGS reactors comparable.

3 RESULTS AND DISCUSSION

This chapter presents the results of the WGS pilot plant operation with product gas upstream and downstream the RME gas scrubber. Results were determined during two successive 100 hour operations of the WGS pilot plant.

The Fe/Cr based catalyst was activated in previous experiments. The activation procedure and results of the previous experiments can be found in [8] and [12].

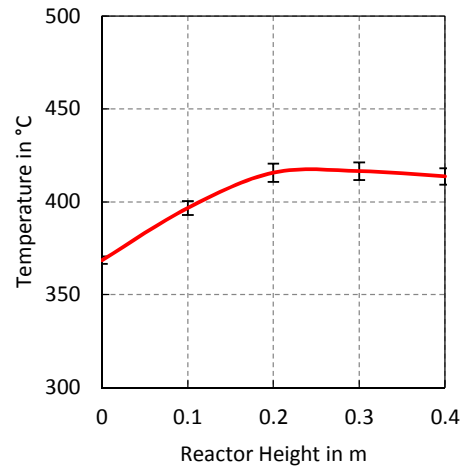3.1 Operation with Product Gas Upstream the RME Gas Scrubber

Table III shows the WGS pilot plant operation parameters and the figures during the operation with product gas upstream the RME gas scrubber.

Table III: Operation data of the WGS pilot plant with gas upstream the RME gas scrubber during the 100 hours of operation. The GHSV is given for one reactor. The STDGR and the STCR are given for inlet of the first reactor. X_{CO} is given for the whole WGS pilot plant.

GHSV h^{-1}	STDGR -	STCR -	X_{CO} %
478	1.6	2.6	94

The STDGR and STCR were chosen in order to protect the Fe/Cr based catalyst from coking. During this 100 hours of operation, a CO conversion of 94 % was achieved.

Figures 6 to 8 show the temperature profiles along reactors A, B, and C during the 100 hours of operation with product gas upstream the RME gas scrubber.

Figure 6: Temperature profile of reactor A during the 100 hours of operation with product gas upstream the RME gas scrubber.

Figures 6 to 8 indicate that the WGS reaction mainly took place in reactor A (see Figure 6). The temperature increased along the reactor because of the exothermic WGS reaction. After the temperature maximum was reached, the temperature along reactor A decreased. This was the result of two effects. First, the equilibrium composition of the reactive species of the WGS reaction was reached. Therefore, the reaction and consequently the temperature increase stopped. Second, heat losses occurred which finally caused the temperature decrease.

The product gas was cooled actively before it entered reactor B and C. Aim was to achieve about the same reactor inlet temperature at the inlet of all three WGS reactors.

Figure 7: Temperature profile of reactor B during the 100 hours of operation with product gas upstream the RME gas scrubber.

In reactor B, significantly less WGS reaction occurred which only can be dedicated to keep the equilibrium due to the temperature decrease. Consequently, the heat losses exceeded the temperature increase caused by the exothermic reaction. Therefore, the temperature decreased (see Figure 7).
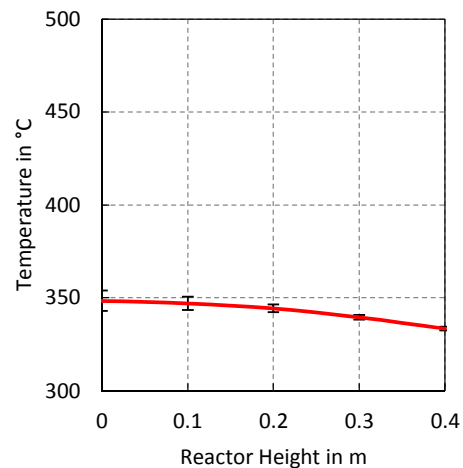
In reactor C the same effects as in reactor B occurred (see Figure 8).
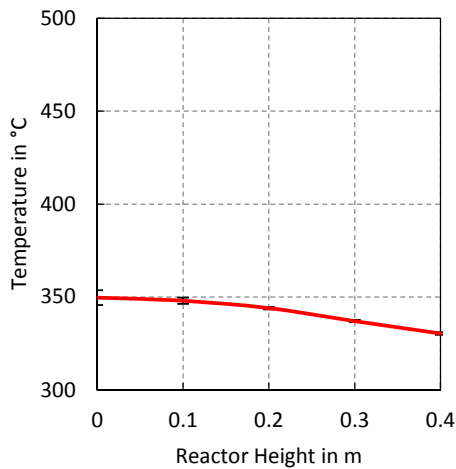
Figure 8: Temperature profile of reactor C during the 100 hours of operation with product gas upstream the RME gas scrubber.

Figures 9 to 12 show the concentrations (dry basis) of the reactive species of the WGS reaction at the inlet and outlet of the WGS pilot plant for the reactors A, B, and C.

Figure 9 shows that the CO content decreased significantly.
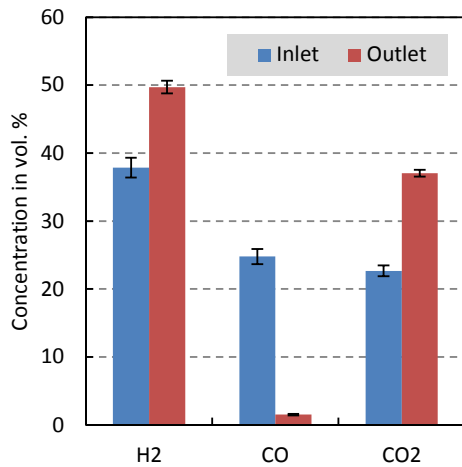
Figure 9: Concentrations (dry basis) of the reactive WGS components at the inlet and outlet of the WGS pilot plant during the 100 hours of operation with product gas upstream the RME gas scrubber.

Figures 10 to 12 also show that the WGS reaction mainly occurred in reactor A (Compare Figures 6 to 8).
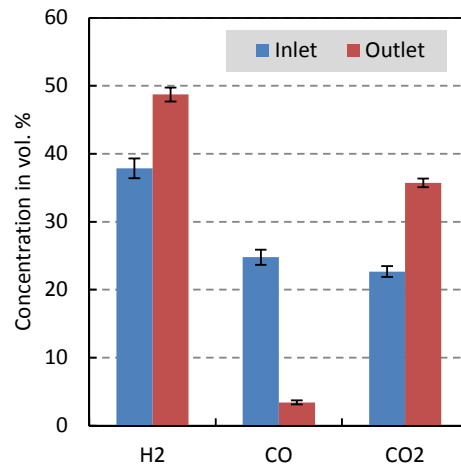
Figure 10: Concentrations (dry basis) of the reactive WGS components at the inlet and outlet of reactor A of the WGS pilot plant during the 100 hours of operation with product gas upstream the RME gas scrubber.
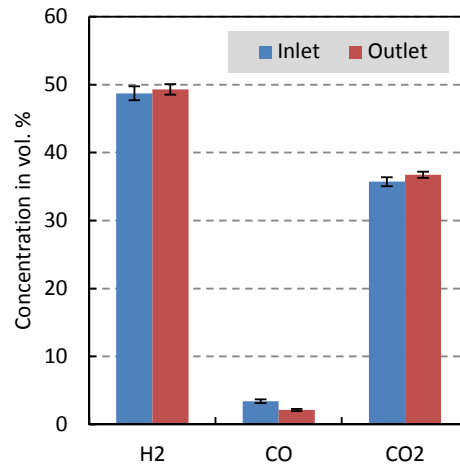
Figure 11: Concentrations (dry basis) of the reactive WGS components at the inlet and outlet of reactor B of the WGS pilot plant during the 100 hours of operation with product gas upstream the RME gas scrubber.
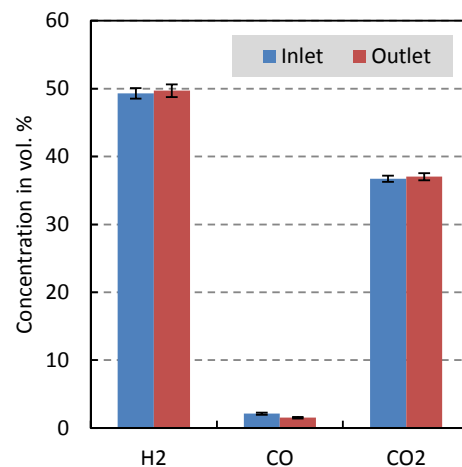
Figure 12: Concentration (dry basis) of the reactive WGS components at the inlet and outlet of reactor C of the WGS pilot plant during the 100 hours of operation with product gas upstream the RME gas scrubber.

Table IV shows the concentrations of the main gas components at the inlet and outlet of all three reactors during the 100 hours of operation with product gas upstream the RME gas scrubber. It can be seen that the CHP plant in Oberwart provided product gas with a steady composition of the main components during the 100 hours of operation of the WGS pilot plant.

Table IV: Concentrations (dry basis) of the main gas components during the 100 hours of operation with product gas upstream the RME gas scrubber.

	H_2 vol. %	CO vol. %	CO_2 vol. %	CH_4 vol. %
Inlet	37.9±1.5	24.8±1.1	22.7±0.8	10.5±0.5
Outlet A	48.7±1.0	3.4±0.3	35.7±0.7	8.9±0.4
Outlet B	49.3±0.8	2.1±0.2	36.8±0.5	8.8±0.3
Outlet C	49.7±0.9	1.5±0.1	37.0±0.5	8.6±0.3
	C_2H_y vol. %	N_2 vol. %	O_2 vol. %	
Inlet	2.8±0.3	1.3±0.2	0.08±0.03	
Outlet A	2.2±0.2	1.1±0.2	0.03±0.01	
Outlet B	2.1±0.3	1.0±0.2	0.03±0.01	
Outlet C	2.0±0.2	1.0±0.2	0.03±0.01	

In addition, Table IV indicates that a H_2 concentration of about 50 vol. % was reached at the outlet of the WGS pilot plant. Along the WGS pilot plant, the dry gas volumetric flow rate increased by a factor of 1.22. With a product gas output of about 1.18 Nm^3/h (dry basis) per kg biomass (dry and ash free, see [14]) a specific H_2 production of about 63 g H_2 per kg biomass was achieved.

Table V shows the concentration of the sulfur components during the 100 hours of operation with product gas upstream the RME gas scrubber.

Table V: Concentrations (dry basis) of the sulfur components during the 100 hours of operation with product gas upstream the RME gas scrubber. BDL=Below Detection Limi

	H_2S vol. ppm	COS vol. ppm	C_4H_4S vol. ppm
Inlet	104±10	3.1±0.5	5.6±1.7
Outlet A	107±8	BDL	5.1±1.4
Outlet B	108±14	BDL	5.4±0.8
Outlet C	110±12	BDL	5.3±1.0

It can be seen that the concentrations of all sulfur components except COS were nearly constant.

During the 100 hours of operation with product gas upstream the RME gas scrubber, tar and ammonia samples were taken at the inlet and outlet of the WGS pilot plant. Table VI shows the results of these samples.

Table VI: Tar and NH_3 concentration (dry basis) at the inlet (reactor A) and outlet (reactor C) of the WGS pilot plant during the 100 hours of operation with product gas upstream the RME gas scrubber. The measurements were single sample measurements. Therefore, no standard deviation could be calculated.

	GCMS Tar mg/Nm^3	Gravimetrical Tar mg/Nm^3	NH_3 vol. ppm
Inlet	8144	169	3350
Outlet	5831	50	2840

Table VI shows that the tar content decreased along the WGS pilot plant because the WGS pilot plant offered a reactive environment and consequently a certain residence time for the tar reduction. The NH_3 content decreased because of the higher volumetric dry gas flow rate after the WGS pilot plant. No chemical NH_3 reaction occurred according to these results.

3.2 Operation with Product Gas Downstream the RME Gas Scrubber

Table VII shows the WGS pilot plant operation parameters and figures during the operation with product gas downstream the RME gas scrubber.

Table VII: Operation data of the WGS pilot plant with gas downstream the RME gas scrubber during the 100 hours of operation. GHSV is given for one reactor. The STDGR and the STCR are given for inlet of the first reactor. X_{CO} is given for the whole WGS pilot plant.

GHSV h^{-1}	STDGR -	STCR -	X_{CO} %
394	1.2	2.0	92

The STDGR and STCR were chosen in order to protect the Fe/Cr based catalyst from coking and carbon deposition. During these 100 hours of operation an overall CO conversion of 92 % was achieved.

Figures 13 to 15 show the temperature profiles along reactors A, B, and C during the 100 hours of operation with product gas downstream the RME gas scrubber.
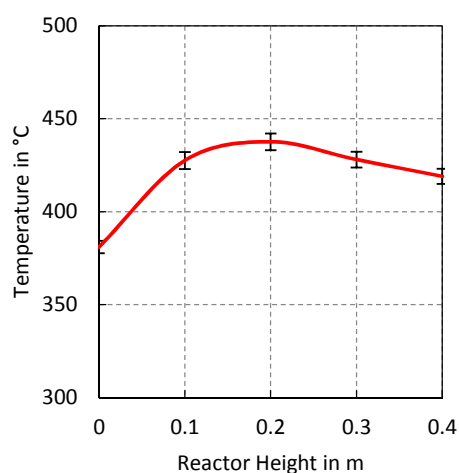
Figure 13: Temperature profile of reactor A during the 100 hours of operation with product gas downstream the RME gas scrubber.

Figures 13 to 15 indicate again that the WGS reaction mainly occurred in reactor A (see Figure 13). The temperature increased along the reactor because of the exothermic WGS reaction. After the temperature maximum was reached, the temperature along reactor A decreased. This was the same result as already observed during the test with product gas upstream the RME gas scrubber.

The product gas was cooled before it entered reactor B and C. Aim was to achieve about the same reactor inlet temperature at the inlet of all three WGS reactors.

Figure 14: Temperature profile of reactor B during the 100 hours of operation with product gas downstream the RME gas scrubber.

In reactor B nearly no WGS reaction took place. Consequently, the heat losses were higher than the temperature increase caused by the exothermic reaction. Therefore, the temperature decreased (see Figure 14).

In reactor C the same effects as in reactor B occurred (see Figure 15).
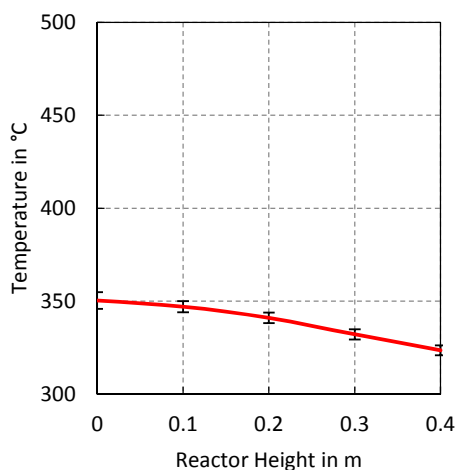
Figure 15: Temperature profile of reactor C during the 100 hours of operation with product gas downstream the RME gas scrubber.

Figures 16 to 19 show the concentrations of the reactive species of the WGS reaction at the inlet and outlet of reactors A, B, and C.

Figure 16 shows that the CO content decreased

significantly along all three reactors. The same result was observed during the test with product gas upstream the RME gas scrubber.
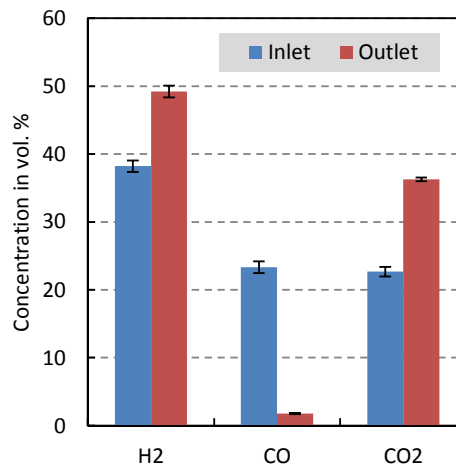
Figure 16: Concentration (dry basis) of the reactive WGS components at the inlet and outlet of the WGS pilot plant during the 100 hours of operation with product gas downstream the RME gas scrubber.

Figures 17 to 19 also show that the WGS reaction mainly took place in reactor A (Compare Figures 13 to 15).
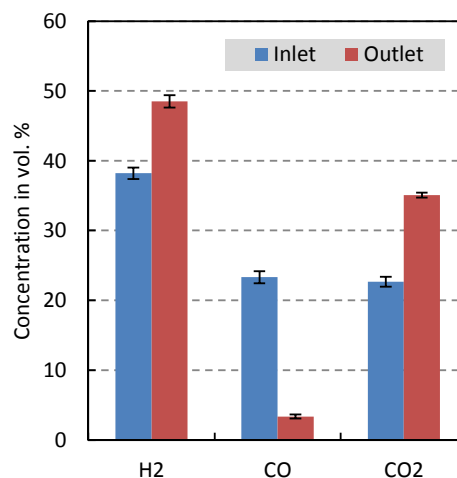
Figure 17: Concentration (dry basis) of the reactive WGS components at the inlet and outlet of reactor A of the WGS pilot plant during the 100 hours of operation with product gas downstream the RME gas scrubber.

Figure 18: Concentration (dry basis) of the reactive WGS components at the inlet and outlet of reactor B of the WGS pilot plant during the 100 hours of operation with product gas downstream the RME gas scrubber.

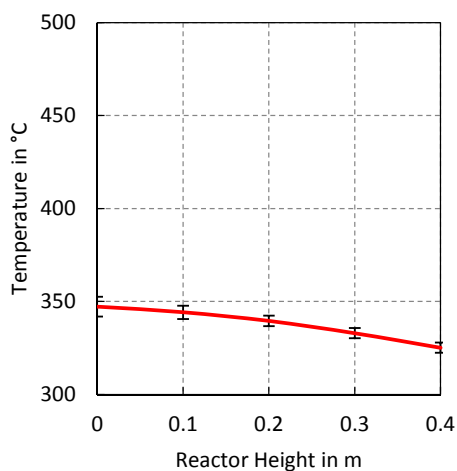**Figure 19:** Concentration (dry basis) of the reactive WGS components at the inlet and outlet of reactor C of the WGS pilot plant during the 100 hours of operation with product gas downstream the RME gas scrubber.

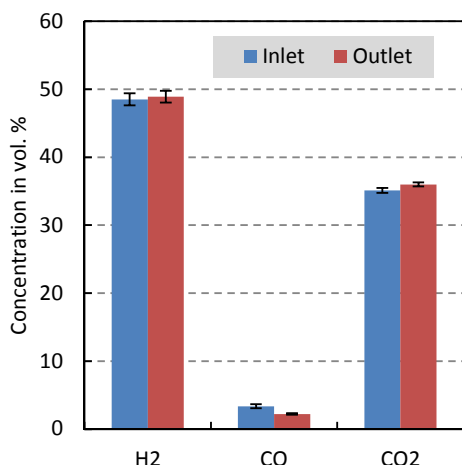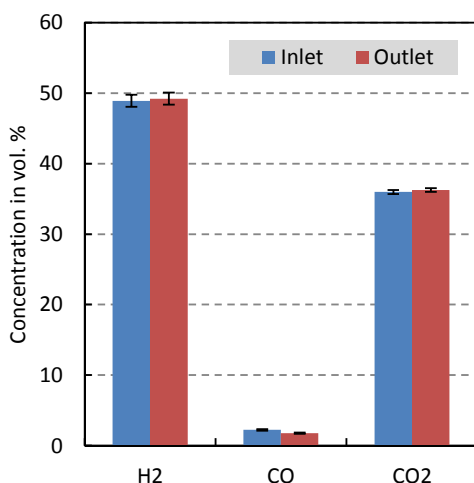Table VIII shows the concentrations of the main gas components at the inlet and outlet of all three reactors during the 100 hours of operation with product gas downstream the RME gas scrubber. Again, it can be seen that the CHP plant in Oberwart provided product gas with a steady composition during this 100 hours of operation of the WGS pilot plant.

Table VIII: Concentrations (dry basis) of the main gas components during the 100 hours of operation with product gas downstream the RME gas scrubber.

	H_2 vol. %	CO vol. %	CO_2 vol. %	CH_4 vol. %
Inlet	38.2±0.8	23.3±0.9	22.7±0.7	10.0±0.4
Outlet A	48.5±0.9	3.4±0.3	35.1±0.4	8.6±0.3
Outlet B	48.9±0.9	2.2±0.1	36.0±0.3	8.5±0.3
Outlet C	49.2±0.9	1.8±0.1	36.3±0.3	8.4±0.3
	C_2H_y vol. %	N_2 vol. %	O_2 vol. %	
Inlet	2.8±0.3	2.7±0.3	0.3±0.04	
Outlet A	2.2±0.3	2.2±0.2	0.03±0.01	
Outlet B	2.2±0.2	2.1±0.2	0.03±0.01	
Outlet C	2.2±0.2	2.1±0.2	0.03±0.01	

In addition, Table VIII indicates that a H_2 concentration of about 50 vol. % was reached at the outlet of the WGS pilot plant. This is the same concentration as during the operation with product gas upstream the RME gas scrubber. Along the WGS pilot plant the dry gas volumetric flow rate increased by a factor of 1.22. With a product gas output of about 1.18 Nm^3/h (dry basis) per kg biomass (dry and ash free, see [14]) a specific H_2 production of about 63 g H_2 per kg biomass was also achieved. The same result was achieved during the operation of the WGS pilot plant with product gas upstream the RME gas scrubber.

Table IX shows the concentration of the sulfur components during the 100 hours operation with product gas downstream the RME gas scrubber.

Table IX: Concentrations (dry basis) of the sulfur components during the 100 hours of operation with product gas downstream the RME gas scrubber. BDL=Below Detection Limit

	H_2S vol. ppm	COS vol. ppm	C_4H_4S vol. ppm
Inlet	91±13	3.8±0.9	5.6±1.6
Outlet A	79±12	BDL	5.1±1.0
Outlet B	59±13	BDL	5.6±0.9
Outlet C	44±9	BDL	5.7±1.0

During the 100 hours of operation with product gas downstream the RME gas scrubber, no tar and NH_3 samples were taken. [8] and [12] provide data of tar and NH_3 samples taken during the operation of the WGS pilot plant with product gas downstream the RME gas scrubber.

4 CONCLUSION AND OUTLOOK

During both 100 hours of operation with product gas upstream as well as downstream the RME gas scrubber no significant difference regarding the performance of the WGS pilot plant could be observed.

In both cases, a CO conversion of more than 92 % was achieved. Consequently, the CO concentration of the product gas could be lowered to less than 2.0 vol. % (dry basis) at the outlet of the WGS pilot plant.

During the 100 hours of operation with product gas upstream the RME gas scrubber, the WGS pilot plant operated flawlessly and the Fe/Cr based catalyst showed no performance decrease caused by the higher tar and NH_3 content in the product gas which is an important as well as encouraging result for a future application.

Within the overall 200 hours of operation and with this experimental setup, no catalyst deactivation could be overserved.

Future work should proof the long term stability of the Fe/Cr based catalyst during operation with product gas upstream the RME gas scrubber.

5 ABBREVIATIONS AND ACRONYMS

BDL	Below Detection Limit
CHP	Combined Heat and Power
d.b.	Dry Basis
DFB	Dual Fluidized Bed
FPD	Flame Photometric Detector
FR	Flow Record
GC	Gas Chromatograph
GCMS	Gas Chromatography Mass Spectroscopy
ORC	Organic Rankine Cycle
RME	Rapeseed Methyl Ester
TCD	Thermal Conductivity Detector

6 SYMBOLS

c_i	Volumetric fraction of component i in -
GHSV	Gas Hourly Space Velocity in h^{-1}
ΔH	Enthalpy of formation in kJ/mol
STDGR	Steam to Dry Gas Ratio in -
STCR	Steam to Carbon Ratio in -
$V_{Catalyst}$	Catalyst volume in m^3
$\dot{V}_{Dry}$	Volumetric dry gas flow rate in Nm^3/h
$\dot{V}_{H2O}$	Volumetric steam flow rate in Nm^3/h
X_{CO}	CO conversion in -

7 REFERENCES

[1] Liu K. et.al., Hydrogen and Syngas Production and Purification Technologies, (2010), Book, Wiley VCH.

[2] Balat H., Hydrogen from biomass – Present scenario and future prospects, (2010), International Journal of Hydrogen Energy, Vol. 36, pag. 7416-7426.

[3] Mueller S., Hydrogen from Biomass for Industry– Industrial Application of Hydrogen Production Based on Dual Fluid Gasification, (2013), PhD Thesis, Vienna University of Technology.

[4] Hofbauer H., Biomass CHP Plant Guessing– A Success Story, (2003), CPL Press.

[5] Kaltschmitt M. et.al., Energie aus Biomasse, (2009), Book, Springer Verlag.

[6] Diaz N., Hydrogen Separation from Producer Gas Generated by Biomass Steam Gasification, (2013), PhD Thesis, Vienna University of Technology.

[7] Twigg M. V., Catalyst Handbook Chapter 6: The Water-gas-shift Reaction, (1989), Book, Manson Publishing.

[8] Fail S., Biohydrogen Production Based on the Catalyzed Water Gas Shift Reaction in Wood Gas, (2014), PhD Thesis, Vienna University of Technology.

[9] Gordon S., Computer program for calculation of complex chemical equilibrium composition, rocket performance, incident and reflected shocks and Chapman-Jouguet detonations, (1971), Report, NASA Lewis Research Center.

[10] Kotik J., Ueber den Einsatz von Kraft-Waerme-Kopplungsanlagen auf Basis der Wirbelschicht-Dampfvergasung fester Biomasse am Beispiel des Biomassekraftwerks Oberwart, (2010), PhD Thesis, Vienna University of Technology.

[11] Corella J. et.al., 140 g H_2/kg biomass d.a.f. by a CO-shift reactor downstream from a FB biomass gasifier and a catalytic steam reformer, (2008), International Journal of Hydrogen Energy, Vol. 33, pag. 1820-1826.

[12] Fail S. et.al., Wood Gas Processing To Generate Pure Hydrogen Suitable for PEM Fuel Cells, (2014), ACS Sustainable Chemistry & Engineering, Vol. 2(12), pag. 2690-2698.

[13] Wolfesberger U. et.al., Tar content of composition in producer gas of fluidized bed gasification of wood-influence of temperature and pressure, (2009), Environmental Process & Sustainable Energy, Vol. 28(3), pag. 372-379.

[14] Kirnbauer F. et.al., Performance improvement of dual fluidized bed gasifiers by temperature reduction: The behavior of tar species in the product gas, (2013), Fuel, Vol. 108, pag. 534-542.

8 ACKNOWLEDGEMENTS

9   LOGO SPACE

bioenergy2020+

TECHNISCHE
UNIVERSITÄT
WIEN
Vienna University of Technology

energie
BURGENLAND

AIR LIQUIDE
Creative Oxygen

COMET

Competence Centers for
Excellent Technologies

FFG

Michael Kraussler, Matthias Binder, Silvester Fail, Antonio Plaza, Alberto Cortes, and Hermann Hofbauer.

Validation of a kinetic model for the catalyzed water gas shift reaction applying a Fe/Cr catalyst processing product gas from biomass steam gasification.

VALIDATION OF A KINETIC MODEL FOR THE CATALYZED WATER GAS SHIFT REACTION APPLYING A FE/CR CATALYST PROCESSING PRODUCT GAS FROM BIOMASS STEAM GASIFICATION

Kraussler M.[1], Binder M.[2], Fail S.[2], Plaza A.[3], Cortes A.[3], Hofbauer H.[1,2]
[1]Bioenergy2020+ GmbH, Wienerstrasse 49, 7540 Guessing, Austria
[2]Vienna University of Technology, Institute of Chemical Engineering, Getreidemarkt 9, 1060 Vienna, Austria
[3]University of Granada, Acera de San Ildefonso 48, 18071 Granada, Spain

ABSTRACT: In this work, a kinetic model of the catalyzed water gas shift reaction applying a Fe/Cr based catalyst found from investigations in a micro reactor test rig is validated with experimental data from a pilot plant water gas shift reactor. The reactor was fed with product gas from an industrial biomass dual fluidized bed steam gasification plant. The validation was done with product gas upstream a rapeseed methyl ester gas scrubber and product gas downstream a rapeseed methyl ester gas scrubber of the biomass gasification plant. In both cases, the calculated and measured values of the concentrations at the outlet of the reactor showed good agreement. However, the model shows inaccuracy regarding the temperature profile at the entrance of the reactor. If the kinetic model can be improved and adapted, it could be useful for basic design and engineering of an industrial scale water gas shift reactor applying a Fe/Cr based catalyst and processing product gas from biomass steam gasification.
Keywords: Biomass, Gasification, Hydrogen, Modelling, Product Gas, Water Gas Shift

1 INTRODUCTION

Today, hydrogen is an important resource for a wide range of applications in chemical industry [1]. More than 95 % of this hydrogen is produced by steam reforming of natural gas and other processes with fossil fuels as feedstock. With the background of the climate change, a CO_2 neutral method of hydrogen production needs to be established [2].

Biomass steam gasification is a proven technology and CO_2 neutral alternative to steam reforming of natural gas [3].

A promising technology for biomass steam gasification is the dual fluidized bed (DFB) process [4,5]. The commercial biomass gasification plants in Guessing and Oberwart have been using this technology for several years. Both plants generate a product gas with a H_2 content of about 40 vol. % (dry basis). The other components are about 25 vol. % CO (d.b.), 20 vol. % CO_2 (d.b.), and 10 vol. % CH_4 (d.b.). In addition, small amounts of N_2, O_2, higher hydrocarbons, and about 100 vol. ppm H_2S (d.b.) are contained. The high H_2 content makes the product gas a promising CO_2 neutral H_2 source [6]. A process which can further increase the hydrogen content of the product gas is the exothermic water gas shift (WGS) reaction (see Equation 1).

$$CO + H_2O \overset{-\Delta H}{\longleftrightarrow} CO_2 + H_2 \qquad (1)$$
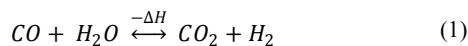
It converts carbon monoxide and steam to carbon dioxide and hydrogen. In order to reach economic reaction rates, catalysts are necessary. Suitable catalysts are based on Fe/Cr formulations. At the amount of about 100 vol. ppm H_2S, the Fe/Cr based catalyst seems to be robust against sulfur poisoning [7].

In [8], a kinetic model for the Fe/Cr based catalyzed WGS reaction processing product gas was proposed. This model takes effects of H_2S on the Fe/Cr based catalyst into account.

This paper validates the kinetic model with experimental data from a WGS pilot plant located at the plant site of the biomass steam gasification plant in Oberwart, Austria. Therefore, product gas from the biomass gasification plant was processed in a pilot plant

WGS reactor applying a Fe/Cr based catalyst. The experimental results were compared with numerical calculations based on the kinetic model in Equation (2).

The non-linear molar and energy balances of an adiabatic ideal plug flow reactor were solved with a numerical method. For this purpose, a finite difference method was used.

In this work, the solutions of the molar and energy balances are described. Consequently, the numerical equation system is derived. Finally, the experimental approach is shown and the calculated and experimental results are compared.

2 MATERIALS AND METHODS

At the beginning of this chapter, the chemical kinetic law of the WGS reaction catalyzed by the Fe/Cr based catalyst which was presented in [8] is introduced.

Furthermore, the molar and energy balances of the pilot plant WGS reactor are derived. Consequently, the numerical balances are introduced.

Finally, the pilot plant WGS reactor and the measurement methods which were used for the validation process are described.

2.1 The Kinetic Model of a WGS Reaction Catalyzed by a Fe/Cr Based Catalyst

The kinetic model of the WGS reaction was derived at Vienna University of Technology from results obtained in a laboratory scale chemical kinetics test rig. Starting point was the mathematical approach for the reaction rate $r(c_i, T)$ in Equation 2.

$$r(c_i, T) = k_0 \cdot \exp\left(\frac{-E_a}{R \cdot T}\right) \cdot$$

$$\cdot p_{CO}^a \cdot p_{H2O}^b \cdot p_{CO2}^c \cdot p_{H2}^d \cdot \qquad (2)$$

$$\cdot \left(1 - \frac{K_{MAL}}{K_g}\right)$$

The reaction rate is a function of the reactive species (CO, H_2O, CO_2, and H_2) and the temperature. Other

components which are contained in the product gas of the biomass steam gasification process were considered inert.

The reaction rate is described by the rate constant k_0, the activation energy E_a, and the reaction exponents (a,b,c, and d) of each component i which is a reactant of the WGS reaction (see Equation 1). p_i is the partial pressure, R the general gas constant, and T the temperature. K_{MAL} is the mass action law and K_g the equilibrium constant calculated by thermo-physical properties.

The partial pressure of each component i can be expressed by the overall absolute pressure p and the volumetric concentration c_i:

$$p_i = c_i \cdot p \qquad (3)$$

The buildup and function of the test rig for chemical kinetics at Vienna University of Technology can be found in [8]. The experiments led to the following values for the parameters of Equation 2 (see Table I).

Table I: Parameters of the kinetic model for the WGS reaction catalyzed by a Fe/Cr based catalyst.

Parameter	Value	Unit
k_0	117.8	mol/g_{cat} kPa s
E_a	102E+3	J/mol
a	1.77	-
b	0.23	-
c	-0.17	-
d	-0.12	-

2.2 Balances of the Ideal Adiabatic Plug Flow Reactor

For the validation of the kinetic model with experimental data, the molar and the energy balances of an ideal adiabatic plug flow reactor was derived.

2.2.1 Derivation of the Molar Balance of the Ideal Adiabatic Plug Flow Reactor

Figure 1 shows the illustration for the derivation of the molar balance of the pilot plant WGS reactor.
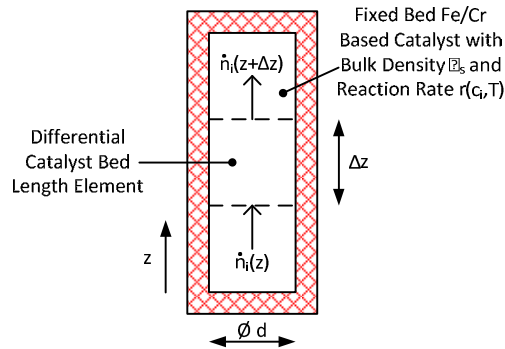
Figure 1: Illustration for the calculation of the molar balance of the pilot plant WGS reactor.

The molar balance of each reactive component i leads to

$$\dot{n}_i(z + \Delta z) - \dot{n}_i(z) = \pm r(c_i, T) \cdot \rho_s \cdot \Delta z \cdot \frac{d^2 \cdot \pi}{4} \qquad (4)$$

$$\frac{\dot{n}_i(z + \Delta z) - \dot{n}_i(z)}{\Delta z} = \pm r(c_i, T) \cdot \rho_s \cdot A \qquad (5)$$

$\dot{n}_i$ is the molar flow of component i and A is the cross section of the catalyst bed. ρ_s is the bulk density of the Fe/Cr based catalyst. $\pm$ indicates if component i is an educt or a product of the WGS reaction.

The limiting process lim $\Delta z \rightarrow 0$ leads to the following differential equation:

$$\frac{d\dot{n}_i}{dz} = \pm r(c_i, T) \cdot \rho_s \cdot A \qquad (6)$$

Replacement of the molar flow rate $\dot{n}_i$ of each component i with the overall molar flow rate $\dot{n}$ and the volumetric concentration of each component i leads to

$$\frac{dc_i}{dz} = \pm r(c_i, T) \cdot \rho_s \cdot A \cdot \frac{1}{\dot{n}} \qquad (7)$$

This step is valid because of the equimolar character of the WGS reaction and the assumption of ideal gas behavior. Consequently, the overall molar flow rate is constant.

Equation 7 is the starting point for the numerical solution of the molar balance of the pilot plant WGS reactor.

2.2.2 Derivation of the Energy Balance of the Ideal Adiabatic Plug Flow Reactor

Figure 2 shows the drawing for the derivation of the energy balance of the pilot plant WGS reactor.
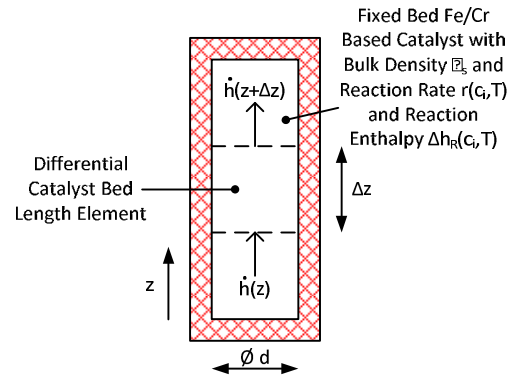
Figure 2: Illustration for the calculation of the energy balance for the pilot plant WGS reactor.

The energy balance of the differential element leads to

$$\dot{h}(z + \Delta z) - \dot{h}(z) =$$
$$= \pm \Delta h_R(c_i, T) \cdot r(c_i, T) \cdot \rho_s \cdot \Delta z \cdot A \qquad (8)$$

With the formation enthalpy $\Delta h_R(c_i, T)$ of the WGS reaction and the overall enthalpy flow $\dot{h}$. The limiting process lim $\Delta z \rightarrow 0$ and the overall molar heat capacity $c_P(c_i, T)$ of the gas stream lead to

$$\frac{dT}{dz} = \pm \Delta h_R(c_i, T) \cdot r(c_i, T) \cdot \rho_s \cdot A \cdot \frac{1}{c_P(c_i, T)} \qquad (9)$$

Equation 9 is the starting point for the numerical solution of the energy balance of the pilot plant WGS reactor. With Equations 7 and 9, the numerical solution for the pilot plant WGS reactor can be derived.

2.3 The Finite Difference Model for the Ideal Plug Flow Reactor

The non-linear behavior of Equations 7 and 9 make an analytical solution difficult. Therefore, a numerical approach was appropriate. The finite difference method was chosen for solving Equations 7 and 9. This numerical method is easy to apply and its accuracy is high enough for this work.

Figure 3 shows the concept of the finite difference method for the solution of Equations 7 and 9. Please note that superscript indices which refer to the finite difference method should not be mixed up with exponents.
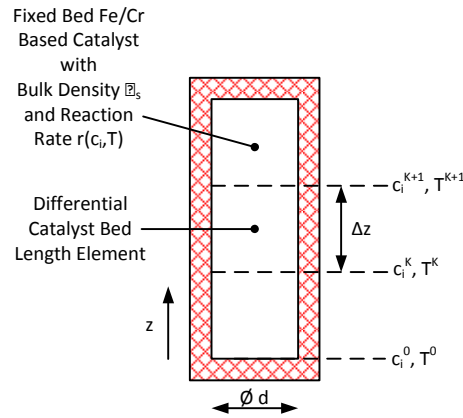
Figure 3: Illustration of the finite difference approach for solving Equations 7 and 9.

Introduction of the differential quotient in Equation 7 leads to Equations 10 and 11.

$$\frac{c_i^{K+1} - c_i^K}{\Delta z} = \pm r(c_i^K, T^K) \cdot \rho_s \cdot A \cdot \frac{1}{\dot{n}} \qquad (10)$$

$$c_i^{K+1} = \pm r(c_i^K, T^K) \cdot \rho_s \cdot A \cdot \frac{1}{\dot{n}} \cdot \Delta z + c_i^K \qquad (11)$$

Equation 11 enables the calculation of the concentration profiles of CO, H_2O, CO_2, and H_2 along the bed length of the pilot plant WGS reactor if the boundary conditions c_i^0 at the beginning of the reactor are given.

Introduction of the differential quotient in Equation 9 leads to Equation 12 and 13.

$$\frac{T^{K+1} - T^K}{\Delta z} =$$
$$= \pm \Delta h_R(c_i, T) \cdot r(c_i, T) \cdot \rho_s \cdot A \cdot \frac{1}{c_P(c_i, T)} \qquad (12)$$

$$T^{K+1} =$$
$$= \pm \Delta h_R(c_i, T) \cdot r(c_i, T) \cdot \rho_s \cdot A \cdot \frac{1}{c_P(c_i, T)} \cdot \Delta z + \qquad (13)$$
$$+ T^K$$

Equation 13 enables the calculation of the temperature profile along the bed length of the pilot plant WGS reactor if the boundary condition T^0 at the entrance of the reactor is given.

Equations 11 and 13 form an equation system which describes the concentration and temperature profile along the pilot plant WGS reactor. This equation system was solved using an algorithm which was written in Scilab™ [9].

The thermophysical properties of the product gas components were calculated by NASA polynomials [10].

Input values for the numerical calculation were the steam volumetric flow rate $\dot{V}_{H2O}$, the dry gas volumetric flow rate $\dot{V}_{Dry}$, the kinetic model coefficients in Table I, the reactor length L, the reactor diameter d, the concentrations at the reactor inlet c_i^0, and the reactor inlet temperature T^0.

2.4 Biomass Steam Gasification Plant in Oberwart

The pilot plant WGS reactor processed product gas from the biomass steam gasification combined heat and power (CHP) plant in Oberwart. Figure 4 shows a simplified flowchart of the process.

The plant is based on the DFB steam gasification technology which is described in detail in [4] and [5].

The CHP plant generates district heat and electricity from biomass (woodchips) as feedstock. Table II shows the main operation parameters of the CHP plant.

Table II: Main operation parameters of the CHP plant in Oberwart [6].

Parameter	Value	Unit
Fuel Power	8.7	MW
District Heat Power	4.0	MW
Electrical Power	2.8	MW

Biomass is fed into the biomass dryer. In the next step, the screw conveyor transports the biomass into the gasifier. In the gasifier, the biomass is in contact with steam and the bed material olivine at about 850 °C. No oxygen is needed for the gasification process. The result is a product gas with high hydrogen content (about 40 vol. %, d.b.). The product gas is cooled, cleaned by a bag house filter and by a rapeseed methyl ester (RME) gas scrubber. In the RME gas scrubber, tar, NH_3, and other condensable fractions of the product gas are removed before the product gas is fed into gas engines for electricity generation.

There is the possibility to take a partial flow of the product gas for experimental work from two different extraction points along the product gas line (see Figure 4). The first extraction point is upstream the RME gas scrubber and the second extraction point is downstream the RME gas scrubber after the product gas blower. Table III shows the conditions at the two different extraction points.
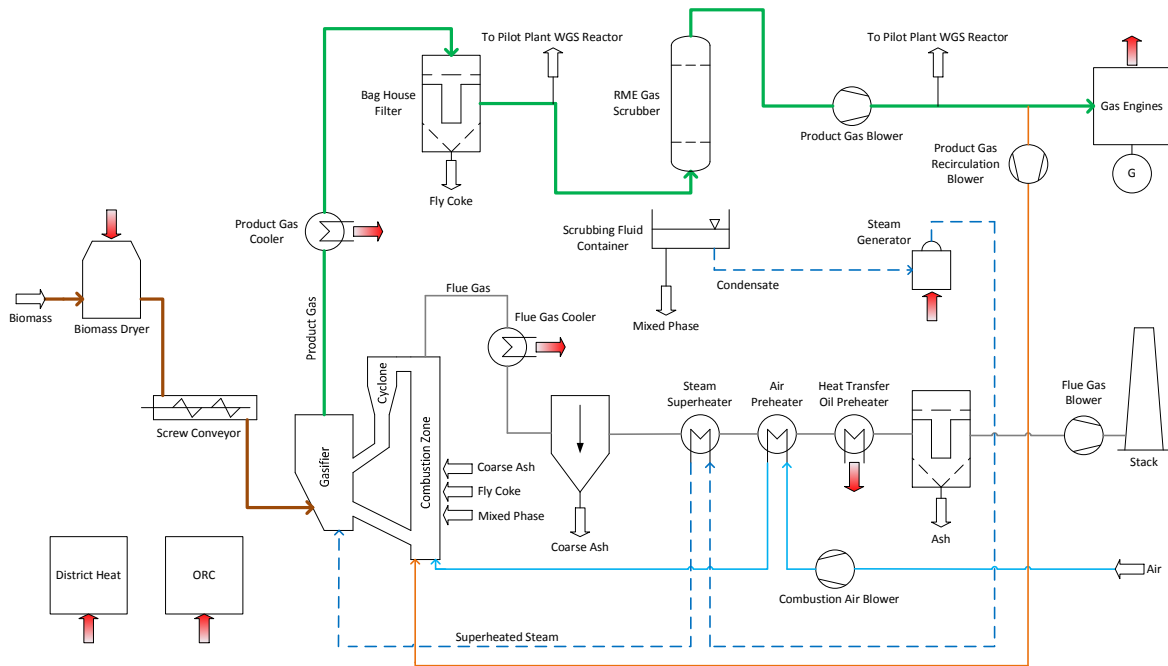
Figure 4: Simplified flowchart of the CHP plant in Oberwart. Heat sources and heat sinks of the process are indicated by arrows.

Table III: Operation conditions at the experimental extraction points (see Figure 4) of the CHP plant under full load operation.

Parameter	Upstream RME Scrubber	Downstream RME Scrubber	Unit
Temperature	~ 150	~ 40	°C
H_2O Content	~ 35	~ 7	vol. %

For the validation of the kinetic model, the product gas was successively taken from both extraction points.

A detailed description of the CHP plant in Oberwart can be found in [11].

2.5 The Pilot Plant WGS Reactor

Figure 5 shows a simplified flowchart of the pilot plant WGS reactor located at the plant site of the CHP plant in Oberwart. The unit consisted of a cylindrical thermal insulated reactor. At the bottom of the reactor a screen plate was used for carrying the Fe/Cr based catalyst. The catalyst bed diameter was 9 cm and its height was about 40 cm resulting in a catalyst bed volume of about 2.5 liters. Seven thermocouples were used to measure and record the temperature profile along the pilot plant WGS reactor. The temperature profile allowed a conclusion on the activity of the Fe/Cr based catalyst due to the exothermic behavior of the WGS reaction.
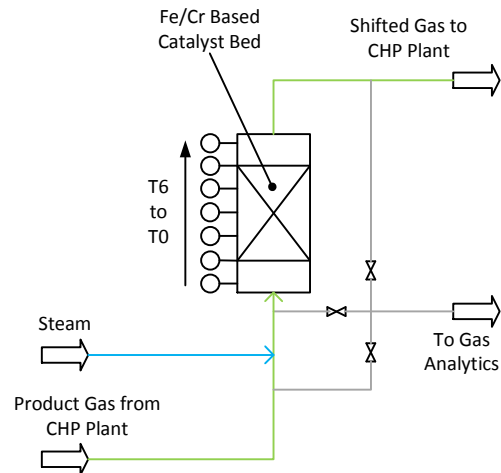
Figure 5: Simplified flowchart of the pilot plant WGS reactor which was used for processing product gas from the CHP plant in Oberwart.

The pilot plant WGS reactor processed a partial flow of the product gas of the CHP plant from the two extractions points (see Figure 4). The product gas was mixed with a certain amount of steam which was provided by a steam generator. The gas inlet temperature was adjusted with a heating section. The pilot plant WGS reactor operated at ambient pressure.

After the product gas was processed in the reactor, it was recycled back to the CHP plant. A sampling flow of the processed gas upstream the steam addition, at the inlet, and at the outlet of the pilot plant WGS reactor was sent to the gas analytical line and subsequently to a gas chromatograph in order to measure the dry gas composition.

2.6 Measurement of the Temperature Profile along the Pilot Plant WGS Reactor and Measurement of the Gas Components

Figure 5 shows the position of the thermocouples (type J) along the pilot plant WGS reactor. Thermocouple T0 was positioned before the fixed bed Fe/Cr based catalyst. Therefore, it was not in the reactive zone. T1 to T5 were positioned along the catalyst bed with a distance of 10 cm to each other. T1 was positioned directly at the beginning of the catalyst bed and T5 was positioned directly at the end of the catalyst bed. T6 was outside the catalyst bed. Those thermocouples enabled the measuring and recording of the temperature profile along the investigated pilot plant WGS reactor.

A gas chromatograph (Clarus 500^{TM} from Perkin Elmer) was used to measure the gas composition at the inlet and at the outlet of the pilot plant WGS reactor. A thermo- conductivity detector (TCD) enabled the quantification of different components in the gas stream. CO, CO_2, CH_4, N_2, and O_2 were measured. Other minor gas components in the product gas were neglected and not further discussed in this paper. The gas chromatograph was not able to measure the H_2 concentration. Consequently, the H_2 concentration was calculated as the difference of the sum of the other measured components to hundred percent.

Figure 6 shows the setup of the gas conditioning before the gas chromatograph. The gas stream passed two gas washing bottles filled with glycol at a temperature of about -5 °C in order to condense and separate the steam. Therefore, a dry gas stream could be assumed after the gas washing bottles. The dry gas stream passed another gas washing bottle filled with glass wool in order to prevent aerosols from entering the gas chromatograph. After the glass wool bottle, a gas meter recorded the volumetric dry gas flow.
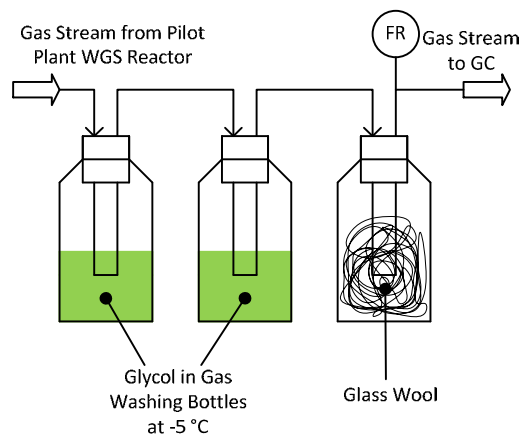
Figure 6: Setup of gas conditioning upstream the gas chromatograph.

The steam content in the product gas upstream the steam addition, at the inlet of the reactor, and at the outlet of the reactor was determined with a gravimetrical method. The gas stream passed the gas washing bottles for a certain time whereas the volumetric flow was recorded. Subsequently, the gas washing bottles were weighed. Consequently, the steam content upstream the steam addition, at the inlet, and at the outlet of the reactor could be determined.

The volumetric dry gas flow rate was calculated by

the water balance of the pilot plant WGS reactor.

2.7 Characteristic Figures of the Pilot Plant WGS Reactor

The operation of the pilot plant WGS reactor could be characterized by a series of key figures calculated according Equations 14 to 16.

The first figure (Equation 14) was the gas hourly space velocity (GHSV). It is the reverse residence time. It was calculated as the ratio of the volumetric dry gas flow rate and the catalyst volume in the reactor. It indicates the stress of the catalyst.

$$GHSV = \frac{\dot{V}_{Dry}}{V_{Catalyst}} \qquad (14)$$

The second figure (Equation 15) was the steam to dry gas ratio (STDGR). This figure describes the ratio of the volumetric steam flow rate to the volumetric dry gas flow rate in the feed of the pilot plant WGS reactor.

$$STDGR = \frac{\dot{V}_{H2O}}{\dot{V}_{Dry}} \qquad (15)$$

The third figure (Equation 16) was the steam to carbon ratio (STCR). This figure is the ratio of the volumetric steam flow rate and the volumetric flow rate of all gas components which include at least one carbon atom. The value of the STCR must not be too low in order to avoid coking on the surface of the catalyst.

$$STCR = \frac{\dot{V}_{H2O}}{\dot{V}_{Dry} \cdot (c_{CO} + c_{CO2} + c_{CH4})} \qquad (16)$$

All three figures described the conditions in the pilot plant WGS reactor. They make different WGS reactors comparable to each other.

3 RESULTS AND DISCUSSION

In this chapter, a comparison between experimental results from the pilot plant WGS reactor and calculations with the mathematical model is presented. For this comparison, two 100 hour steady state test runs were selected. The dry gas composition at the inlet, at the outlet, and the temperature profile along the pilot plant WGS reactor are considered.

The operation of the pilot plant WGS reactor with product gas upstream and downstream the RME gas scrubber is compared. CO, H_2O, CO_2, and H_2 were considered as reactive species. The other components (CH_4, N_2, and O_2) were considered to be inert during the WGS reaction.

3.1 Validation of the Kinetic Model with Product Gas Upstream the RME Gas Scrubber

This section compares the experimental results with the calculated results from the numerical approach. The pilot plant WGS reactor was operated with product gas upstream the RME gas scrubber of the CHP plant. The steam content at the inlet of the pilot plant WGS reactor was set to about 60 vol. %. The temperature along the reactor and the dry gas composition at the inlet and at the outlet of the reactor were measured.

The measured values were from 100 hours of steady

state operation of the pilot plant WGS reactor with product gas upstream the RME gas scrubber. Table IV shows the characteristic values of the operation with product gas upstream the RME gas scrubber.

Table IV: Characteristic values of the pilot plant WGS reactor operation with product gas upstream the RME gas scrubber.

GHSV	STDGR	STCR
h^{-1}	-	-
621	1.5	2.5

Figure 7 shows the measured and calculated concentrations (dry basis) of H_2, CO, and CO_2 including the error bars at the inlet and at the outlet of the pilot plant WGS reactor.
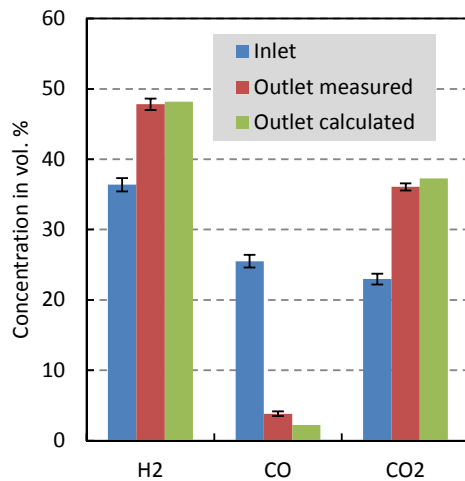
Figure 7: Concentrations (dry basis) of the main gas components H_2, CO, and CO_2 at the pilot plant WGS reactor inlet, outlet (measured), and outlet (calculated with Equation 11 and 13). Error bars show the standard deviation of the measured values.

Figure 7 shows good accordance regarding the concentrations of H_2, CO, and CO_2 at the outlet of the pilot plant WGS reactor. The difference of the CO concentration of the measured and calculated values at the outlet is higher compared to the difference of CO_2 and H_2. This can be explained due to the slightly oscillating steam content in the product gas upstream the RME gas scrubber. This was caused by different fractions of biomass with different water contents and therefore, oscillating steam content in the product gas.

Table V shows the concentrations of all measured and calculated components at the inlet and outlet of the pilot plant WGS reactor.

The concentrations at the outlet of the reactor are near to the equilibrium composition for the chosen operation parameters. The lower concentrations of the non-reactive components CH_4, N_2, and O_2 at the outlet of the reactor compared with the concentrations of the reactor inlet can be explained by the dilution effect due to higher dry gas flow rate at the pilot plant WGS reactor outlet caused by the stoichiometry of the WGS reaction.

Table V: Concentrations (dry basis) of the gas components at the inlet and at the outlet of the pilot plant WGS reactor during operation with product gas upstream the RME gas scrubber. Measured (mea.) values and calculated (calc.) values are shown.

	H_2 vol. %	CO_2 vol. %	CO vol. %
Inlet	36.3 ± 1.0	23.0 ± 0.8	25.5 ± 0.9
Outlet mea.	47.8 ± 0.8	36.1 ± 0.5	3.8 ± 0.3
Outlet calc.	48.1	37.3	2.2
	CH_4 vol. %	O_2 vol. %	N_2 vol. %
Inlet	10.9 ± 0.4	0.1 ± 0.04	4.2 ± 1.6
Outlet mea.	9.1 ± 0.4	0.03 ± 0.002	3.2 ± 1.1
Outlet calc.	8.9	0.08	3.4

Table VI shows the mean values of the thermocouples along the pilot plant WGS reactor with product gas upstream the RME gas scrubber during the 100 hours steady state operation.

Table VI: Mean values of the thermocouples along the pilot plant WGS reactor during operation with product gas upstream the RME gas scrubber. T0 and T6 are not in contact with the catalyst bed.

Thermocouple	Value	Unit
T0	355.4 ± 1.6	°C
T1	366.3 ± 1.4	°C
T2	394.3 ± 3.6	°C
T3	415.2 ± 5.2	°C
T4	418.3 ± 5.0	°C
T5	416.5 ± 4.4	°C
T6	362.9 ± 3.5	°C

The exothermic WGS reaction caused a temperature increase along the reactor (see Figure 8). At a certain point, the temperature decreased because of heat losses. In addition, the equilibrium composition was reached. Therefore, the reaction stopped and consequently the temperature decreased further.
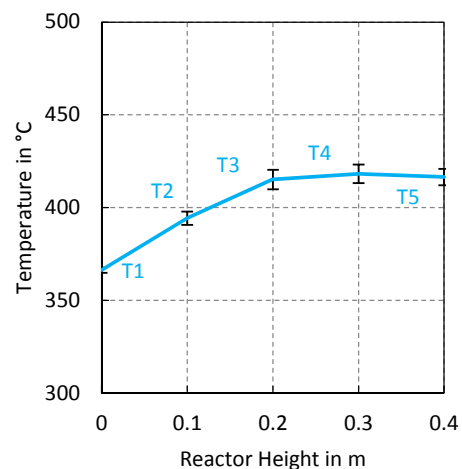
Figure 8: Temperature profile along the pilot plant WGS reactor operated with product gas upstream the RME gas scrubber.

3.2 Validation of the Kinetic Model with Product Gas Downstream the RME Gas Scrubber

This time, the pilot plant WGS reactor was operated with product gas downstream the RME gas scrubber of the CHP plant in Oberwart. This section compares the experimental results with the calculated results from the mathematical model.

The measured values were found during another 100 hours of steady state operation of the pilot plant WGS reactor.

Table VII shows the operation data of the pilot plant WGS reactor.

Table VII: Characteristic values of the pilot plant WGS reactor with product gas downstream the RME gas scrubber.

GHSV	STDGR	STCR
h^{-1}	-	-
524	1.2	2.2

Figure 9 shows the concentrations of H_2, CO, and CO_2 (d.b.) at the inlet as well as the measured and calculated concentrations of the reactive species of the WGS reaction. The main difference compared to the data in Section 3.1 is that the gas is cooled and cleaned by the RME gas scrubber of the CHP plant. Consequently, the tar content in the product gas was lower.
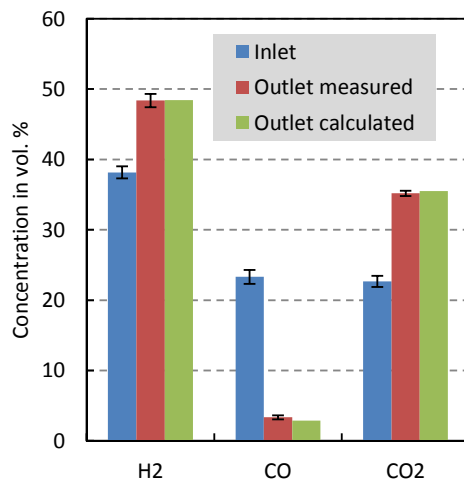
Figure 9: Concentrations (dry basis) of the main gas components H_2, CO, and CO_2 at the pilot plant WGS reactor inlet, outlet (measured), and outlet (calculated with Equation 11 and 13). Error bars show the standard deviation of the measured values.

The calculated data in Figure 9 regarding the CO concentration are in better agreement to the experimental results than in Section 3.1. This can be explained by the product gas composition downstream the RME gas scrubber. The steam content in the product gas was very constant over the 100 hours of operation because the RME gas scrubber operated at a steady temperature level. This steady temperature level led to a certain and constant amount of steam in the product gas downstream the RME gas scrubber.

Table VIII shows the mean values of the concentration (d.b.) of all measured components at the pilot plant WGS reactor inlet and outlet. The

concentrations at the outlet of the reactor are near the equilibrium concentrations for the chosen operation parameters. The lower concentration of CH_4 and the other non-reactive components at the outlet of the reactor can be explained by the dilution effect due to higher dry gas flow rate at the pilot plant WGS reactor outlet.

Table VIII: Mean values of the concentrations (dry basis) of the main components at the inlet and outlet of the pilot plant WGS reactor during operation with product gas downstream the RME gas scrubber.

	H_2 vol. %	CO_2 vol. %	CO vol. %
Inlet	38.2 ± 0.9	22.7 ± 0.8	23.3 ± 1.0
Outlet mea.	48.3 ± 1.0	35.2 ± 0.4	3.4 ± 0.3
Outlet calc.	48.3	35.5	2.9
	CH_4 vol. %	O_2 vol. %	N_2 vol. %
Inlet	10.0 ± 0.4	0.25 ± 0.03	5.6 ± 1.6
Outlet mea.	8.7 ± 0.4	0.03 ± 0.01	4.4 ± 1.1
Outlet calc.	8.4	0.21	4.7

Table IX shows the mean values of the thermocouples along the pilot plant WGS reactor during the 100 hours operation with product gas downstream the RME gas scrubber.

Table IX: Measured values of the thermocouples along the pilot plant WGS reactor during operation with product gas downstream the RME gas scrubber.

Thermocouple	Value	Unit
T0	353.3 ± 3.2	°C
T1	381.0 ± 3.4	°C
T2	427.4 ± 4.6	°C
T3	437.4 ± 4.5	°C
T4	427.9 ± 4.2	°C
T5	418.9 ± 4.0	°C
T6	357.9 ± 3.9	°C

Figure 10 shows the temperature profile along the pilot plant WGS reactor with measured data.
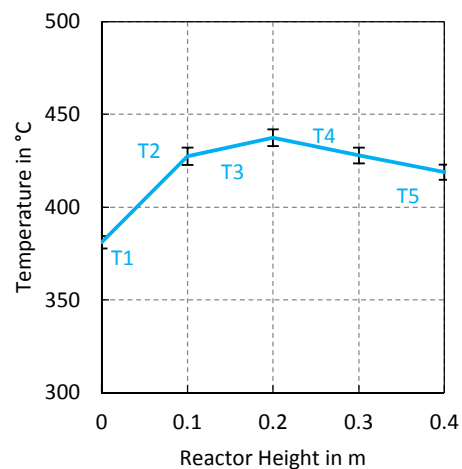
Figure 10: Temperature profile along the pilot plant WGS reactor operated with product gas downstream the RME gas scrubber.

The temperature profiles behave similar to the temperature profiles in Section 3.1, Figure 8. However, it indicates that the activity of the catalyst seemed to be higher in Figure 10 compared to Figure 8 as the temperature increase was steeper and the reaction was finished in a height slightly below 20 cm compared to slightly above 20 cm in Figure 8.

4 CONCLUSION AND OUTLOOK

The results of the numerical solution of the molar and energy balance applying the kinetic model compared with the experimental values show good accordance regarding the gas composition at the pilot plant WGS reactor outlet. These results were obtained by operating a pilot plant WGS reactor with real product gas from an 8 MW industrial DFB gasification plant.

Future work should focus on the improvement of the kinetic model in order to consider aging effects of the catalyst which occur during long term operations of the WGS unit.

Such a kinetic model is a valuable tool for designing and engineering of an industrial scale WGS unit.

5 ACRONYMS AND ABBREVIATIONS

CHP	Combined Heat and Power
d.b.	Dry Basis
DFB	Dual Fluidized Bed
FPD	Flame Photometric Detector
FR	Flow Record
GC	Gas Chromatograph
ORC	Organic Rankine Cycle
RME	Rapeseed Methyl Ester
TCD	Thermal Conductivity Detector
WGS	Water Gas Shift

6 SYMBOLS

A	Cross section of catalyst bed in m^2
a,b,c,d	Reaction rate exponents in -
c_i	Volumetric fraction of component i in -
c_P	Overall molar heat capacity in J/mol K
d	Catalyst bed diameter in m
dz	Differential length element in m
E_a	Activation energy in J/mol
GHSV	Gas Hourly Space Velocity in h^{-1}
$\dot{h}$	Overall enthalpy flow in J/s
ΔH	Enthalpy of formation in kJ/mol
Δh_R	Reaction enthalpy in J/mol
k_0	Rate constant in mol/g_{cat} kPa s
$\dot{n}_i$	Molar flow rate of component i in mol/s
$\dot{n}$	Overall molar flow rate in mol/s
p_i	Partial pressure of component i in kPa
p	Absolute pressure in kPa
ϱ_s	Catalyst bulk density in kg/m^3
R	General gas constant in J/mol K
r	Reaction rate in mol/g_{cat} s
STDGR	Steam to Dry Gas Ratio in -
STCR	Steam to Carbon Ratio in -
T	Temperature in K
$V_{Catalyst}$	Catalyst volume in m^3
$\dot{V}_{Dry}$	Volumetric dry gas flow rate in Nm^3/h
$\dot{V}_{H2O}$	Volumetric steam flow rate in Nm^3/h
Δz	Length element in m

7 REFERENCES

[1] Liu K. et.al., Hydrogen and Syngas Production and Purification Technologies, (2010), Book, Wiley VCH.

[2] Balat H., Hydrogen from biomass – Present scenario and future prospects, (2010), International Journal of Hydrogen Energy, Vol. 36, pag. 7416-7426.

[3] Mueller S., Hydrogen from Biomass for Industry– Industrial Application of Hydrogen Production Based on Dual Fluid Gasification, (2013), PhD Thesis, Vienna University of Technology.

[4] Hofbauer H. Biomass CHP Plant Guessing – A Success Story, (2003), CPL Press.

[5] Kaltschmitt M. et.al., Energie aus Biomasse, (2009), Book, Springer Verlag.

[6] Diaz N., Hydrogen Separation from Producer Gas Generated by Biomass Steam Gasification, (2013), PhD Thesis, Vienna University of Technology.

[7] Twigg M. V., Catalyst Handbook Chapter 6: The Water-gas-shift Reaction, (1989), Book, Manson Publishing.

[8] Fail S., Biohydrogen Production Based on the Catalyzed Water Gas Shift Reaction in Wood Gas, (2014), PhD Thesis, Vienna University of Technology.

[9] www.scilab.org, 19.05.2015

[10] Gordon S., Computer program for calculation of complex chemical equilibrium composition, rocket performance, incident and reflected shocks and Chapman-Jouguet detonations, (1971), Report, NASA Lewis Research Center.

[11] Kotik J., Ueber den Einsatz von Kraft-Waerme-Kopplungsanlagen auf Basis der Wirbelschicht-Dampfvergasung fester Biomasse am Beispiel des Biomassekraftwerks Oberwart, (2010), PhD Thesis, Vienna University of Technology.

9   LOGO SPACE